

CORRELATION OF RHEOLOGICAL PROPERTIES  
OF LIQUID FIRE RETARDANT  
WITH AERIALY DELIVERED PERFORMANCE

Final Report

to

UNITED STATES DEPARTMENT OF AGRICULTURE  
FOREST SERVICE  
INTERMOUNTAIN FOREST & RANGE EXPERIMENT STATION

A report of research performed under the  
auspices of the Intermountain Forest and  
Range Experiment Station, Ogden, Utah.



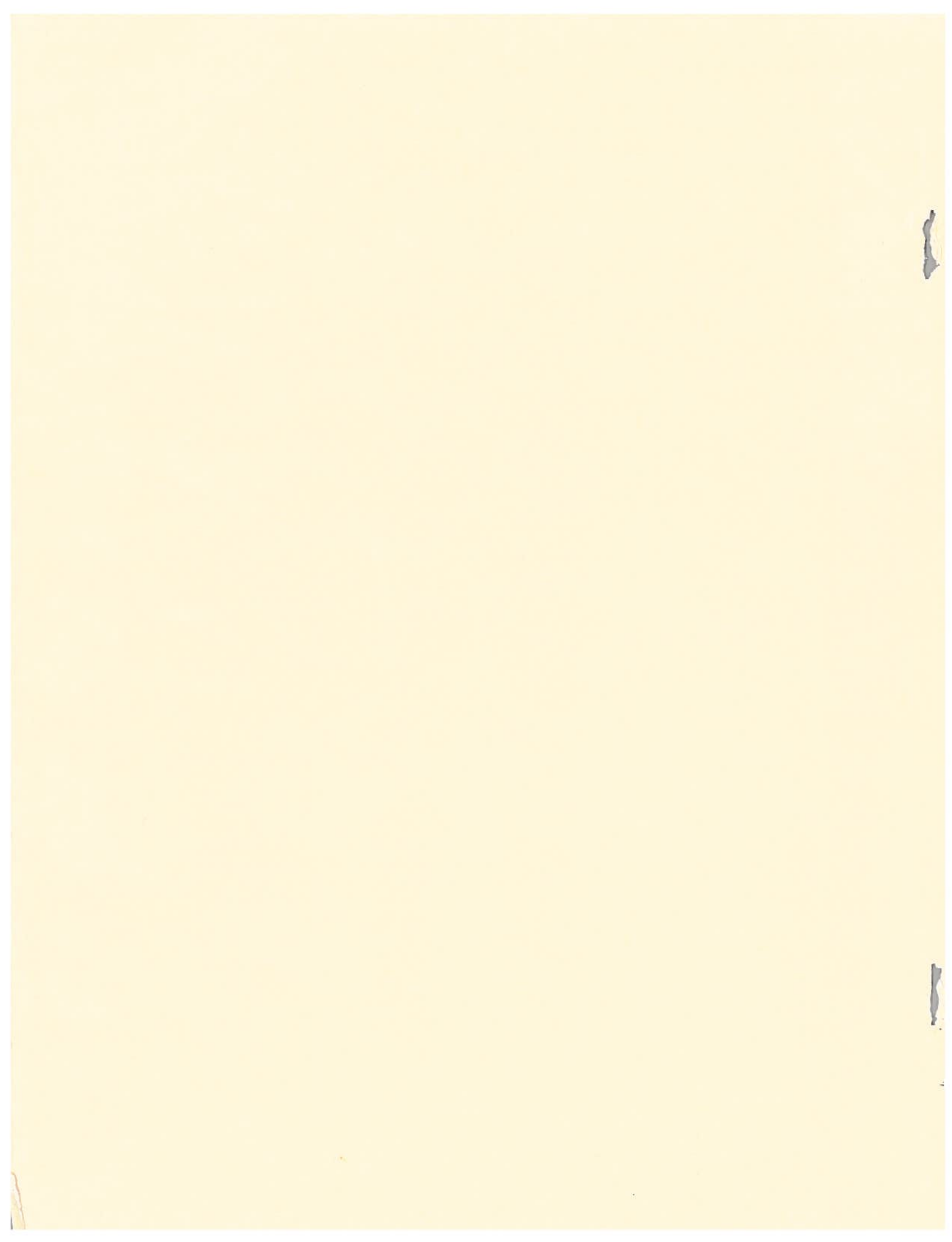
---

**Shock Hydrodynamics**

---

A DIVISION OF **Whittaker**

---



CORRELATION OF RHEOLOGICAL PROPERTIES  
OF LIQUID FIRE RETARDANT  
WITH AERIALY DELIVERED PERFORMANCE

FINAL REPORT  
(8990-08)

by

W. H. Andersen  
R. E. Brown  
N. A. Louie  
K. G. Kato  
J. A. Burchfield  
J. D. Dalby  
L. Zernow

Contract 26-3198

Period Covered: 3 March 1975 Through 1 August 1976

1 August 1976

INTERMOUNTAIN FOREST & RANGE EXPERIMENT STATION

USDA Forest Service

Ogden, Utah 84401

The research conducted under this contract is a part of a program to improve fire control technology, specifically through the use of fire retardant chemicals and delivery systems whose chemical and/or design characteristics are tailored to fuel and fire situation needs. This program is being conducted at the Northern Forest Fire Laboratory. Information or questions regarding these studies should be directed to the:

Northern Forest Fire Laboratory  
Drawer G  
Missoula, Montana 59801

SHOCK HYDRODYNAMICS DIVISION  
WHITTAKER CORPORATION  
4710-16 Vineland Avenue  
North Hollywood, California 91602

1  
2  
3  
4

5  
6  
7  
8

## ACKNOWLEDGEMENT

The authors wish to acknowledge the assistance given them by the Contract Monitor, Mr. Charles W. George, and his group at the Northern Forest Fire Laboratory during the field test experiments conducted at Chico, California, and by Mr. Damon H. Swanson of the Honeywell Corporation. Discussion with Mr. George regarding various aspects of the program was also helpful to the success of the program.

10 11 12

13 14 15

TABLE OF CONTENTS

	Page
SUMMARY . . . . .	viii
1. INTRODUCTION . . . . .	1
1.1 Scope of the Present Program . . . . .	1
2. MEASUREMENT OF FLUID RHEOLOGICAL PROPERTIES . . . . .	2
2.1 Viscous and Elastic Nature of Fire Retardants Solutions . . . . .	2
2.2 Fire Retardant Thickener Selection . . . . .	3
2.3 Experimental Procedure . . . . .	4
2.3.1 Sample Preparation . . . . .	4
2.3.2 Rotoviscometry . . . . .	4
2.4 Experimental Results . . . . .	6
2.4.1 Apparent Viscosity Measurements . . . . .	6
2.4.2 Elastic Strain (Recoverable Shear) Measure- ments . . . . .	13
2.4.3 Reexamination of the Rheological Properties of Phos-Chek XA . . . . .	16
2.5 Discussion of Results . . . . .	16
2.5.1 Estimated Power Law Relationships of Apparent Viscosity . . . . .	16
2.5.2 Yield Stress Estimates . . . . .	22
2.5.3 Recoverable Shear . . . . .	24
2.5.4 Estimated Effective Viscosity . . . . .	27
2.6 Surface Tension Measurements . . . . .	30
3. EXPERIMENTAL FIELD TEST PROCEDURES . . . . .	32
3.1 Field Test Conditions . . . . .	32
3.1.1 Test Grid and Ground Contour Pattern . . . . .	32
3.1.2 Test Tank and Gating System . . . . .	32
3.1.3 Aircraft Speed, Drop Height and Wind . . . . .	33
3.1.4 Retardants and Test Matrix . . . . .	35
3.2 Measurement of Terminal Droplet Size . . . . .	35
3.2.1 High Speed Photography . . . . .	37
3.2.2 Rotating Impact Samplers . . . . .	39
3.2.3 Impact Sampler Cards . . . . .	41
3.2.4 Reduction of the Camera Data . . . . .	42

TABLE OF CONTENTS (Concluded)

	Page
3.2.5 Reduction of the Impact Sampler Data . . . . .	44
4. EXPERIMENTAL RESULTS . . . . .	52
4.1 Correlations of Droplet Size . . . . .	69
4.1.1 Comparison of Camera and Sampler Data . . . . .	69
4.1.2 Effect of Ground Concentration . . . . .	70
4.1.3 Comparison of Retardants . . . . .	71
4.1.4 Effect of Air Speed . . . . .	74
4.1.5 Temporal Aspects of Droplet Impaction on the Ground . . . . .	75
4.1.6 Droplet Impact Velocities . . . . .	75
4.2 Ground Contour Pattern . . . . .	80
5. CORRELATION WITH THEORY . . . . .	81
5.1 Terminal Droplet Size . . . . .	84
5.1.1 Mass Mean Diameter Equations . . . . .	84
5.1.2 Droplet Size In and Near the Effective Ground Pattern . . . . .	87
5.1.3 Effect of Gum Thickener Concentration . . . . .	89
5.1.4 Effect of Aircraft Velocity . . . . .	89
5.1.5 Application to Retardant Development . . . . .	89
5.1.6 Droplet Size in the Ineffective Ground Pattern. . . . .	91
5.1.7 Droplet Size Distribution . . . . .	91
6. CONCLUSIONS . . . . .	93
REFERENCES . . . . .	95



## LIST OF FIGURES

Figure	Title	Page
1	Apparent Viscosity as Measured on the Brookfield LVF Viscometer as a Function of Relative Guar Gum Concentration in Phos-Chek XA . . . . .	5
2	Shear Stress versus Shear Rate for Special Phos-Chek Formulation 263 . . . . .	7
3	Shear Stress versus Shear Rate for 4:1 Mixture of Special Formulations 263 and 9333 . . . . .	7
4	Shear Stress versus Shear Rate for Phos-Chek XA . . . . .	8
5	Shear Stress versus Shear Rate for a 1:1 Mixture of Special Formulations 263 and 9333 . . . . .	9
6	Shear Stress versus Shear Rate for a 1:3 Mixture of Special Formulations 263 and 9333 . . . . .	10
7	Shear Stress versus Shear Rate for a 1:9 Mixture of Special Formulations 263 and 9333 . . . . .	11
8	Shear Stress versus Shear Rate for Special Phos-Chek Formulation 9333 . . . . .	12
9	Apparent Viscosities of Special Phos-Chek Formulations as a Function of Shear Rate . . . . .	14
10	Measured Elastic Deformation Angle for Special Formulation 9333 as a Function of Shear Rate . . . . .	15
11	Estimated Recoverable Shear of Special Phos-Chek Formulation 263 as a Function of Shear Rate . . . . .	17
12	Estimated Recoverable Shear of 4:1 Mixture of Special Formulations 263 and 9333 . . . . .	17
13	Estimated Recoverable Shear of Phos-Chek XA as a Function of Shear Rate from Capillary and Rotational Viscometry Data . . . . .	18
14a	Recoverable Shear of a 1:1 Mixture of Special Formu- lations 263 and 9333 as a Function of Shear Rate . . . . .	19
14b	Recoverable Shear of a 1:3 Mixture of Special Formu- lations 263 and 9333 as a Function of Shear Rate . . . . .	19
15a	Recoverable Shear of a 1:9 Mixture of Special Formu- lations 263 and 9333 as a Function of Shear Rate . . . . .	20

LIST OF FIGURES (Continued)

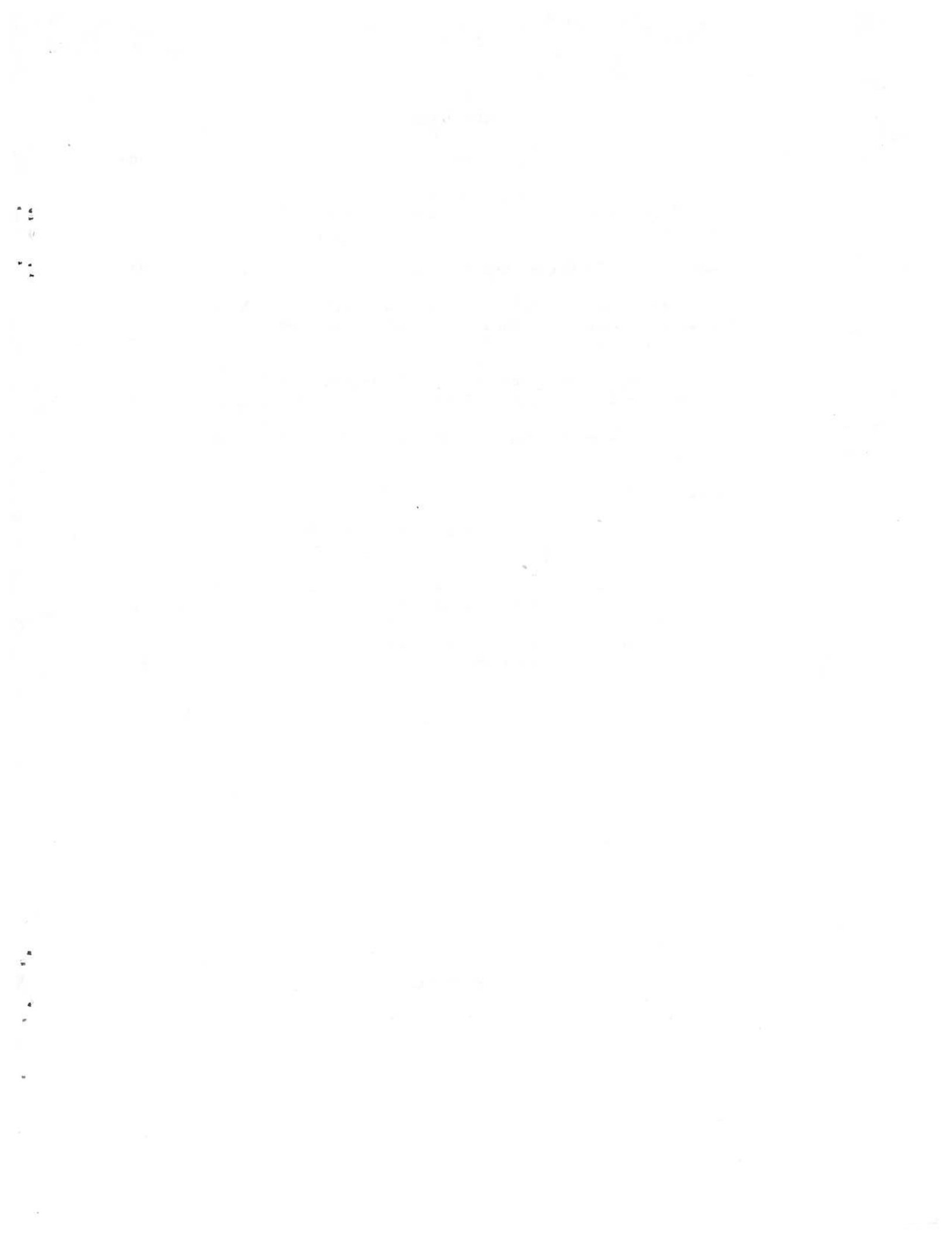
Figure	Title	Page
15b	Recoverable Shear of Special Phos-Chek XA Formulation 9333 as a Function of Shear Rate . . . . .	20
16	Comparison of Rotovisco Data Obtained for a 1.72:1 Mixture of Special Formulations 263 and 9333 With Phos-Chek XA Data . . . . .	21
17	Estimated Yield Stresses of Phos-Chek XA Formulations According to the Reiner-Rivlin Model for a Bingham Body as a Function of Guar Gum Concentration . . . . .	25
18	Recoverable Shear versus Shear Rate for Phos-Chek XA, Special Phos-Chek XA Formulations 9333 and 263 and Mixtures of the Special Formulations . . . . .	26
19	Estimated Effective Viscosity, $\eta_e$ , as a Function of Shear Rate and Guar Gum Concentration in Phos-Chek XA Formula-tion . . . . .	28
20	Surface Tension of the Phos-Chek XA Solutions as a Function of Gum Thickener Concentration . . . . .	31
21a	Bottom View of the Experimental Tank . . . . .	34
21b	Approximate Flow Rate of Retardant from the Tank . . . . .	34
22	Location of the Camera and Impact Samplers in the Test Grid . . . . .	36
23	Schematic of the Camera System Used to Dynamically Observe the Size of the Droplets Produced by the Aerial Dissemination of Liquid Fire Retardants During the Fall-out Process . . . . .	38
24	Rotating Impact Sampler Schemes Used to Prevent Over-loading of Target and Provide Time Resolution of the Droplet Sizes . . . . .	40
25	Schematic of the Camera and Rotating Sample Controls . . . . .	41
26	Correction Factor vs Apparent Image Size . . . . .	43
27	Two Frames of the Camera Film Obtained for Phos-Chek XA (Drop Test No. 147) . . . . .	45
28	Typical Droplet Splotch Patterns Obtained by the Rotating Impact Samplers . . . . .	46

LIST OF FIGURES (Continued)

Figure	Title	Page
29	Experimental Relation Between Droplet Diameter and Splotch Pattern Diameter of the Retardants . . . . .	51
30	Measured Droplet Sizes: Phos-Chek XA (DN 155) . . . . .	53
31	Measured Droplet Sizes: Phos-Chek XA (DN 147) . . . . .	54
32	Measured Droplet Sizes: 0.42 Phos-Chek XA (DN 163) . . . . .	55
33	Measured Droplet Sizes: 0.42 Phos-Chek XA (DN 164) . . . . .	56
34	Measured Droplet Sizes: 1.6 Phos-Chek XA (DN 169) . . . . .	57
35	Measured Droplet Sizes: 1.6 Phos-Chek XA (DN 168) . . . . .	58
36	Measured Droplet Sizes: Phos-Chek XA (DN 161) . . . . .	59
37	Measured Droplet Sizes: Phos-Chek XA (DN 157) . . . . .	60
38	Measured Droplet Sizes: Phos-Chek XA (DN 158) . . . . .	61
39	Measured Droplet Sizes: Fire-Trol (DN 160) . . . . .	62
40	Measured Droplet Sizes: Fire-Trol (DN 240) . . . . .	63
41	Measured Droplet Sizes: Fire-Trol 931 (DN 165) . . . . .	64
42	Measured Droplet Sizes: Fire-Trol 931 (DN 166) . . . . .	65
43	Measured Droplet Sizes: Water (DN 151) . . . . .	66
44	Measured Droplet Sizes: Water (DN 162) . . . . .	67
45	Experimental Effect of Gum Thickener Concentration on Mass Mean Droplet Size of the Phos-Chek XA Solutions . . . . .	74
46	Mass Mean Diameter of the Impacting Droplets vs Time, as Measured by the Camera Technique . . . . .	76
47	Droplet Size Distributions of the Impacting Droplets vs Time, as Measured by the Rotating Impact Samplers . . . . .	77
48	Terminal Velocities of the Droplets vs Drop Diameter, as Measured by the Camera Technique . . . . .	79
49	Apparent Viscosity vs Shear Rate of the Fire Retardant Solutions . . . . .	82

LIST OF FIGURES (Concluded)

Figure	Title	Page
50	Effective Viscosity vs Shear Rate of the Fire Retardant Solutions . . . . .	83
51	Computed Effect of Gum Thickener Concentration of the Droplet Size of the Phos-Chek XA Solutions . . . . .	90
52	Computed Effect of Aircraft Speed on the Mass Mean Droplet Diameter of the Retardants . . . . .	90
53	Computed Size Distribution of the Retardant Droplets In and Near the Effective Ground Pattern . . . . .	92



LIST OF TABLES

Table	Title	Page
I	Power Law Parameters Estimated for the Relation Between Shear Stress and Shear Rate for Special Formulations of Phos-Chek . . . . .	22
II	Summary of Yield Stress Estimates . . . . .	23
III	Power Law Parameters Estimated for the Variation of Elastic Recoverable Shear with Shear Rate for Special Formulations of Phos-Chek . . . . .	27
IV	Estimated Effective Viscosities of Phos-Chek Fire Retardants Containing Various Guar Gum Concentrations . . . . .	29
V	Measured Surface Tensions of the Special Phos-Chek Formulations at 20°C . . . . .	31
VI	Experimental Values of the Spread Factor Constants . . . . .	50
VII	Comparison of the Droplet Sizes Measured by the Camera and Corresponding Sampler . . . . .	69
VIII	Experimental Mass Mean Droplet Diameter of the Retardants In and Near the Effective Ground Pattern . . . . .	72
IX	Computed Droplet Sizes of the Retardants In and Near the Effective Ground Pattern . . . . .	87

Use of trade or firm names is for reader information only, and does not constitute endorsement by the U. S. Department of Agriculture of any commercial product or service.

## SUMMARY

This report describes the results of an investigation of the droplet sizes produced by the aerial dissemination of various liquid fire retardants, and their correlation with the rheological properties of the retardants on the basis of the previously developed liquid breakup model.

Several retardants whose effective viscosities encompass a wide range were selected for study in the field. These retardants included 1.6 Phos-Chek XA, Phos-Chek XA, 0.42 Phos-Chek XA, Fire-Trol 100, Fire-Trol 931 and water. Experimental measurements were made of the effect of gum thickener concentration on the rheological properties of the Phos-Chek XA solutions to complement those made earlier on Phos-Chek XA and the other retardants. It was found that the effective viscosity increases with increase in gum thickener concentration in the shear rate range which controls the droplet size. The surface tension of the Phos-Chek XA solutions was also found to increase with increase in the thickener concentration.

Experimental measurements were made of the droplet sizes produced during the aerial dissemination of the retardants under fixed conditions of tank size and release conditions, drop speed and drop height. These measurements were made simultaneously with some of the retardant drop tests that were conducted by the Honeywell Corporation and the U. S. Forest Service in the fall of 1975 at Chico, California during an experimental tank and gating system study. The measurements were made at various locations in the ground pattern by means of a high speed camera, three rotating impact samplers that covered and protected the splash patterns of the individual drops during the fall of the retardant rain, and a number of impact cards. The subsequent measurements of droplet size on the film and splotch size on the impact samplers were made visually, and the data reduced by a computer. The droplet size distributions (based on mass) at the various locations in the field and at various times were obtained, as were also the corresponding mass mean diameters.

The results of the studies showed a definite trend in the droplet size of the various retardants. The droplet size of the retardants decreased in the order, 1.6 Phos-Chek XA, Phos-Chek XA, 0.42 Phos-Chek XA, Fire-Trol 100, Fire-Trol 931 and water. The droplet size increased with increase in gum thickener concentration and decrease in aircraft speed. The droplet size upstream of the effective (heavy) concentration pattern was slightly smaller than near and within the heavy pattern as predicted by theory.

The droplet sizes of the various samplers for each retardant were averaged and the results compared with theory. It was found that the experimental dependence of the droplet size on the effective viscosity of the retardant was smaller than used in the previous calculations, but that by lowering the viscosity dependence to the experimental value given in the literature the droplet sizes could be correlated in a semi-quantitative manner by retaining the remainder of the model including the theoretical shear rate. The model was modified and simplified for practical use.

The final equations for estimating the terminal mass mean diameter,  $d_m$ , of the droplets produced by the aerial dissemination of a retardant with density,  $\rho_1$ , surface tension,  $\sigma$ , and effective viscosity,  $\eta_e$ , at an aircraft velocity,  $V_a$ , are

$$d_m = \frac{15}{V^{0.7}} \left( \frac{\sigma \eta_e}{\rho_1} \right)^{1/3}$$

$$\dot{S} = \frac{16.36 V^{1.414}}{\rho_1^{1/3} \sigma^{2/3} \eta_e^{1/9}}$$

$$V = 0.7 V_a$$

$$\eta_e = F_{\text{expt}}(\dot{S})$$

where the units of  $d_m$ ,  $V_a$ ,  $\eta_e$ ,  $\sigma$  and  $\rho_1$  are mm, knots, poise, dyne/cm and gm/cc, respectively. The solution of the equations requires the experimental relationship between the effective viscosity of the retardant and the shear rate,  $\dot{S}$ , and this relationship is represented by the last equation, where  $F_{\text{expt}}$  denotes the experimental function. These equations can be used in the development of retardants that will have rheological properties that will produce droplets of a desired size when the retardant is disseminated. Additional field studies should eventually be conducted to provide further information regarding the relation between droplet size and the ground contour pattern (tank and gating system) and aircraft speed, and further theoretical studies should be conducted on the mechanics of liquid breakup and its relation to the ground contour pattern.



## 1. INTRODUCTION

Aircraft have been used for many years to delivery liquid fire retardant solutions to large fires, and over the years a variety of fire retardants, aircraft, and tank and gating systems have been used in fighting fires. During this time it became apparent that the rheological properties of the liquid retardant can have a significant effect on the aerodynamic breakup and dispersion characteristics of the retardant, subsequent to its release from the aircraft.<sup>1,2</sup> This will affect both the particle size of the retardant that interacts with the fuel complex on the ground, and the localized area concentration of the dispersed retardant. It was also found that these properties can influence the wetting-out characteristics of a fuel element (e.g., brush or tree) by the retardant rain. It is thus evident that the effectiveness and efficiency of aerial fire fighting operations depends in part on the rheological properties of the liquid retardant.

On the preceding basis, the U. S. Forest Service sponsored a program with Shock Hydrodynamics whose overall purpose was to establish the relationships between the rheological properties of a liquid fire retardant and the drop behavior, breakup and dispersion characteristics, and wetting-out properties of the retardant. The initial portions of this work have been completed and are described in references 3 and 4. In this initial effort, analytical models were developed that describe many aspects of the aerodynamic breakup and dispersion characteristics of liquid retardants, including final droplet size, in terms of the important fluid properties that control the breakup such as viscosity, elasticity and surface tension, and the important delivery system parameters such as aircraft speed and altitude and the tank and gating system. These models provide a fundamental basis for further understanding the breakup and dispersion characteristics of aerially delivered liquid fire retardants, and for potentially controlling these characteristics for optimum or specific applications by means of controlled retardant rheology or delivery conditions. Some preliminary understanding of the effect of retardant rheology on the wetting-out characteristics of fuels by a retardant rain was also obtained in these studies.

### 1.1 SCOPE OF THE PRESENT PROGRAM

The purpose of the present program was to establish the actual (experimental) relationship between the rheological properties of fire retardants and their full scale aerial drop behavior in the field, including the effect of fluid rheology on the terminal droplet size distribution and dispersion pattern. Toward this objective, a number of retardants whose effective viscosities encompass a wide range were selected for study in the field. These retardants included 1.6 Phos-Chek XA, Phos-Chek XA, 0.42 Phos-Chek XA, Fire-Trol 100, Fire-Trol 931 and water. In the selection of these retardants, experimental measurements were made of the effect of gum thickener concentration on the rheological properties of Phos-Chek solutions to complement the measurements previously made on standard Phos-Chek XA and the two Fire-Trol retardants. These rheology measurements are discussed first in the following sections of the report.

Experimental measurements were subsequently made of the actual droplet sizes produced by the aerial dissemination of these retardants, and these measurements together with the corresponding ground dispersion patterns are then discussed. The droplet size measurements were made simultaneously with some of the tests that were conducted by Honeywell and the U. S. Forest Service in the fall of 1975 at Chico, California during an experimental tank and gating system (ETAGS) study. The report concludes with a comparison of the experimental droplet sizes obtained for the retardants with those estimated on the basis of theory, together with a preliminary modification of the theoretical model based on experiment and further analysis.

## 2. MEASUREMENT OF FLUID RHEOLOGICAL PROPERTIES

In this section there are presented the results of studies of the effect of guar gum concentration on the apparent viscosity, elasticity, effective viscosity, yield stress and surface tension of the basic Phos-Chek XA formulation. The corresponding measurements for standard Phos-Chek XA, Fire-Trol 100 and Fire-Trol 931 are given in references 3 and 4. Discussion of the implications of the role of gum thickener concentration on the aerial dissemination characteristics of the retardants will be included in later sections of the report.

### 2.1 VISCIOUS AND ELASTIC NATURE OF FIRE RETARDANT SOLUTIONS

It was previously shown<sup>3,4</sup> that the effective viscosity,  $\eta_e$ , helps control the aerodynamic breakup behavior and final droplet size of an aerially delivered fire retardant, and is related to the apparent viscosity,  $\eta$ , and recoverable shear (i.e., elastic strain),  $s$ , of the fluid by the equation

$$\eta_e = \eta(1 + s) \quad (1)$$

where the value of both  $\eta$  and  $s$  may depend on the shear rate of the liquid while it is undergoing breakup. Terminal droplet size increases with increase in  $\eta_e$ . On the previous programs, measurements were made of the viscous and elastic properties of the contemporary liquid retardants Phos-Chek XA, Fire-Trol 100 and Fire-Trol 931. It was found that all of these retardants undergo shear thinning, which causes the real (apparent) viscosity exhibited during liquid breakup to be much less than that measured by the normal (low shear rate) Brookfield Viscometer.<sup>®</sup> However due to its elastic nature, the effective viscosity of the Phos-Chek XA, which is a gum thickened retardant, remains relatively high during breakup. On the basis of theory, this results in a relatively large final droplet size of the broken-up liquid. On the other hand Fire-Trol 100, which is a clay thickened retardant, is nonelastic in nature and consequently exhibits its reduced (shear thinned) viscosity during breakup. This results in a droplet size that is smaller than that of Phos-Chek. Fire-Trol 931 has a lower apparent viscosity than Fire-Trol 100 but exhibits some elasticity which (presumably) causes its terminal droplet size to be comparable to that of Fire-Trol 100.

## 2.2 FIRE RETARDANT THICKENER SELECTION

A thickener is added to a fire retardant solution in order to increase its viscosity and consequently its terminal droplet size. However as shown in Eq. (1) it is the effective viscosity, which results from both viscosity and elasticity while the liquid is undergoing shear, that controls the aerodynamic breakup characteristics of the liquid and its final droplet size. In the initial stages of the program the decision was made to study in the field all three of the currently used fire retardants, i.e., Phos-Chek XA, Fire-Trol 100 and Fire-Trol 931, as well as water. However, in order to more effectively elucidate the effect of the rheological properties, it was considered desirable to also conduct tests on fluids in which the rheological properties are varied independently of the retardant composition, i.e., to vary the properties by merely adjusting the thickener concentration. Since on the basis of theory an elastic liquid offers the widest range of possibilities for varying the liquid breakup characteristics and final droplet size, and experimental drop studies have demonstrated the superiority of gum-thickened over clay-thickened and unthickened fluids, it was concluded that the measurements should be made on a gum-thickened fluid in which the gum-thickener concentration is varied independently of the remaining ingredients.

There are various gums that could be considered for the studies, and the effect of gum composition should probably eventually be studied. For the present program, however, it was believed that the primary end objectives would be best attained by using the conventional Phos-Chek XA composition, but varying the guar gum content since there is data which showed that the guar gum concentration can be varied over a relatively wide concentration range without difficulties. This eliminated the problems that could have arisen in attempting to use a different gum. Moreover, since much experimental drop data is presently available with various tank and gating systems for the standard Phos-Chek XA composition, a wider range of information can be correlated from tests with this basic retardant composition.

Two special Phos-Chek formulations were prepared by the Monsanto Company for this investigation:

- i. Phos-Chek XA Special Formulation 10 min-visc-9333, 233998 (whose guar gum thickener concentration was a factor of 2.00 greater than that of Phos-Chek XA), and
- ii. Phos-Chek XA Special Formulation 10 min-visc-263, 233998 (whose guar gum thickener concentration was a factor of 0.42 that of Phos-Chek XA).

The designations 10 min-visc-9333 and 10 min-visc-263 describe the apparent viscosity of 68.39 grams of each formulation in 500 grams of water, ten minutes after preparation, determined using a Brookfield LVF Viscometer with a number 4 spindle at 60 rpm. The proportional quantities of the other dry ingredients (i.e., diammonium phosphate, iron oxide and the corrosion and spoilage inhibitors) of the Phos-Chek XA formulations were held constant in the two special formulations. Additional formulations

were prepared by mixing together given amounts of each of these two formulations. From the results of the rheology measurements on the various liquid solutions, two different concentrations of gum thickened retardant were eventually selected for study in the field tests, viz, 0.42 Phos-Chek XA and 1.6 Phos-Chek XA, where the numbers 0.42 and 1.6 indicate Phos-Chek XA formulations with a gum concentration that is a factor of 0.42 and 1.6 of that contained in the standard Phos-Chek XA formulation.

## 2.3 EXPERIMENTAL PROCEDURE

### 2.3.1 Sample Preparation

In addition to the "as received" samples of Phos-Chek XA, special formulation 263, and special formulation 9333, mixtures of the latter two formulations were made. These additional dry mixtures had weight ratios of "263" to "9333" of 4:1, 1.72:1, 1:1, 1:3 and 1:9.

The aqueous retardant fluids were prepared in the following manner. To 500 grams of water (Arrowhead Puritas Water, Inc., Spring Water) was added 68.4 grams of the powdered Phos-Chek formulation. The mixture was mixed in a Proctor-Silex Model 8040 blender for 30 seconds at the lowest blender speed (i.e., 12,000 rpm) and 2.5 min. at the highest speed (i.e., 21,000 rpm). The mixing propeller of this blender has four blades, each 1.0 in. long and approximately 0.26 in. wide.

For purposes of quality control, the apparent viscosity of each retardant solution was measured, 10 min. after preparation, with a Brookfield LVF Viscometer using a #4 spindle at 60 rpm. The retardant fluids were placed in a 600 ml low-form beaker for these measurements. The average apparent viscosities of these retardant mixtures at the effective shear rate under these conditions (i.e., 12.5 sec<sup>-1</sup>) are shown in Figure 1.

### 2.3.2 Rotoviscometry

The viscosity and elasticity measurements were made at 20±1°C using the Model RVI Haake Rotoviscometer<sup>®</sup> with ELZ Visco-Elastic attachment. The details of the measurements with this instrument have been discussed previously,<sup>3,4</sup> and need only be summarized here. Briefly, for the viscosity measurements the viscous drag on a motor driven rotor immersed in a standard cup of the liquid is measured as a torque which is displayed as a scale reading, S<sub>c</sub>, on a previously calibrated scale. Different diameter rotors (designated MVI, MVII and MVIII) and motor speeds are used to encompass different shear rate ranges. Under steady shear conditions, the shear rate,  $\dot{S}$ , shear stress,  $\sigma$ , and apparent viscosity,  $\eta$ , of the liquid are given by

$$\dot{S} = B/U \quad (2)$$

$$\sigma = afS_c \quad (3)$$

$$\eta = \sigma/\dot{S} \quad (4)$$

where B and f are known geometric instrument constants, a is the known scale sensitivity, and U is a speed factor which varies inversely with the

Ratio of Special Formulations 9333 to 263

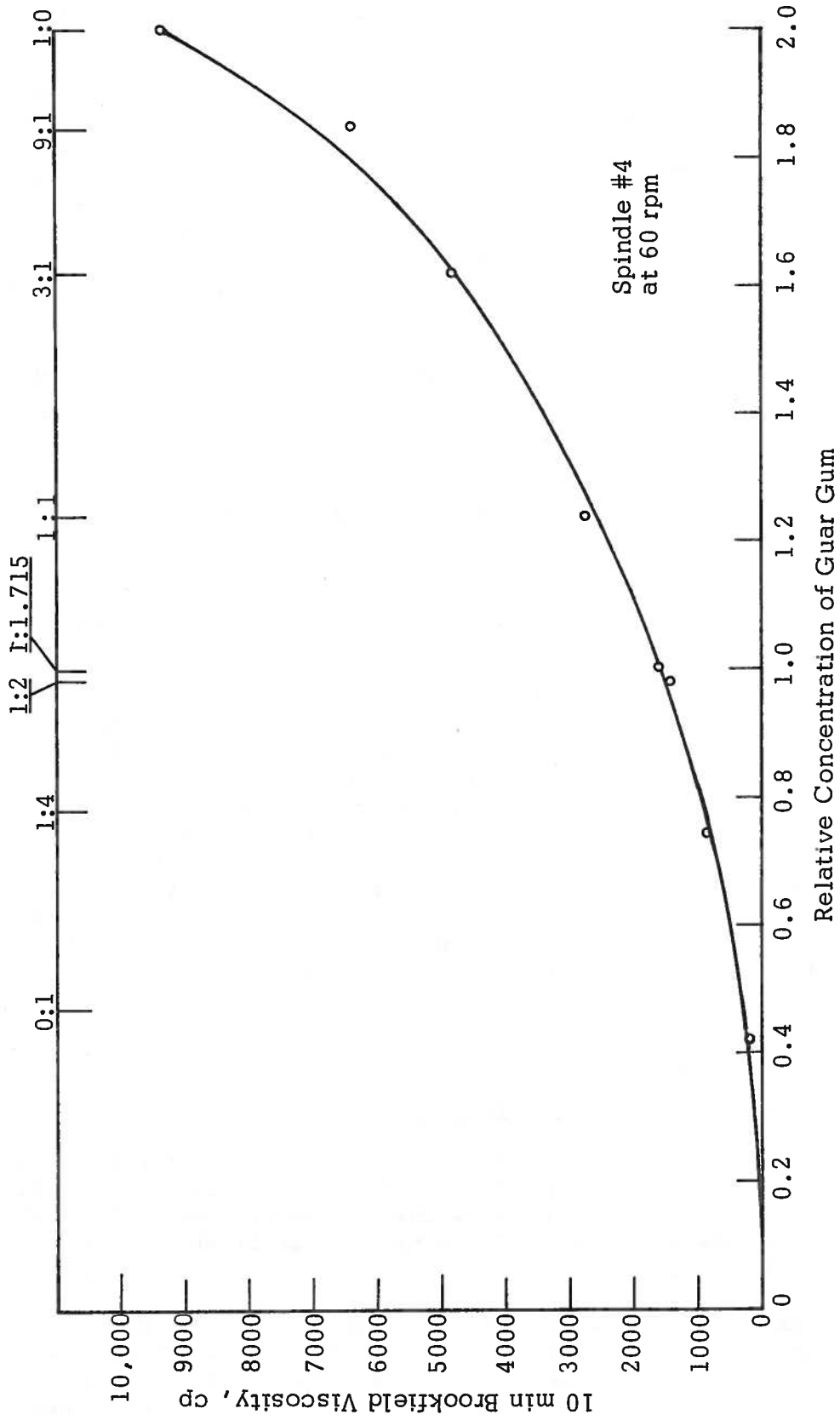


Figure 1. Apparent Viscosity as Measured on the Brookfield LVF Viscometer as a Function of Relative Guar Gum Concentration in Phos-Chek XA.

angular velocity of the rotor. A 100:1 gear reducer was attached to the motor drive and the flexible drive cable in order to extend the measurements to shear rates as low as  $0.01 \text{ sec}^{-1}$ .

The measurement of fluid elasticity utilizes the ELZ attachment which permits the measurement of the restoring moment of the rotor as the result of the fluid elasticity (if any) when the rotor is suddenly disconnected from the drive shaft. Thus if the fluid exhibits elastic behavior, the sudden termination of the rotational torque causes the rotor to spring back, or recoil. The angular displacement,  $\phi$ , of this restoration (called the elastic relaxation angle), is directly related to the elastic strain, which is usually discussed in terms of the elastic angle of deformation,  $\gamma$ , where

$$\tan \gamma = \phi/C = \eta \dot{S}/G \quad (5)$$

$$G = \sigma/\tan \gamma \quad (6)$$

$G$  is the shear modulus of the fluid, and  $C$  is a known geometric rotor constant. The recoverable shear (elastic strain),  $s$ , and the relaxation time,  $t_r$ , of the liquid are related to the shear modulus and shear rate by

$$t_r = \eta/G = s/\dot{S} \quad (7)$$

A further point of special importance regarding the elasticity measurements is that the dissipation of kinetic energy of the rotor at the moment of decoupling occurs presumably in less than 0.1 sec according to manufacturing specifications. This limits the maximum shear rate of the elasticity measurements to the shear rate that corresponds to a relaxation time equal to or greater than about 0.1 sec rather than the shear rate limit of the instrument. This was discussed in ref. 4. Since the lower limit of valid shear rate range measurements is controlled by the yield point of the liquid, only a limited range of elasticity vs shear rate can thus be determined by this instrument, which limits the accuracy with which the data can be extrapolated to higher shear rates. This will be discussed further.

## 2.4 EXPERIMENTAL RESULTS

### 2.4.1 Apparent Viscosity Measurements

Complete analyses were performed on the retardant samples described previously with the exception of the 1.72:1 mixture whose gum concentration is identical to that of the standard Phos-Chek XA formulation, and for which a more limited analysis was made for the purpose of confirming the previously reported Phos-Chek XA data.

The shear stress vs shear rate data obtained for the special Phos-Chek formulations are shown in Figures 2 through 8. The experimental data for these fluids were corrected using the Krieger-Maron-Elrod treatment, as discussed in ref. 3. With the exception of the 263 formulation, these

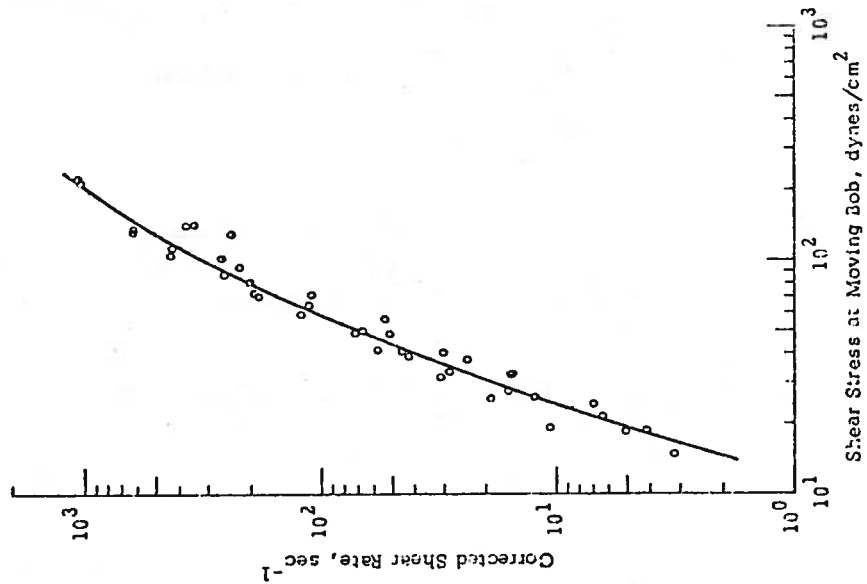


Figure 2. Shear Stress versus Shear Rate for Special Phos-Chek Formulation 263.

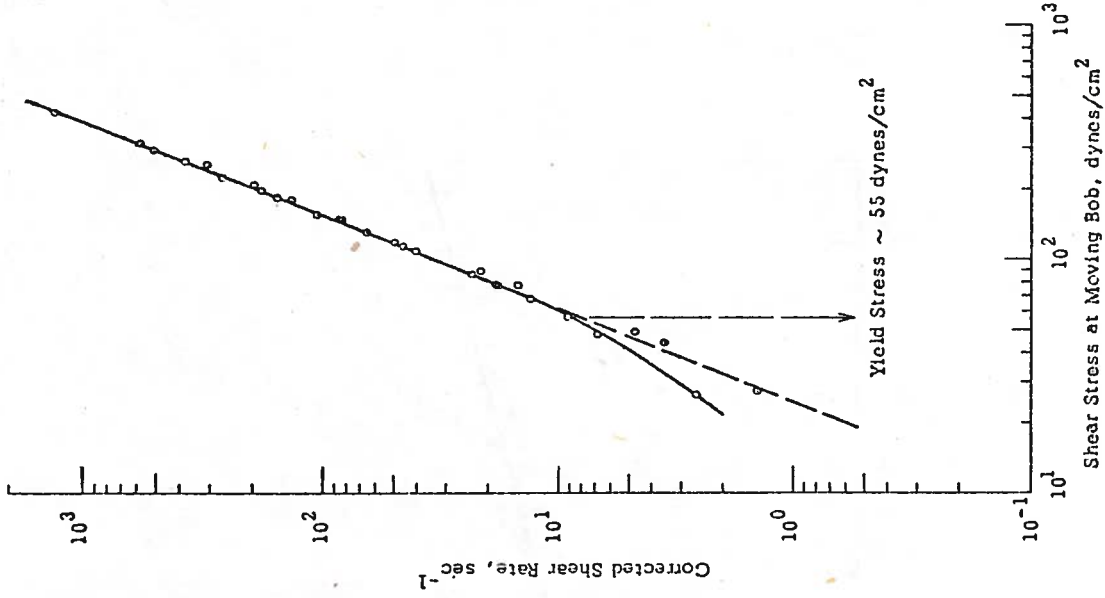


Figure 3. Shear Stress versus Shear Rate for 4:1 Mixture of Special Formulations 263 and 9333.

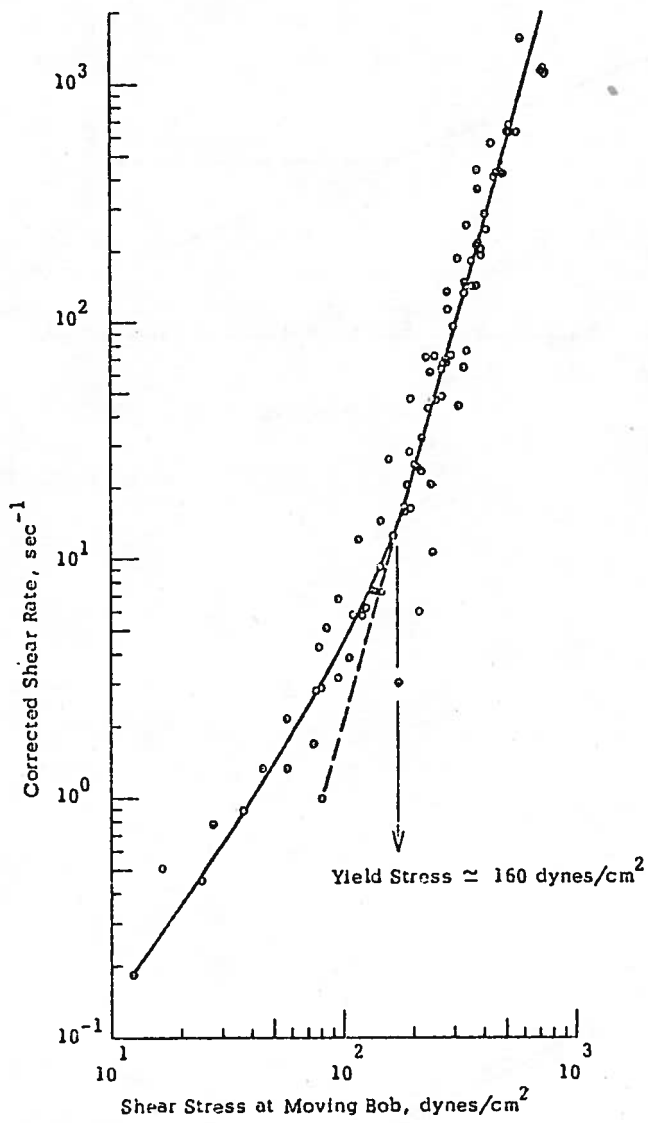


Figure 4. Shear Stress versus Shear Rate for Phos-Chek XA.



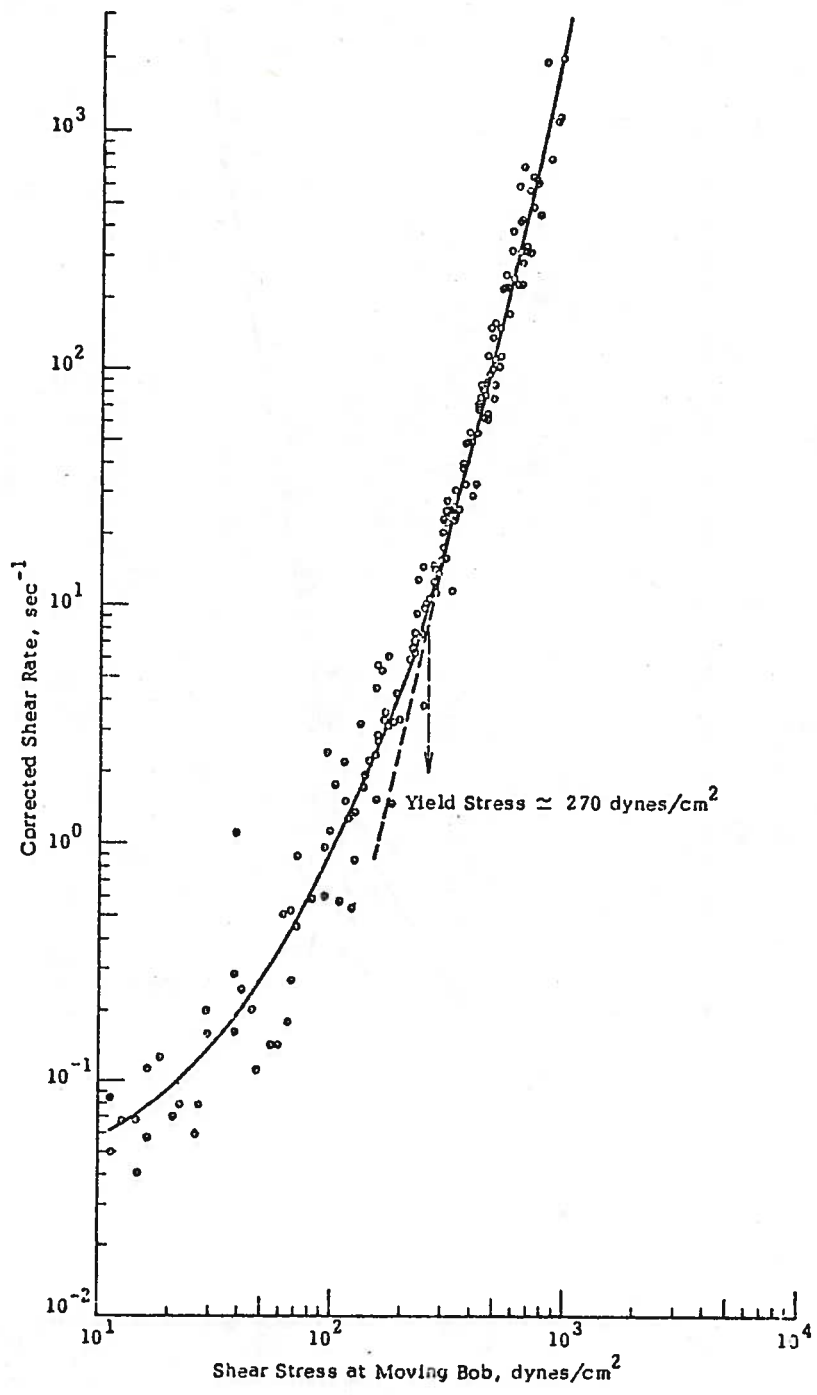


Figure 5. Shear Stress versus Shear Rate for a 1:1 Mixture of Special Formulations 263 and 9333.

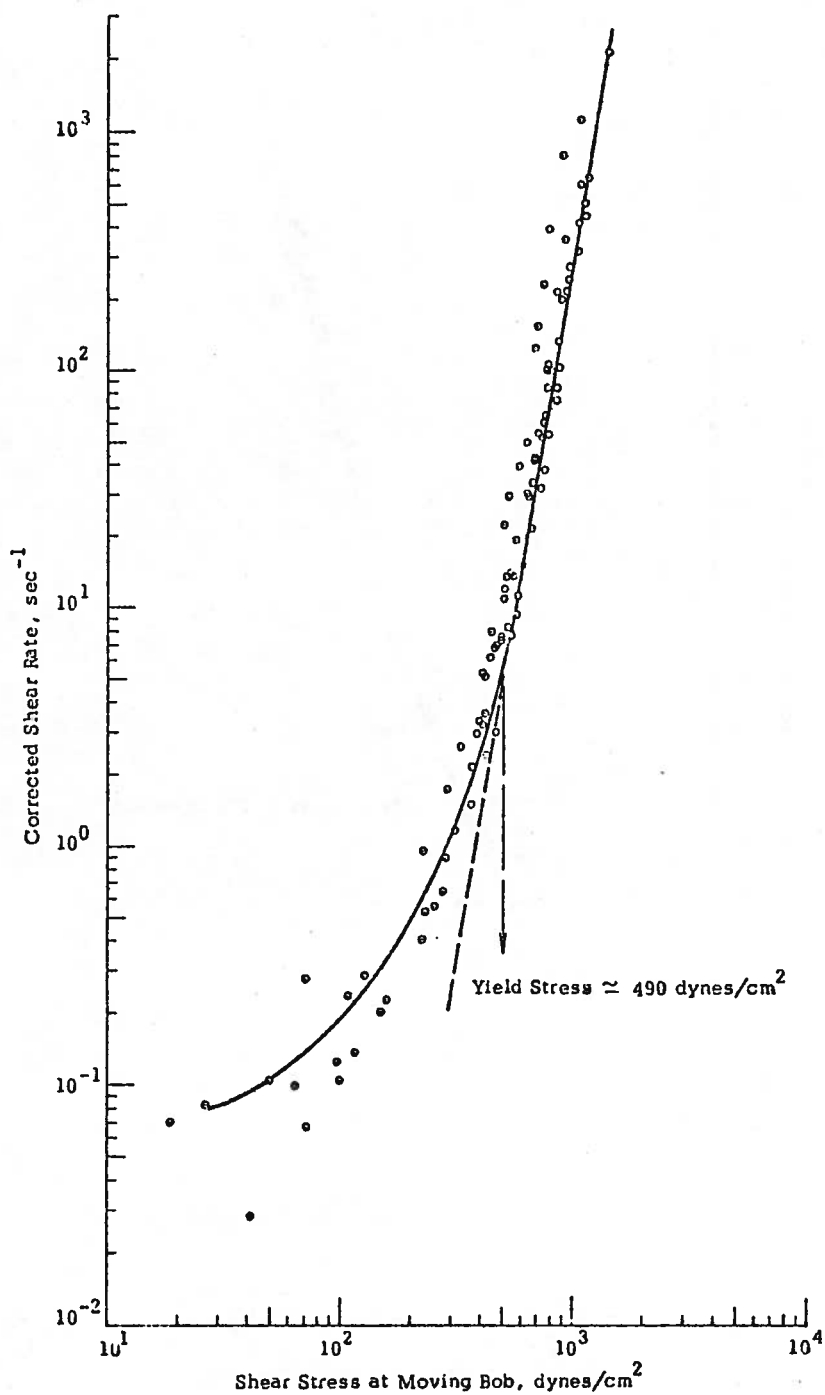


Figure 6 . Shear Stress versus Shear Rate for a 1:3 Mixture of Special Formulations 263 and 9333.

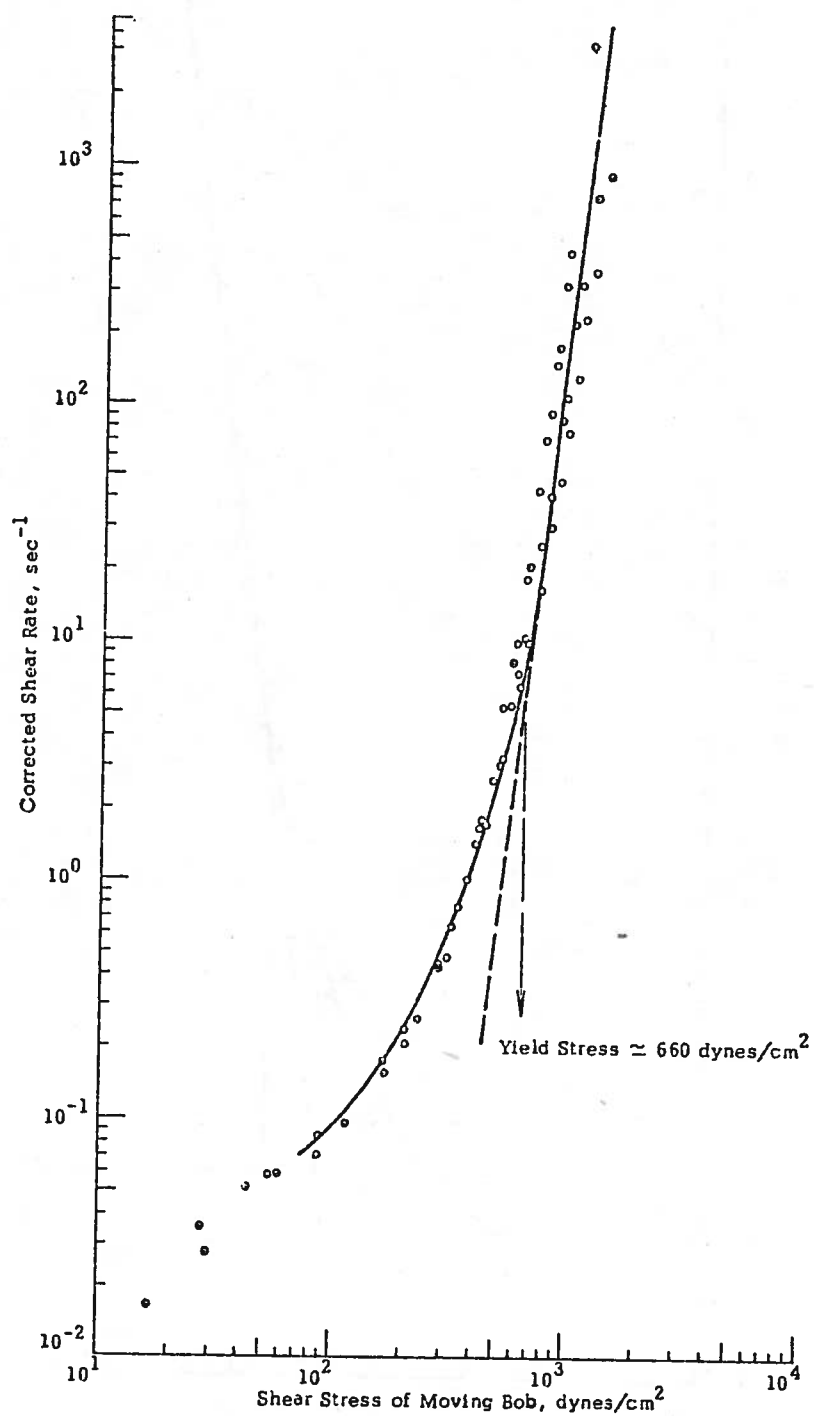


Figure 7. Shear Stress versus Shear Rate for a 1:9 Mixture of Special Formulations 263 and 9333.

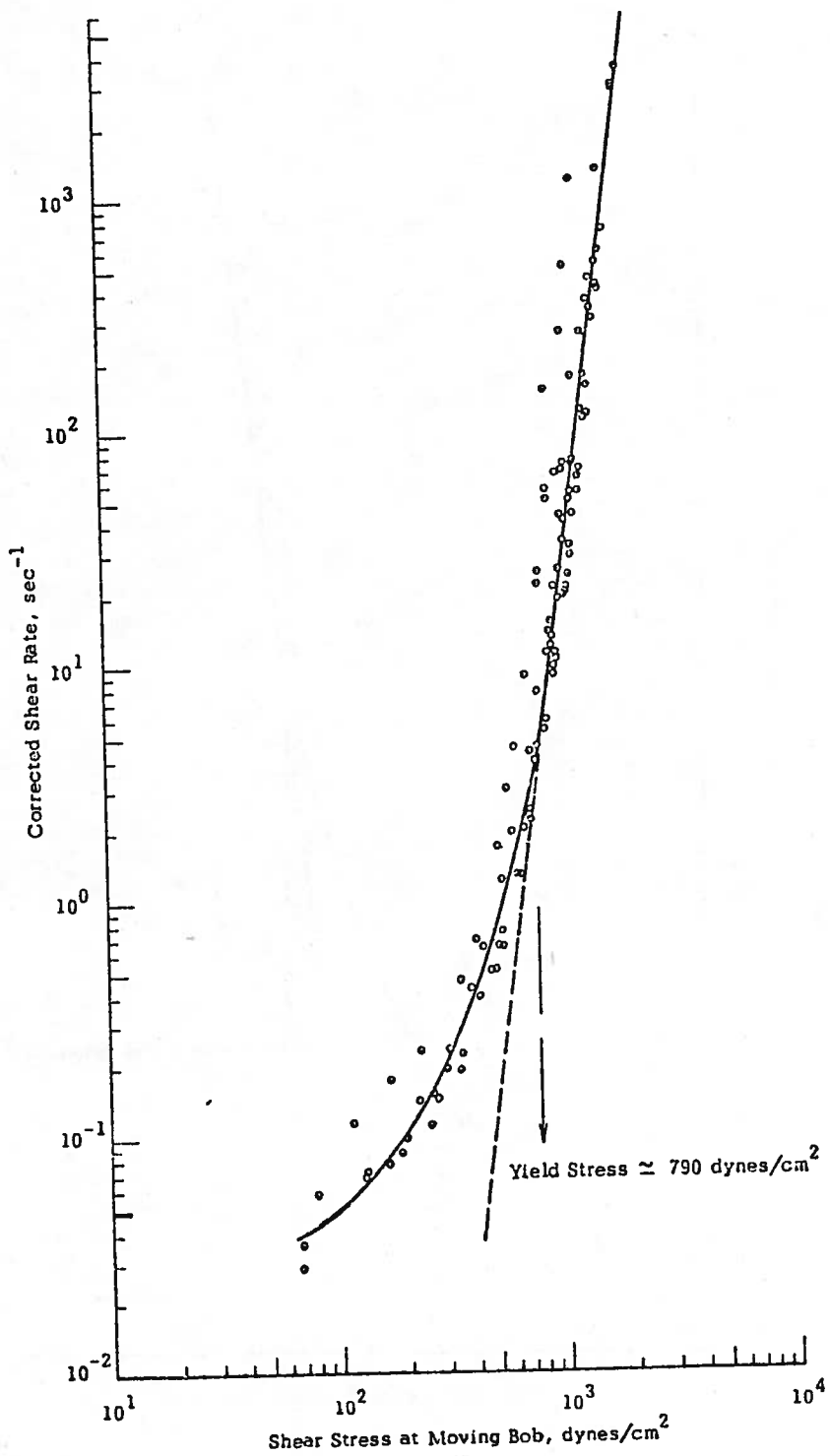


Figure 8. Shear Stress versus Shear Rate for Special Phos-Chek Formulation 9333.

retardant fluids were found to exhibit power law behavior, i.e., the shear stress,  $\sigma(S)$ , exerted on the rotating bob is related to the shear rate by

$$\sigma = b\dot{S}^n \quad (8)$$

where  $b$  and  $n$  are constants. This power law behavior is obeyed under conditions in which the shear stress within the measuring fluid gap between the rotating bob and the stationary beaker wall exceed the yield stress. When the shear stress within the gap falls below the yield stress a plug forms inward from the stationary walls, thus decreasing the effective measuring gap size. The deviation from linearity of the log-log plot of shear stress vs shear rate is believed to occur under plug flow conditions, i.e., the geometry of the measuring gap changes and therefore the true apparent viscosity using Eqn. (4) cannot be obtained from the measured value of shear stress. Thus a method of estimating the yield stress can be made by locating the point of transition between linearity and non-linearity on the log-log plot of shear stress vs shear rate, as shown in Figures 3 - 8.

From the linear portions of the log (shear stress) vs log (shear rate) plots the apparent viscosities were estimated. These estimates are shown in Figure 9. It may be seen that at constant shear rate within the experimental shear rate range, the apparent viscosity decreases monotonically with decrease in gum thickener concentration.

#### 2.4.2 Elastic Strain (Recoverable Shear) Measurements

All of the special Phos-Chek formulations exhibited elastic behavior under the conditions of the rotoviscometry experiments. It was observed that for each of the retardant fluids the elastic angle of deformation increases with shear rate and then levels off at high shear rates as shown in Figure 10 for Phos-Chek Special Formulation 9333, and in Figures 2 and 3 in ref. 4 for Phos-Chek XA and Fire-Trol 931. When the relaxation times,  $t_r$ , are estimated directly from the experimental data, i.e., from Eqn. (7), there was generally observed for the formulations investigated that the plateaus of the elastic angle of deformation vs shear rate plots are reached as  $t_r$  approaches and falls below 0.1 sec. These general occurrences are caused by the mechanical response of the Rotoviscometer and are not characteristic of the fluids themselves. According to manufacturer specifications, the response time of the Rotoviscometer with ELZ attachment is 0.1 sec. Since the theoretical relaxation time of these fluids decrease with increasing shear rate (at least over the shear rate range studied) the instrument time response effectively limits the maximum shear rate at which the elastic deformation can be measured.

The intrinsic yield stress of each retardant can further limit the shear rate range over which elastic deformation angles can be measured. Special consideration had to be given to those measurements of the elastic deformation angle which were taken under conditions of plug flow. When plug flow occurs the gap geometry changes and as a consequence the geometric factor  $C$  decreases. If this is not taken into account the apparent estimated strain (see Eqn. (5)) is lower than the true strain. Because of these two factors (i.e., mechanical response time of the instrument, and the occurrence of plug flow), the shear rate range within which valid measurements can be made was found to be quite limited for the Phos-Chek formulations.

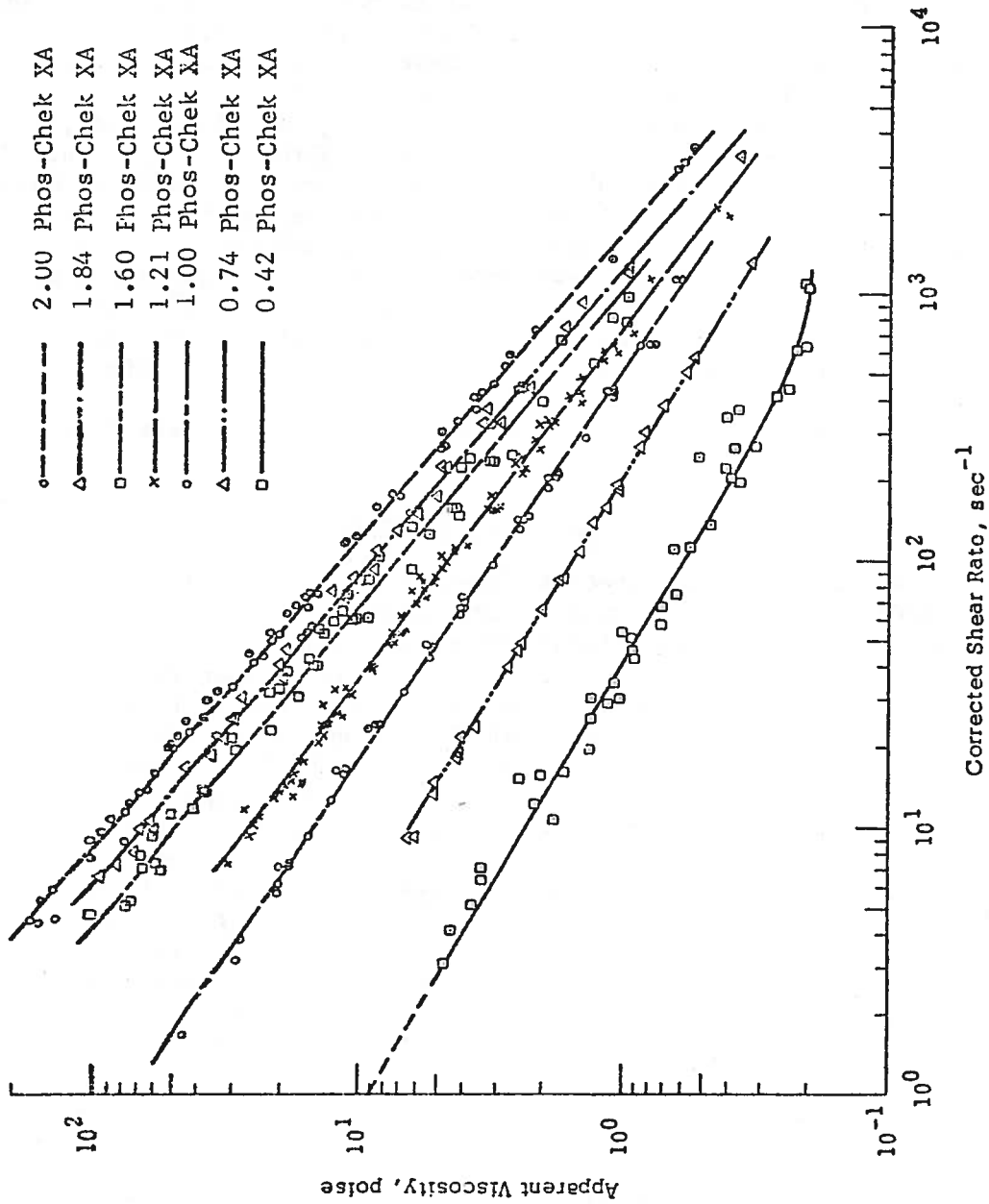


Figure 9. Apparent Viscosities of Special Phos-Chek Formulations as a Function of Shear Rate.

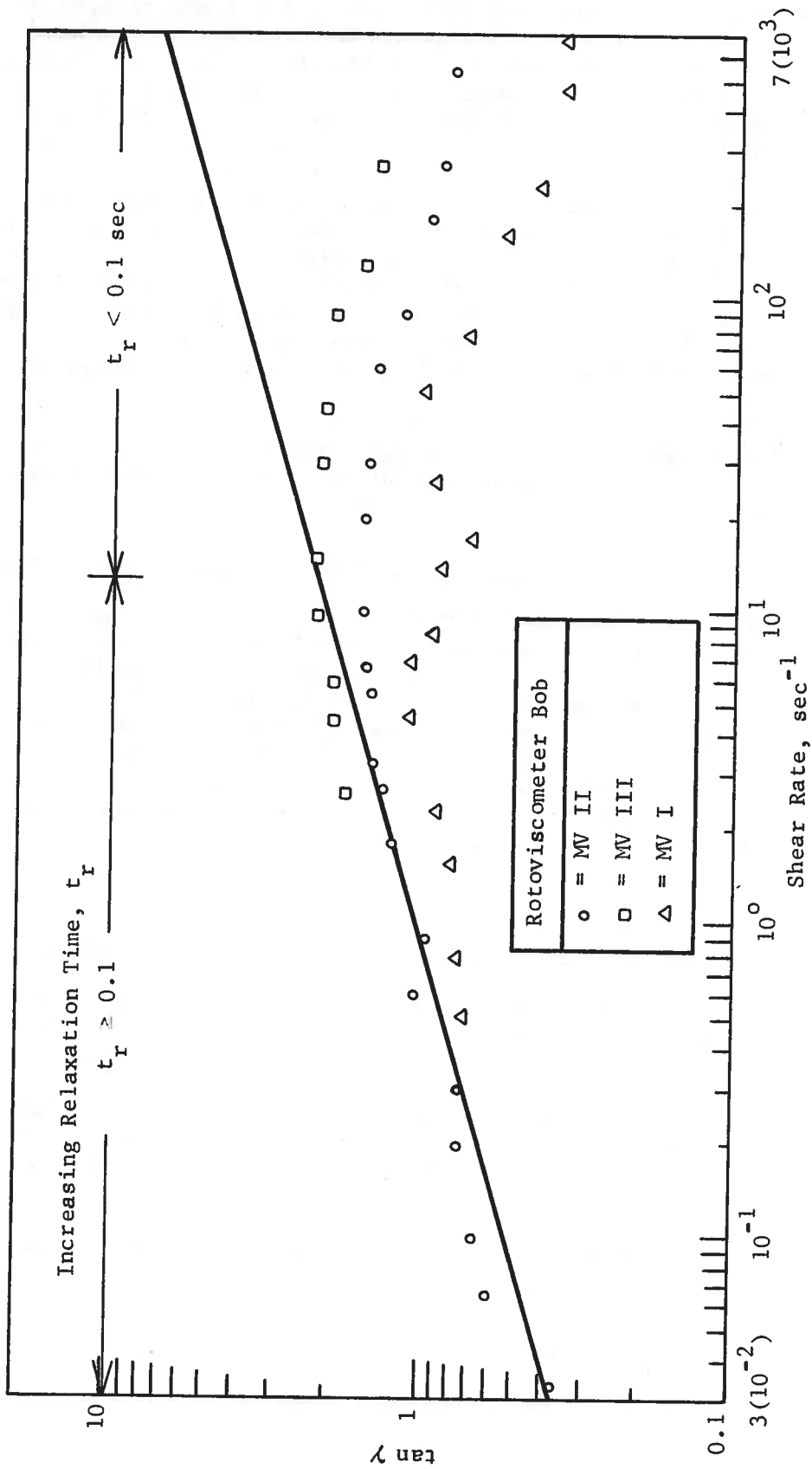


Figure 10. Measured Elastic Deformation Angle for Special Formulation 9333 as a Function of Shear Rate.

The experimental data obtained for which  $t_r > 0.1$  sec for the preceding retardant fluids are shown in Figures 11 through 15. In these figures, log-log plots of elastic strain (or recoverable shear) vs shear rate are shown. The plots appear to be linear in the shear rate regimes where plug flow does not occur (or where the effective measuring gap size is not significantly effected by the presence of a plug). However the validity of extrapolating the data up in a linear manner for one or two decades in shear rate is not known. The assumption of power law relationships are based on the fact that the Phos-Chek XA data obtained by the rotoviscometer, when coupled with the Edgewood Arsenal capillary viscometer data obtained for the XA formulation, obeys this type of treatment over several orders of magnitude of shear rate.<sup>4</sup> Also this treatment was tested by correcting the data for the reduction in the gap size where curvature occurs. These corrected data were found to lie close to the extrapolated line drawn for each retardant.

It should also be noted that since the deformation angle measurement is dependent upon the elastic component within the entire gap, these data are plotted as a function of the average shear rate.

#### 2.4.3 Reexamination of the Rheological Properties of Phos-Chek XA

Based on the composition data for Special Formulations 263 and 9333 supplied by Monsanto, a 1.72:1 mixture of these two retardants should duplicate the Phos-Chek XA formulation. Abbreviated determinations of the shear stresses and elastic strains were performed to confirm the above and to verify the previous results. The data obtained with the 1.72:1 mixture shown in Figures 16a and b were found to be in reasonably good agreement with the Phos-Chek XA data previously reported in ref. 3 and 4. The curves drawn through the data are the best fit curves estimated for Phos-Chek XA (see Figures 4 and 13).

### 2.5 DISCUSSION OF RESULTS

#### 2.5.1 Estimated Power Law Relationships of Apparent Viscosity

As expected, the apparent viscosity of the Phos-Chek fire retardant increases with guar gum concentration, at least over the shear rate range investigated (see Figure 9). Definite trends of added guar gum thickener are reflected in the values of the power law parameters (see Eqn. (8)) derived from least square analyses of the shear stress vs shear rate data. These trends are shown in Table I. As the guar gum thickener concentration increases, the value of the intercept parameter,  $b$ , increases and the slope,  $n$ , decreases.

The apparent viscosities can be estimated directly from the power law constants given in Table I. Combining Eqn. (4) and (8) gives

$$\eta = b\dot{\gamma}^{n-1} \quad (9)$$

This equation gives the apparent viscosity as a function of shear rate.



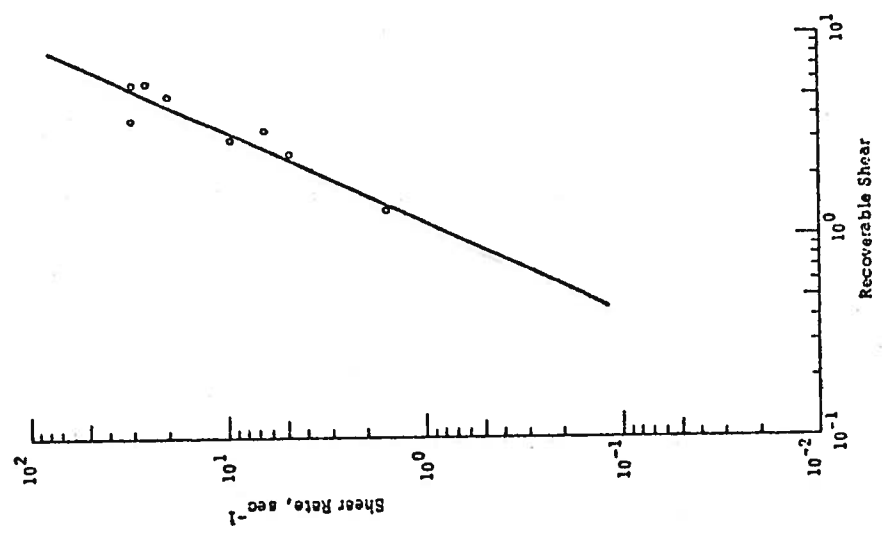


Figure 11. Estimated Recoverable Shear of Special Phos-Chek Formulation 263 as a Function of Shear Rate.

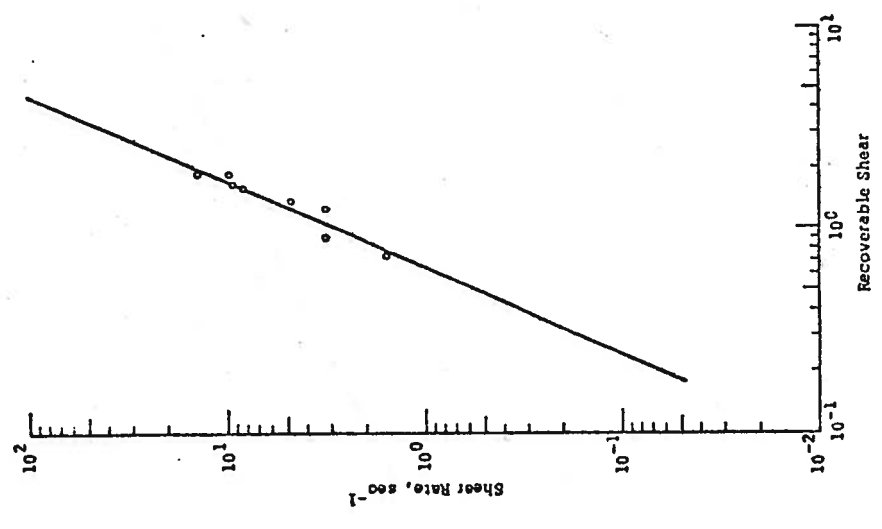


Figure 12. Estimated Recoverable Shear of a 4:1 Mixture of Special Formulations 263 and 9333.

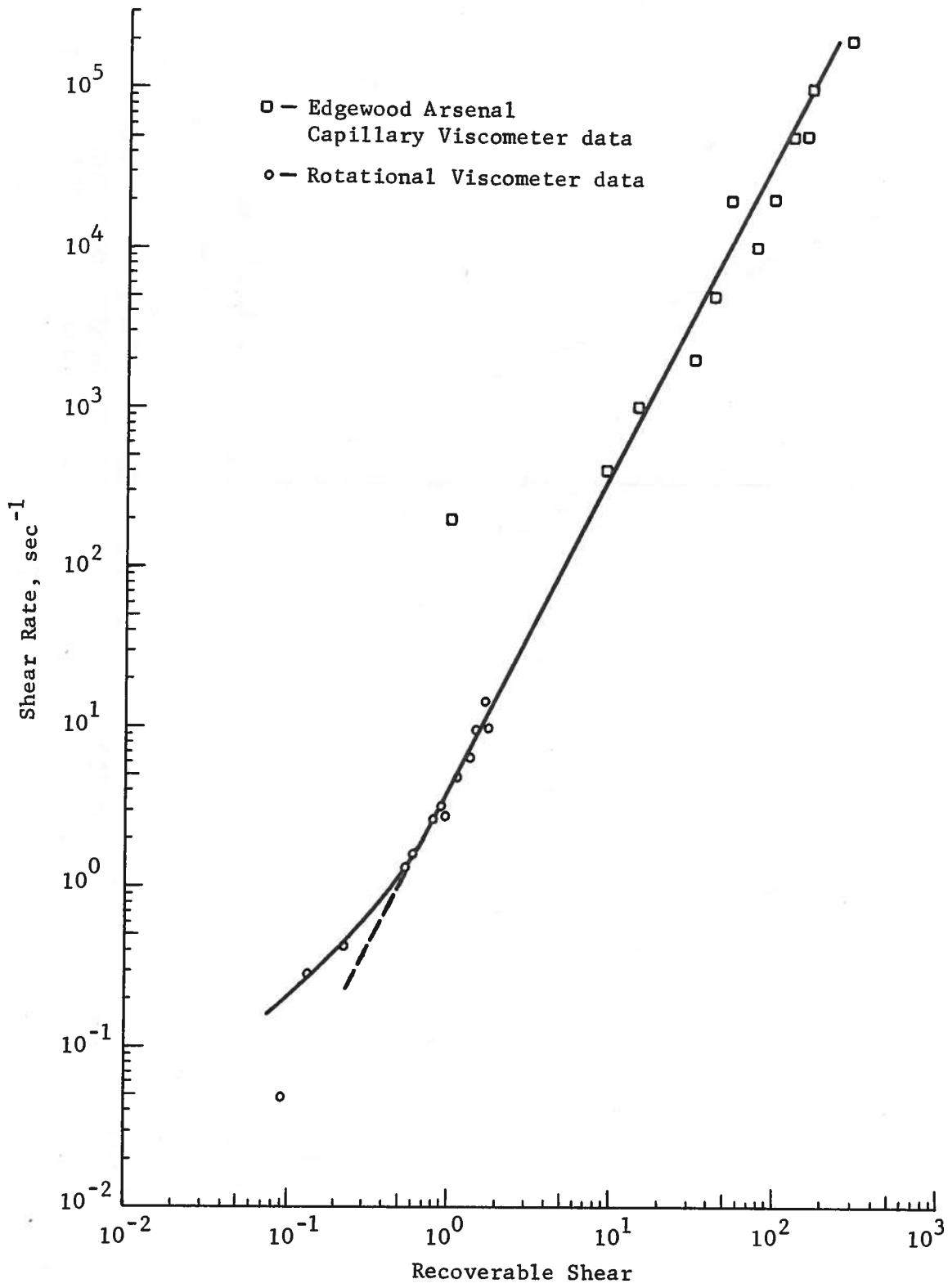


Figure 13. Estimated Recoverable Shear of Phos-Chek XA as a Function of Shear Rate From Capillary and Rotational Viscometry Data.

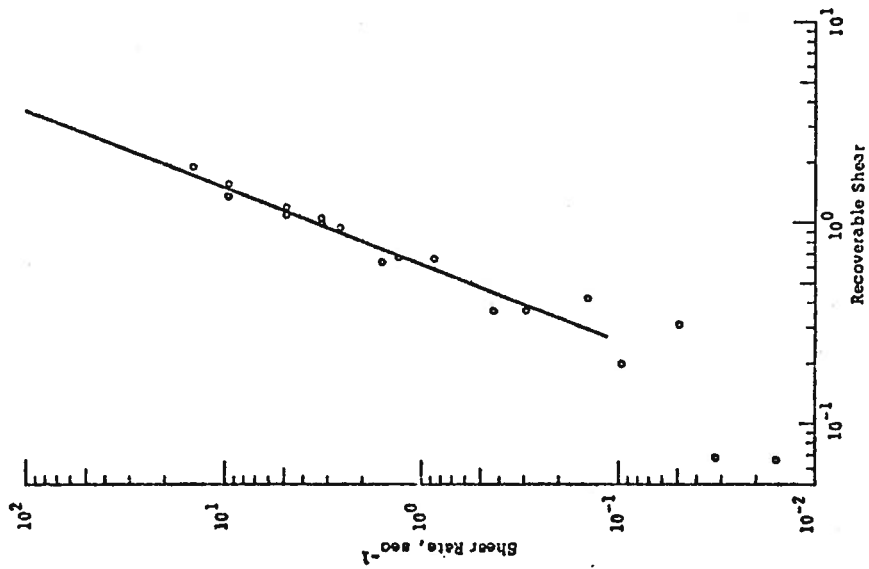


Figure 14a. Recoverable Shear of a 1:1 Mixture of Special Formulations 263 and 9333 as a Function of Shear Rate.

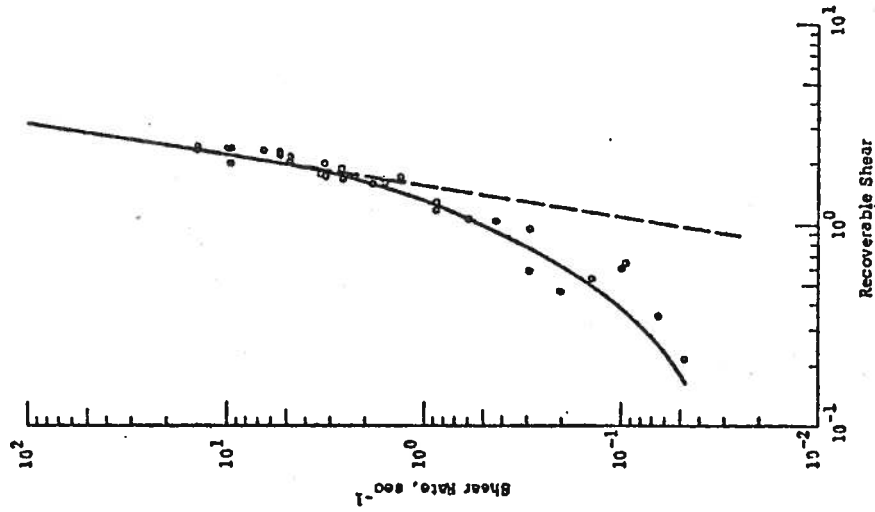


Figure 14b. Recoverable Shear of a 1:3 Mixture of Special Formulations 263 and 9333 as a Function of Shear Rate.

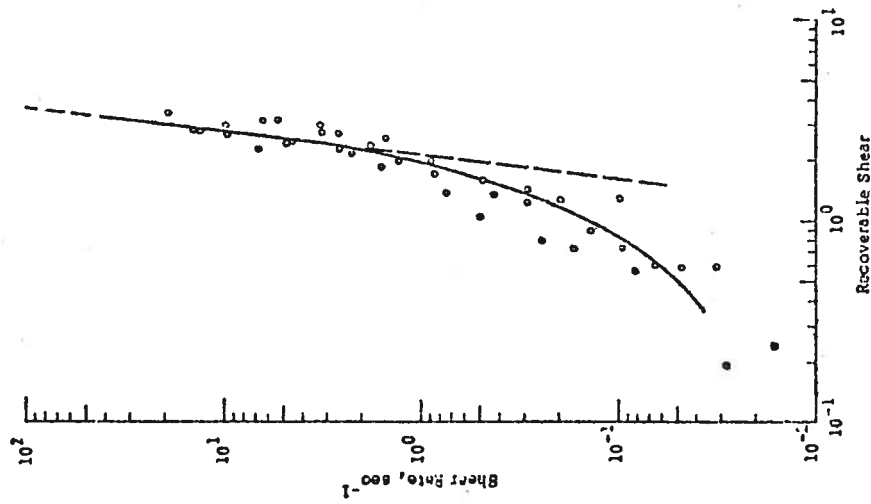


Figure 15a. Recoverable Shear of a 1:9 Mixture of Special Formulations 263 and 9333 as a Function of Shear Rate.

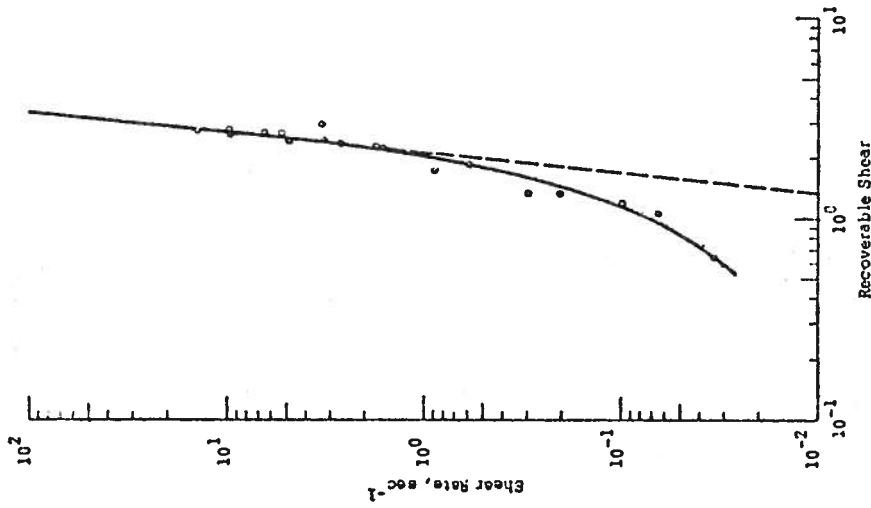
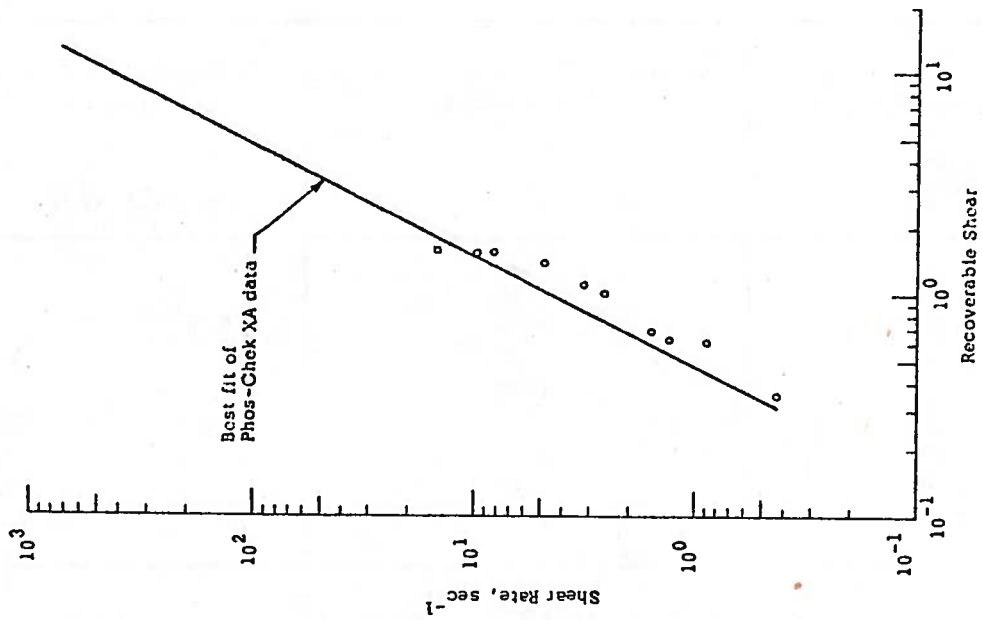
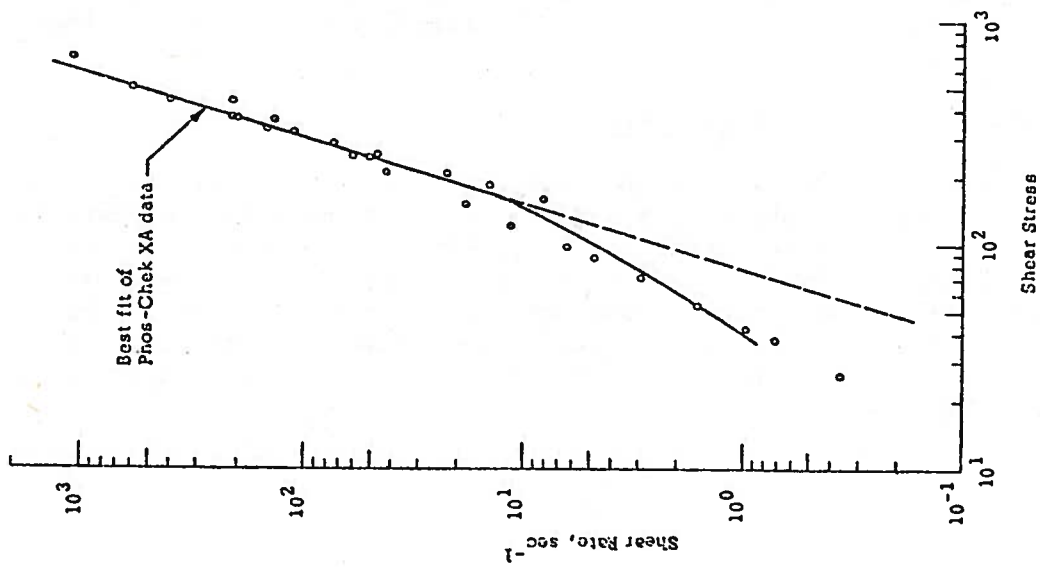


Figure 15b. Recoverable Shear of Special Phos-Chek Formulation 9333 as a Function of Shear Rate.



(a) Shear Stress vs Corrected Shear Rate

(b) Recoverable Shear vs Shear Rate

Figure 16. Comparison of Rotovisco Data Obtained for a 1.72:1 Mixture of Special Formulations 263 and 9333 With Phos-Chek XA Data.

TABLE I. POWER LAW PARAMETERS ESTIMATED FOR THE RELATION BETWEEN SHEAR STRESS AND SHEAR RATE FOR SPECIAL FORMULATIONS OF PHOS-CHEK

Mixture Ratio of Special Formulations  263 and 9333 (ratio of parts)	Relative Concentration of Guar Gum Thickener	Parameters of Power Law Equation, $\sigma = b\dot{S}^n$	
		b (dynes/cm <sup>2</sup> )	n (dimensionless)
1:0	0.42	*	*
4:1	0.74	24.8	0.40
Phos-Chek XA	1.00	67.8	0.33
1.72:1	1.00	**	**
1:1	1.21	149.	0.23
1:3	1.60	335.	0.16
1:9	1.84	478.	0.14
0:1	2.00	650.	0.10

\* Does not obey power law relationship. Better fit obtained with a polynomial  $\log \sigma = a_0 + a_1 \log \dot{S} + a_2 \log^2 \dot{S} + \dots$ , where for a third order fit the coefficients  $a_1 = 1.097(0)$ ,  $0.191(1)$  and  $0.072(2)$ .

\*\* Approximately the same as Phos-Chek XA.

The uncertainties in the apparent viscosities are estimated to be within the calibration uncertainty of 4.1%. The reproducibility of the measurements did tend to decrease somewhat as the retardant fluidity increases. Thus the experimental precision in determining the shear stresses of Special Formulation 263 is believed to be slightly lower than for the 9333 Formulation.

### 2.5.2 Yield Stress Estimates

Two methods were employed for the estimate of yield stress. The first method involved graphical interpretation. The point on the power law plots of shear stress versus shear rate (see Figures 2-8) where the data departed from linearity was considered to be an indication of the presence of plug flow. Since the shear stresses measured are at or close to the rotating bob ( $\sigma_b$ ), this type of estimate should be on the high side since the plug should form near the stationary beaker wall where the shear stresses approach  $\sigma_c$ . That is,

$$\sigma_c \sim 1/R_c^2, \sigma_b \sim 1/R_b^2 \tag{10}$$

Since  $R_c > R_b$ ,  $\sigma_c < \sigma_b$

The yield stress values obtained by this graphical approach are summarized in Table II.

TABLE II. SUMMARY OF YIELD STRESS ESTIMATES

Mixture Ratio of Special Formulations  (parts 263:9333)	Estimated Yield Stress (dynes/cm <sup>2</sup> )	
	Graphical Method	R-R Model*
1:0	--	15 ± 6
4:1	55	54 ± 21
Phos-Chek XA and 1.72:1	160	146 ± 22
1:1	270	204 ± 73
1:3	490	478 ± 64
1:9	660	603 ± 66
0:1	790	772 ± 80

\*Based on the Reiner-Rivlin Calculation.

The Reiner-Rivlin model for a plastic or Bingham body was also employed for the estimate of yield stress.<sup>3</sup> This model is based on Newtonian flow, i.e.,

$$\eta = (\sigma - Y) / (-dv/dr) \quad (11)$$

$$-dv/dr \approx r \, dw/dr \quad (12)$$

where Y is the yield stress and w is the angular velocity within the fluid (or measuring gap). Integrating Eqn. (11) between  $w = \omega$  (at the bob wall), and 0 (at the beaker wall) gives<sup>3</sup>

$$\omega = \frac{-dv/dr}{(\sigma - Y)} \left[ \frac{M}{2\pi k} \left( \frac{1}{R_b^2} - \frac{1}{R_c^2} \right) - Y \ln (R_c/R_b) \right] \quad (13)$$

It can be shown that the curve  $\omega$  versus  $\sigma$  approaches the stress axis at the yield stress tangentially (i.e.,  $d\omega/d\sigma \rightarrow 0$ ) because the gap distance ( $R_b/R$ ) within which laminar fluid flow occurs approaches zero. Thus by assuming Newtonian flow the yield stress, Y, can be estimated from a best fit of  $d\omega/d\sigma$  vs  $\sigma$ , or by graphical means at  $d\omega/d\sigma = 0$ . Following this procedure for each set of data, the mean yield stress values shown in the third column of Table II were obtained. Also shown are the standard deviations about each mean.

The yield stresses estimated by both approaches appear to be in reasonable agreement with each other, although this may be fortuitous since the Reiner-Rivlin model is based on Newtonian flow. There does appear to be a consistent increase, as would be expected, in the yield value with gum thickener concentration as shown in Figure 17.

### 2.5.3 Recoverable Shear

The recoverable shear of these Phos-Chek formulations also appear to vary with shear rate by a power law. This conclusion is based primarily on the observed elastic behavior of the standard Phos-Chek XA fire retardant formulation which has been investigated over several orders of magnitude by capillary viscometry<sup>3</sup> as well as by rotational viscometry<sup>4</sup> (see Figure 13). It was also observed that by the omission of the elasticity data obtained under those conditions whereby gap flow occurs, power law behavior also appears to exist in the other formulations (see Figure 18). The fact that the data in the non-linear shear rate regimes can be made to fall on the estimated best fit line when corrections are made for the estimated changes in gap size caused by plug flow provides a degree of confidence to the data treatment.

When these data are compared with each other an interesting observation is made. As shown in Figure 18 and Table III the recoverable shear at low shear rates decrease with decreasing Guar gum thickener concentration between relative thickener concentrations of 2 and 1. Below relative concentrations of 1 (i.e., relative to the gum concentration in Phos-Chek XA), a reversal occurs and the recoverable shear increases with decreasing gum thickener concentration. From the least square fits of

$$s = c\dot{S}^m \quad (14)$$

this effect is reflected in the values of the coefficient  $c$ , as shown in Table III. Also, it is observed that as the gum thickener concentration increases, the recoverable shear becomes less sensitive to shear rate. This effect is reflected by the decrease in the power term,  $m$ , with concentration.

The mechanical elastic response of the Rotovisco attachment is dependent on the shear stress set up in the fluid by the rotating bob. As the shear stress is increased, the average elastic deformation of the polymer chains increases and consequently the elastic relaxation increases when the shearing is terminated. However, as the gum concentration increases, the average polymer unit length and molecular aggregate volume may decrease because of coulombic and van-der Waals forces, and intra- and intermolecular hydrogen bonding. There could be a corresponding increase in the energy required for unit deformation which could be responsible for the decreasing sensitivity of elastic strain with shear rate as the gum concentration increases.

#### 2.5.3.1 Validity of the Data

Although the elastic strength of the sheared solutions appears to undergo a reversal as the relative gum concentration is increased from 0.42 to 1.0 (the reversal concentration), and then to 2.0, it should be noted



o - mean values  
 [ ] - ( $\pm$ ) standard deviation

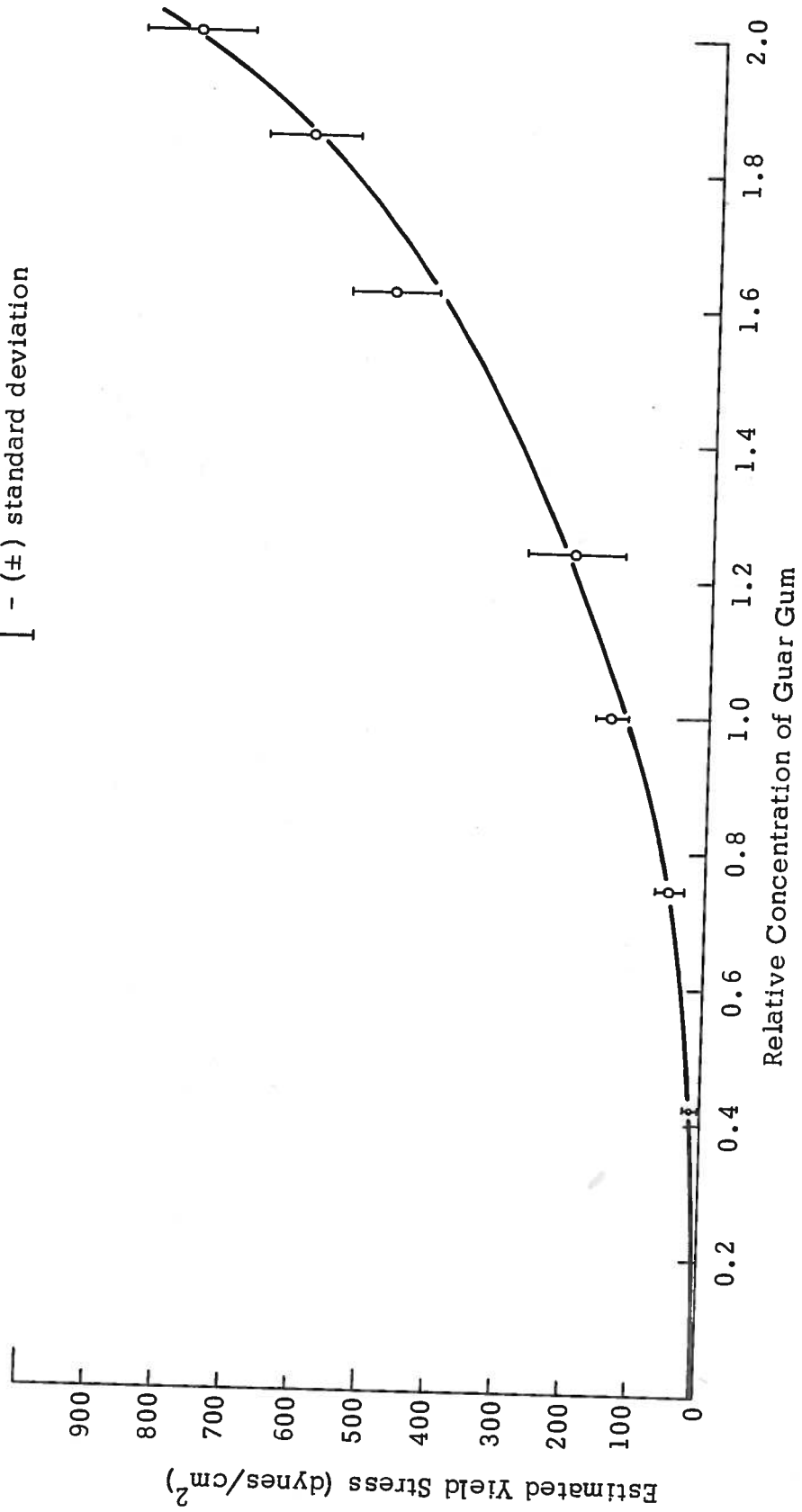


Figure 17. Estimated Yield Stresses of Phos-Chek Formulations According to the Reiner-Rivlin Model for a Bingham Body as a Function of Guar Gum Concentration.

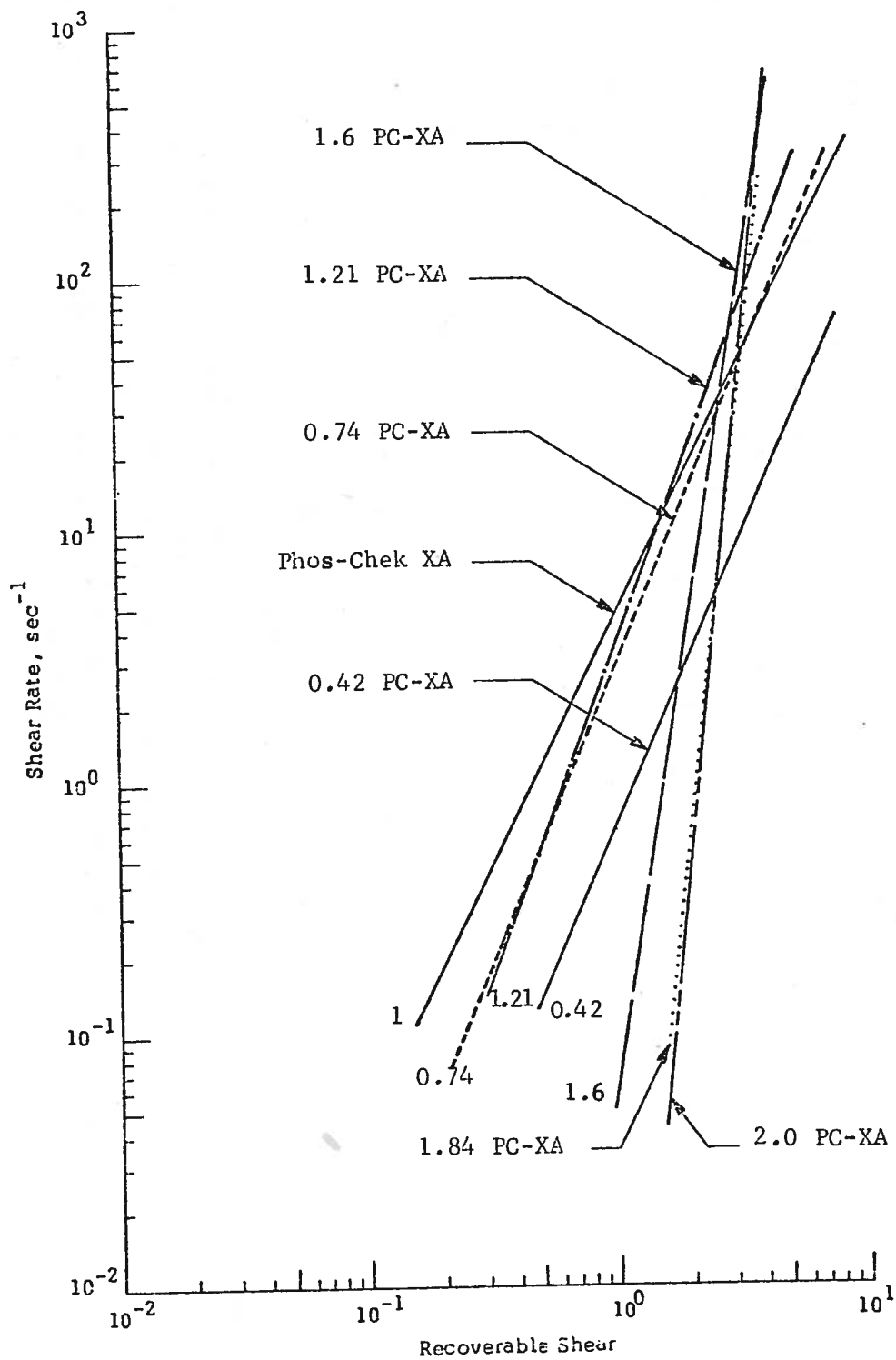


Figure 18. Recoverable Shear versus Shear Rate for Phos-Chek XA, Special Phos-Chek Formulations 9333 and 263 and Mixtures of the Special Formulations.

TABLE III. POWER LAW PARAMETERS ESTIMATED FOR THE VARIATION OF ELASTIC RECOVERABLE SHEAR WITH SHEAR RATE FOR SPECIAL FORMULATIONS OF PHOS-CHEK

Mixture Ratio of Special Formulations 263 and 9333 (ratio of parts)	Relative Concentration of Guar Gum Thickener	Parameters of Power Law Equations $s = c\dot{S}^m$	
		c (dimensionless)	m
1:0	0.42	1.11	0.45
4:1	0.74	0.61	0.43
Phos-Chek XA (or 1.72:1)	1.00	0.49	0.50
1:1	1.21	0.62	0.38
1:3	1.60	1.51	0.16
1:4	1.84	2.07	0.14
0:1	2.00	2.15	0.10

that most of the curves given in Figure 18 are based on a large linear extrapolation of curves based on only a decade or so of experimental data. Only the curve for standard Phos-Chek XA which was studied by the high pressure capillary technique<sup>3</sup> as well as the Rotoviscometer<sup>4</sup> is based on adequate experimental data and can be considered to be completely reliable. As discussed previously, the data obtained by the Rotoviscometer has a very narrow range because it is limited by plug flow at low shear rates and the response time ( $\sim 0.1$  sec) of the instrument at higher shear rates.

It is thus not possible at this time to assess the general validity of the curves shown in Figure 18 (with the exception of standard Phos-Chek). It should also be noted that the 0.42 concentration solution curve runs essentially parallel with the Phos-Chek XA curve, and is thus somewhat out of line with the other solutions studied (the other solutions may be out of line with Phos-Chek XA and the 0.42 solution). The uncertainty is of some importance however, since the recoverable shear data has a significant effect on the effective viscosity curves which help control droplet size (Section 5).

#### 2.5.4 Estimated Effective Viscosity

The effective viscosities of the preceding formulations were estimated as a function of shear rate using Eqn. (1) and incorporating the power law relationships obtained experimentally for  $\eta(\dot{S})$  and  $s(\dot{S})$ . These estimates are summarized in Figure 19 and Table IV.

The apparent viscosities of these retardant fluids (see Figure 9) showed consistent variations with guar gum concentrations at shear rate between about 1 and  $4(10^3)\text{sec}^{-1}$ . As the gum thickener concentration

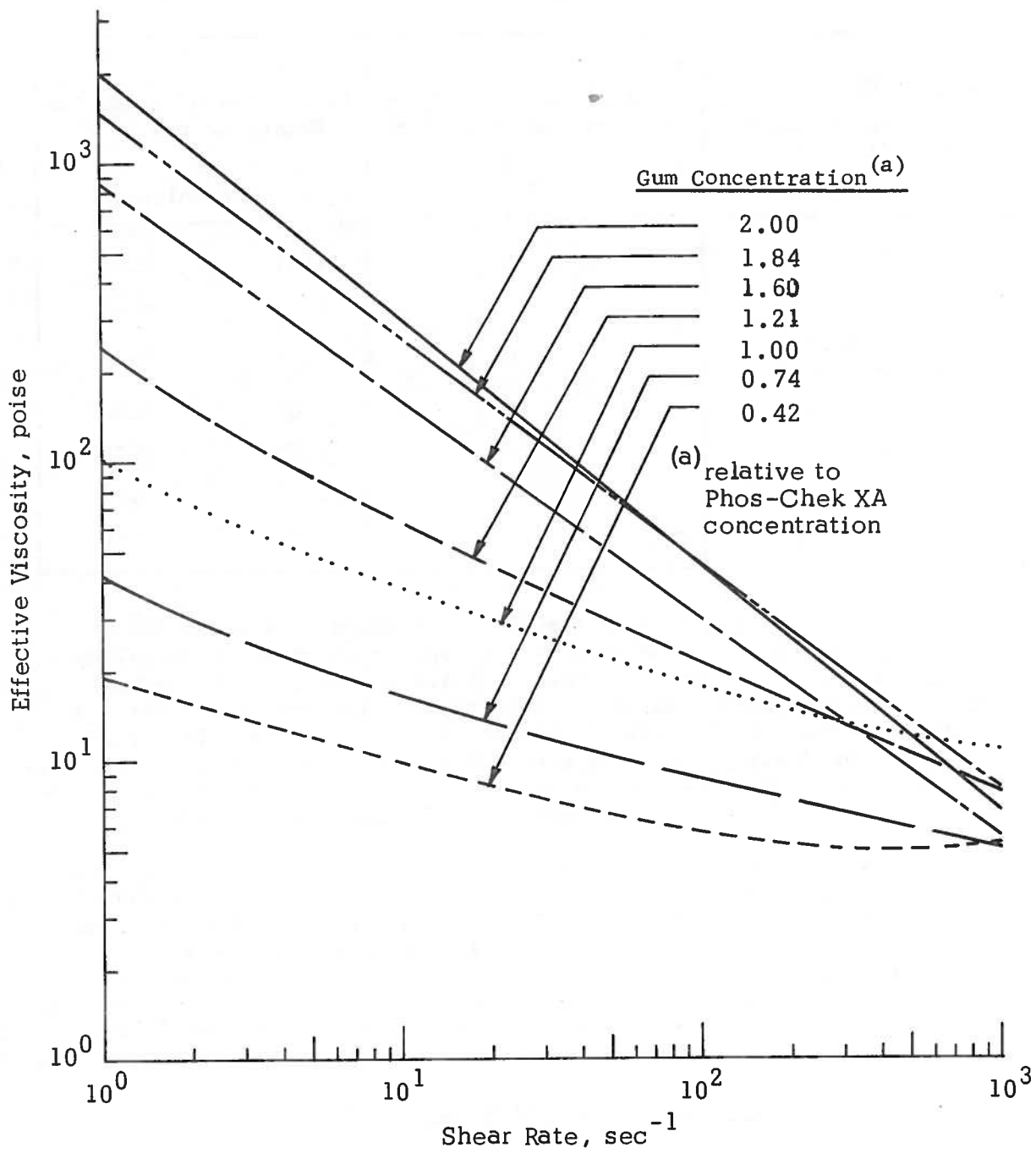


Figure 19. Estimated Effective Viscosity,  $\eta_e$ , as a Function of Shear Rate and Guar Gum Concentration in Phos-Chek XA Formulations.

TABLE IV. ESTIMATED EFFECTIVE VISCOSITIES OF PHOS-CHEK FIRE RETARDANTS CONTAINING VARIOUS GUAR GUM CONCENTRATIONS

Relative Guar Gum Concentration	Brookfield 10 min-Viscosity (poise)	Estimated Effective Viscosity, $\eta_e^*$ (poise)
0.42	2.63	$\eta(\dot{S}) (1 + 1.11\dot{S}^{0.45})$
0.74	8.50	$24.8\dot{S}^{-0.60} (1 + 0.61\dot{S}^{0.43})$
1.00 (Phos-Chek XA)	16.03	$67.8\dot{S}^{-0.67} (1 + 0.49\dot{S}^{0.50})$
1.21	27.20	$149\dot{S}^{-0.76} (1 + 0.62\dot{S}^{0.38})$
1.60	48.11	$335\dot{S}^{-0.84} (1 + 1.51\dot{S}^{0.16})$
1.84	63.80	$478\dot{S}^{-0.86} (1 + 2.07\dot{S}^{0.14})$
2.00	93.33	$650\dot{S}^{-0.90} (1 + 2.15\dot{S}^{0.10})$

\* For the 0.42 Phos-Chek formulation, a quadratic expression is used to express  $\eta(\dot{S})$ , as given in Table I, i.e.,  $\eta(\dot{S}) = \sigma/\dot{S}$ , where  $\sigma$  is given in the footnote.

increases the apparent viscosity increases. However, as shear rate increases the relative differences in apparent viscosity with gum concentration decreases.

The effective viscosities of these fluids follow this same general trend at low shear rates. However, Figure 19 shows that as the shear rate,  $\dot{S}$ , is increased the difference in the values of the various fluids decreases. In the  $\dot{S}$  range of  $10^2 - 10^3 \text{sec}^{-1}$  there is a crossing of the  $\eta_e$  vs  $\dot{S}$  curves, such that the fluids having the higher  $\eta_e$  at low  $\dot{S}$  have the lower  $\eta_e$  at high  $\dot{S}$ . However, the standard XA fluid decreases with increasing  $\dot{S}$  in a manner as to make its value larger than any of the fluids at  $\dot{S}$  greater than about  $600 \text{sec}^{-1}$ . In general, as with the apparent viscosity results it appears that at high shear rates, i.e.,  $>10^3 \text{sec}^{-1}$ , the effective viscosity of the Phos-Chek XA becomes less sensitive or possibly completely insensitive to gum thickener concentration.

The reason for the crossing behavior of the curves at high shear rate is not understood, but it arises from the elastic strain behavior (Figure 18) since the apparent viscosity curves of the various formulations decrease monotonically with decreasing gum concentration and increasing shear rate (Figure 9). The crossing behavior may possibly not be real but rather arise as the result of the data treatment, as noted previously. However, the effective viscosity curve of the standard XA fluid is believed to be

completely correct since the elasticity data obtained at low shear rates using the Rotoviscometer were consistent with- and extrapolated to in a direct fashion - the data obtained at high shear rates using the high pressure capillary tube technique.<sup>4</sup> It is of interest to note that the XA (1.00) formulation and the 0.42 XA formulation appear to parallel each other at high shear rate. It is possible that a similar monotonic limiting behavior exists for the other formulations.

The general behavior of the effective viscosity vs shear rate of the various formulations at high shear rates (Figure 19) was unexpected, i.e., the effective viscosity of the formulations does not increase monotonically with increase in gum thickener concentration (the curves cross). This behavior results because of the non-monotonic behavior of the elastic strain (recoverable shear) of the fluids with shear rate (Figure 18), even though the general behavior of apparent viscosity vs shear rate is normal (Figure 9). This behavior, if real, has certain implications regarding the droplet sizes that would be produced by the aerodynamic breakup of the fluids, and this will be considered later (see Section 5).

As discussed before, the measurements of apparent viscosity and recoverable shear for the standard XA formulation made from the special formulations used in this study were in essential agreement with previous measurements.<sup>3,4</sup> However, the elastic strain (recoverable shear) data was treated in a slightly different manner so as to better take into account, geometric effects of the gap in the measuring head. The result is that  $\eta_e$  of the standard Phos-Chek XA formulation given in Figure 19 is slightly higher at low shear rates than that given in ref. 4, but at high shear rates ( $10^3 \text{ sec}^{-1}$ ) is essentially unaltered.

## 2.6 SURFACE TENSION MEASUREMENTS

Measurements of the surface tension of the special Phos-Chek XA formulations were made at 20°C using a Fisher Surface Tensiometer, Model 120. This tensiometer consists of a du Noüy Torsion balance and a platinum-iridium ring. Conventional procedures were followed in making these measurements.<sup>3</sup> The platinum-iridium ring was cleaned between measurements by rinsing in clean water and heated in the oxidizing portion of a propane gas flame.

The fire retardant mixtures were prepared as described previously. After the samples were prepared they were conditioned at 17-19°C, placed in a 60 cm- diameter glass petri dish, and the surface tension, then measured. The measurements were made when the samples reached approximately 20°C. Attempts were made to minimize the effects of entrapped air bubbles by prolonging the storage time. However, all of the measurements were completed less than 24 hours after the mixtures were prepared.

Unlike water, the fracture of the distended fire retardant surface film, attached to the platinum-iridium ring by the upward pull exerted by the torsion balance was found to be time dependent (i.e., fracture occurs over a time duration of several seconds whereas with water fracture occurs within a second after the upward force is made to just exceed the downward surface tension). During the time period required for the film to break, changes in the film concentration probably occur. In order to minimize the uncertainty and inconsistency in the surface tension measurements resulting from this

time dependency, the scale reading on the tensiometer was taken at the onset of the irreversible elongation of the distended film. Also, each measurement was made as rapidly as possible, within approximately one minute.

The difference between the theoretical and experimental ring calibration was determined to be 0.47 percent. Each measurement of apparent surface tension was corrected for the radius and circumference of the Pt-Ir ring and the density of the fluid (the density of the special Phos-Chek XA formulations was estimated to be 1.06 gm/cc). The data are shown in Table V and Figure 20 (the assumed line is not a statistical fit of the data).

TABLE V. MEASURED SURFACE TENSIONS OF THE SPECIAL PHOS-CHEK XA FORMULATIONS AT 20°C

Relative Guar Gum Concentration	Surface Tension* (dynes/cm)
0.00 (water)	72.8
0.42	33.4
0.74	42.5
1.00 (Phos-Chek XA)	41.2
1.21	44.3
1.60	59.9

\* Relative to handbook value of surface tension of water at 20°C, corrected for density, and instrument.

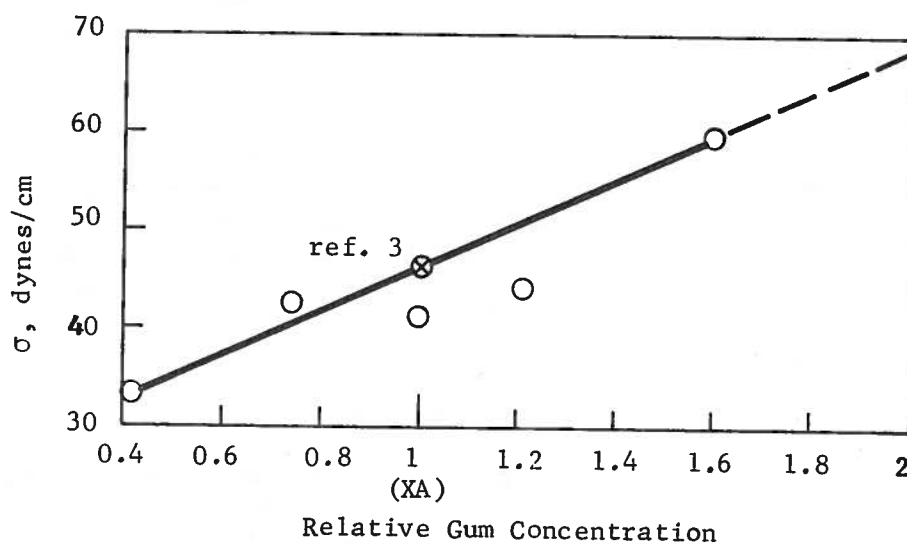


Figure 20. Surface Tension of the Phos-Chek XA Solutions as a Function of Gum Thickener Concentration.

Each surface tension value is an average of at least three determinations. The average deviation was estimated to be 2%. The surface tension for standard Phos-Chek XA (41.2 dynes/cm) is slightly lower than the value (46.3) previously found.<sup>3</sup> However, the earlier value appears to be more consistent with the general trend of the data, as shown in Figure 20. It was not possible to obtain experimental values of surface tension for the solutions with a relative gum concentration greater than 1.6, but their values can be obtained by extrapolation of the data shown in Figure 20.

### 3. EXPERIMENTAL FIELD TEST PROCEDURES

On the basis of the results of the rheological measurements and analysis regarding estimates of droplet size and other factors relating to the aerial dissemination of fluids, recommendations were made to the Forest Service for drop tests that should be conducted to determine the effects of fluid rheology on liquid retardant dissemination, and evaluate the general validity of the previously developed liquid breakup models. Imposed on these recommendations were of course the practical constraints of time and funding limitations. Most of these recommendations were eventually carried out, and this section summarizes the various test factors and procedures that were used to conduct the tests and determine the droplet sizes and ground contour patterns of the disseminated retardants.

#### 3.1 FIELD TEST CONDITIONS

The droplet measurement tests were conducted as part of a series of field tests that were carried out by the Honeywell Corporation and U. S. Forest Service at Chico, California during an experimental tank and gating system (ETAGS) study. Shock's field measurements were carried out during November and December, 1975.

##### 3.1.1 Test Grid and Ground Contour Pattern

The liquid retardants were dropped from a P2V-5F Neptune aircraft on to a Forest Service test grid which ran in the south-to-north direction adjacent to the Chico airport runway. This grid was 1240 ft long and 380 ft wide, but not all the grid was required for the rheology tests. The grid was numbered both lengthwise and crosswise, which defined small rectangular areas within the overall grid pattern. The ground concentration profiles of the disseminated liquid were determined for each test by the Forest Service, who used plastic containers in the center of each grid rectangle to sample the localized weight of retardant rain produced as the result of the dissemination process. The sampling procedure appeared similar to that discussed in ref. 1. Computer techniques were used to reduce the data and generate ground contour concentration patterns. The patterns produced by the various fluids used in the fluid rheology tests were supplied to Shock, and will be discussed later.

##### 3.1.2 Test Tank and Gating System

The tank used to hold the liquid on the aircraft was the experimental tank designed by Honeywell for the ETAGS study. It was made up of several individual compartments with various length to width ratios, and having individual doors. Only one of the compartments (Compartment No. 5)



was used in the rheology tests in order that any difference in test results between the different retardants be due to retardant rheology only, and not due in part to the use of different tanks. According to descriptive drawings supplied by the Forest Service, Compartment No. 5 was located in the middle of the entire compartmented tank, and was 59 inches long, 32 inches wide and 64 inches deep. This compartment carried a load of 460 gallons of retardant in all of the rheology tests (see Figure 21a).

An important consideration in the selection of this compartment was its moderate length to width ratio ( $L/W \approx 2$ ). It was previously shown<sup>4</sup> that the terminal droplet size of the retardant should in principle be relatively insensitive to the aircraft tank (or compartment) dimensions except for very large (single) tank volumes, or tanks with large length/width or width/length ratios. Since it was desirable that the tests be conducted under conditions that the tank dimensions do not have an abnormal effect on the droplet size, Compartment 5 seemed appropriate for the studies. Moreover the dimensions of this compartment are typical of some of the tanks or compartments that are currently in use. Hence, the results obtained with this compartment should also be indicative, for example, of the droplet sizes produced by the individual tanks or compartments of the CL-215, DC-6B, PB4Y2 and C-119 aircraft.

In the use of this compartment to contain the liquid, both doors (2 and 3) of the compartment were opened simultaneously. The door opening time (1.3 sec) was held constant for all the rheology tests (door rate 6). The approximate flow rate curve of the retardant from the compartment under this condition is shown in Figure 21b.\*

### 3.1.3 Aircraft Speed, Drop Height and Wind

In order to most clearly show the effects of fluid rheology on the dissemination characteristics of the various retardants, the liquids were all dropped near a preselected aircraft speed of 130 knots, except for one test with Phos-Chek XA which was also dropped near 180 knots to help elucidate the effect of aircraft speed on the dissemination process. Likewise the liquids were all dropped near a preselected drop height of 300 ft. This height was chosen on the basis that the retardant should be dropped at an altitude that is sufficiently high to (1) ensure the complete breakup of the liquid, (2) prevent damaging liquid impact with the ground, (3) remove most of the forward motion of the droplets so that they fall essentially straight down (neglecting wind effects), and (4) help prevent excessive ground concentration so as to not overload the droplet impact samplers on the ground. On the other hand the drop altitude should not be high enough that droplet evaporation becomes of special significance.

The actual aircraft speed and altitude at which the liquids were dropped in the individual tests usually differed slightly from the preselected values. The actual values are given in the figures that show the measured droplet sizes in the various regions of the ground pattern (Figures 30-44). Although it was desirable for the tests to be conducted under negligible wind conditions, this was not generally possible for practical reasons. The actual magnitude of the wind and its direction are also given in the preceding figures for the various tests.

---

\* This curve is based on data supplied by Mr. Damon Swanson of the Honeywell Corporation.

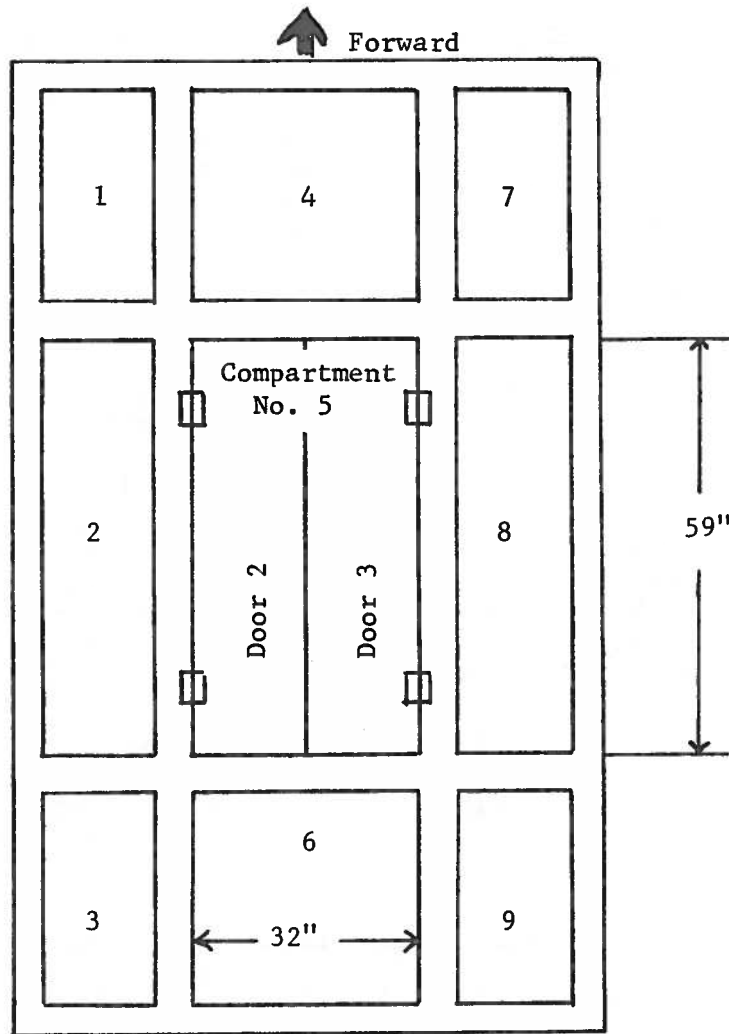


Figure 21a. Bottom View of the Experimental Tank. The Studies Were Conducted Using Compartment No. 5, Which Carried a Load of 460 Gallons of Retardant. Doors 2 and 3 Were Opened Simultaneously During the Drop (Door Rate 6).

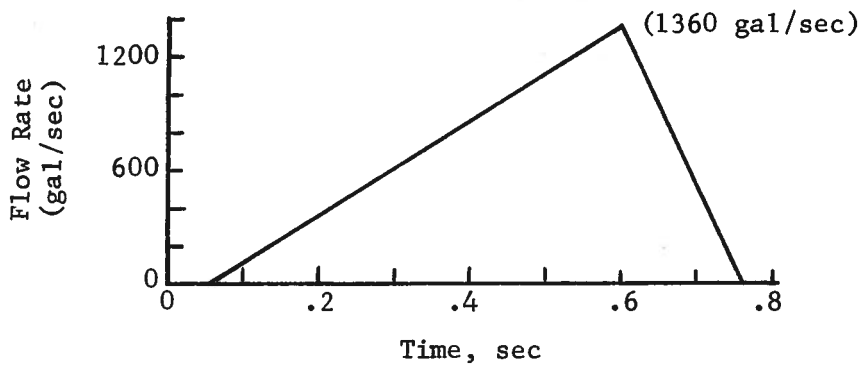


Figure 21b. Approximate Flow Rate of Retardant From Compartment No. 5, Door Rate 6.

### 3.1.4 Retardants and Test Matrix

As noted previously, the tests were conducted on Phos-Chek XA solutions with three different concentrations of gum thickener, viz., 0.42 Phos-Chek XA, Phos-Chek XA, and 1.6 Phos-Chek XA (the numbers 0.42 and 1.6 represent the gum thickener concentration relative to that used in standard Phos-Chek XA), and on Fire-Trol 100, Fire-Trol 931 and water. A small quantity (about a quart) of red paint pigment was added to the water to give it a slightly pink color which assisted in the droplet size measurements of this fluid.

The program called for one successful test on each of the preceding liquids and on the 180 knot drop, i.e., for a minimum of seven drop tests. However, more than triple this number of tests were eventually conducted, although not all the droplet size sensors were employed on all the tests and the drop location was wrong (with respect to the sensors) in several of the tests so that no data was obtained in these tests.

### 3.2 MEASUREMENT OF TERMINAL DROPLET SIZE

The droplet sizes of the rain produced by the aerial dissemination of the liquid retardants were measured by both dynamic and passive techniques, consisting of a high speed camera, three relatively large (~ 4 ft diam.) rotating impact samplers and 29 impact sampler cards (~ 1 ft square). These sensors were located at various fixed positions on the test grid, but one rotating impact sampler was located adjacent (just downstream) to the camera so that their results could be compared. The locations of the sensors were based on the ground concentration pattern produced by an earlier run (drop test No. 38) in which Phos-Chek XA was dropped at 130 knots speed and 300 ft altitude from the No. 5 compartment at door rate 6 (the test conditions). The plot of the pattern produced was displaced slightly so that the center line of the profile was located on the center (21) line of the grid in the crosswise direction. The camera and number 2 rotating impact sampler were then positioned in the center of the heavy concentration region (2 gallons per hundred square feet, designated 2 g/c), which corresponded to the middle of the intersection of the 27/28 lines lengthwise and the 21 line crosswise. The number 1 sampler was displaced to the left slightly and moved upstream to the middle of the intersection of the 24/25 lines lengthwise and the 19 line crosswise, and the number 3 rotating sampler was moved to the right slightly downstream to the 29/30 (lengthwise) and 23 (crosswise) line position.

The 29 impact cards were located at various positions on the fringe and outside of the 1 g/c concentration profile as well as some distance upstream to the middle of this profile. The actual positions were:  
1 (10/11-22), 2 (12/13-16), 3 (12/13-25), 4 (15/16-17), 5 (15/16-13),  
6 (15/16-25), 7 (18/19-13), 8 (18/19-22), 9 (18/19-29), 10 (21/22-10),  
11 (21/22-22), 12 (21/22-30), 13 (23/24-10), 14 (23/24-28), 15 (25/26-9),  
16 (25/26-11), 17 (25/26-29), 18 (25/26-32), 19 (26/27-10), 20 (26/27-31),  
21 (28/29-10), 22 (28/29-32), 23 (29/30-10), 24 (29/30-33), 25 (30/31-33),  
26 (31/32-12), 27(31/32-31), 28 (32/33-30), 29 (33/34-29), where the first pair of numbers indicate the lines in the lengthwise direction between which the samplers were located, and the second number indicates the line in the crosswise direction. Figure 22 shows the location of the camera, the rotating impact samplers and the impact sampler cards in the test grid.

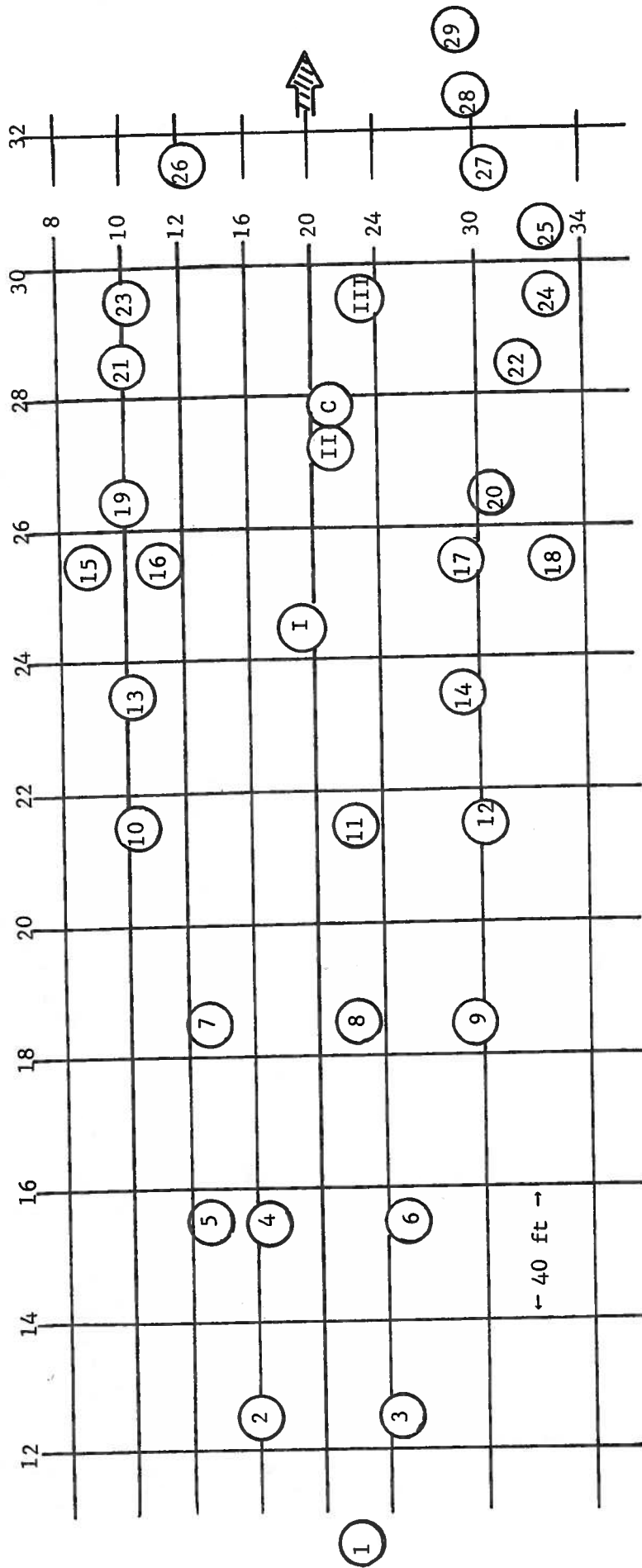


Figure 22. Location of the Camera (C), the Three Rotating Impact Samplers (I, II, III), and the Impact Sampler Cards (circled numbers) in the Test Grid.

The arrangement of the various samplers on the grid was based on the desirability of obtaining detailed information on droplet size at various locations within the higher concentration region of the ground pattern, as well as some subsidiary information outside and upstream of the heavy pattern. However, the information that was actually obtained depended on where the droplets produced by the drop landed with respect to the various sensors. The experimental ground concentration of liquid produced by the falling droplets with respect to the sensors for the various tests are shown in the figures giving droplet size vs ground concentration (Figures 30-44). Generally speaking, reasonable success was attained in the experimental location of the ground pattern produced by the drops with respect to the locations of the sensors.

### 3.2.1 High Speed Photography

The dynamic technique used to measure the sizes of the retardant rain droplets consisted of a high speed camera with telephoto lens which photographed the droplets as they fell in front of a calibrated grid located at some distance from the camera. The general technique was based on the preliminary work and recommendations of the Aerospace Corporation.<sup>5</sup> Prior to the selection of the optical equipment actually used, a significant amount of effort was expended to examine or actually test various possible methods of obtaining the desired data. The possible options included motorized 35mm cameras (Nikon F, Canon F-1, Olympus OM-1MD, Topcon 8000-Supreme 1), regular 16mm cameras of high quality (Beaulieu R16, Bolex H-16EBM) and high speed 16mm cameras (Mitchell HS-16F2, Photo-sonics 16mm-1B, Hycam 41-0004, Fastax WF3). The potential use of special telephoto lenses was also investigated, including Questar 3½ and 7, Celestron 5 and 8, as well as regular telephoto lenses.

A consideration of all the factors involved, including cost and availability, led to the use of a Fastax WF3 camera equipped with a 200mm F/3.2 lens. The camera was situated at the end of a 40 ft long tunnel (Figure 23) fabricated from plastic sheet over a light steel frame, focusing on a region just in front of a 2x2 ft white plastic screen with black tape 2x1 inch grid lines. The tunnel was perpendicular to the south-to-north running test grid, and located on the east side of the grid with the camera pointing west. The depth of the camera field varied from 2 to 3 ft in the tests. In this manner, the image size of the photographed droplets was not severely affected by ambiguous parallax induced errors depending on the droplet location in the field depth.

The camera was powered by a DC power supply with a no-load output of 18.5 VDC. The power supply was switched on manually together with the rotating impact samplers (see Figure 25). The camera speed was set at approximately 250 frames/sec with a 30 mil slit stop. This combination was optimum for obtaining consecutive frames fast enough to record droplet fall velocities up to 50 ft/sec, and an effective exposure time ( $\sim 4 \times 10^{-5}$  sec) that was short enough to record the individual drops but still allow a sufficiently long camera run time to generally encompass the overall settling time of the droplet cloud. Color EKTACHROME 7241 EF430 film was used in the tests. The overall film magnification was approximately 0.02.

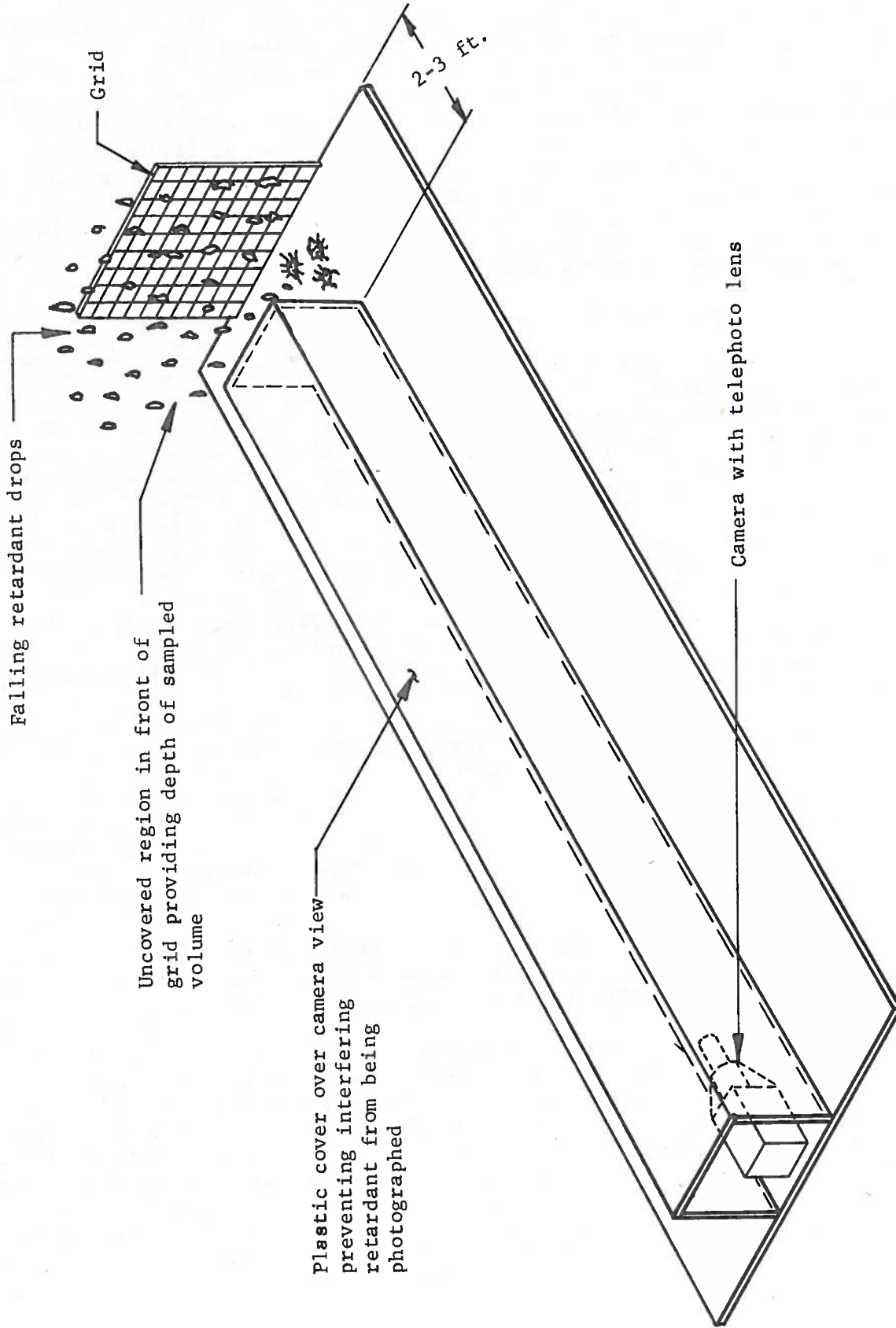


Figure 23. Schematic of the Camera System Used to Dynamically Observe the Size of the Droplets Produced by the Aerial Dissemination of Liquid Retardants During the Fallout Process.

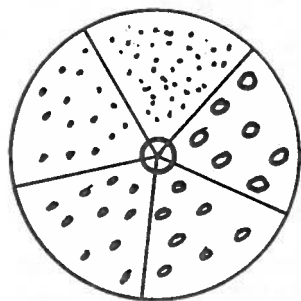
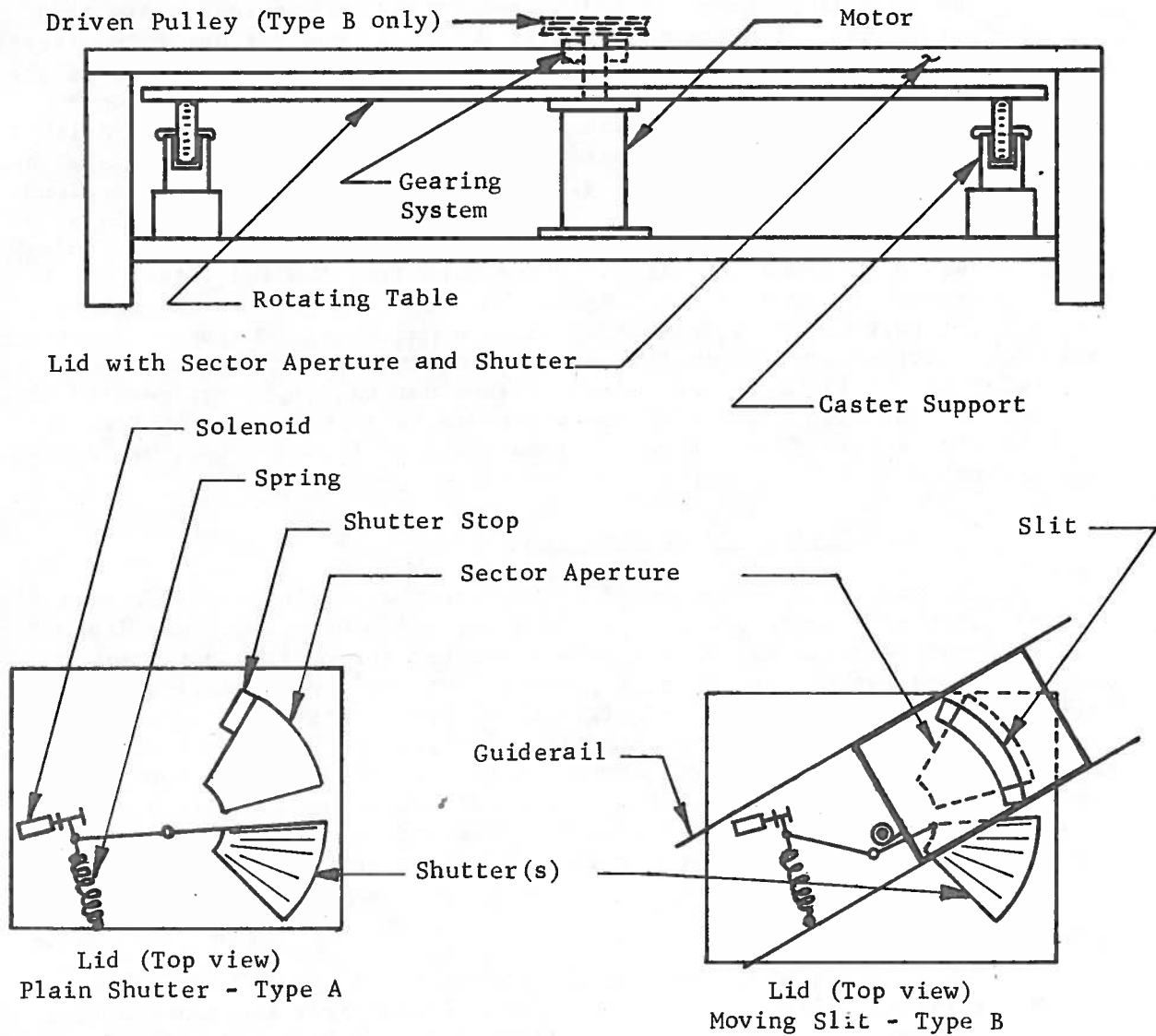
The general performance of the camera system was reasonably good, but the results suggest certain potential modifications for any future tests. Generally speaking the main difficulties encountered were the result of the field conditions including (1) inaccuracy in the position of the drop so that few in any droplets fell in the field view of the camera, (2) variable overcast (or evening) lighting conditions which sometimes provided less than optimum light, and (3) significant wind interaction with the droplet cloud which in some cases for some fluids (Fire-Trol 100) caused the droplets to fall at an angle and coat the grid with liquid which destroyed the viewing area. It was also found (particularly for Fire-Trol 100 and water), that the droplets appear more distinct against a dark (the grid lines) rather than a light background under some lighting conditions. The use of a darker background with strong external lighting (side and front) may thus be preferable to the light background color (and natural lighting) used in the studies. It was also found that for water and to some extent the Fire-Trol liquids, that a larger magnification (and smaller field of view) would have been desirable.

### 3.2.2 Rotating Impact Samplers

The passive technique used to measure the droplet sizes consisted of flat cardboard samplers which provided a surface upon which the individual falling droplets could impact and give a splotch (or splash) pattern whose size was a measure of the spherical diameter of the impacting droplet that could be obtained from suitable calibration experiments. In order to avoid oversaturation in the high concentration (1-2 g/c) region of the ground pattern, three specially built rotating impactor samplers were designed and fabricated for use in this portion of the pattern. These samplers rotated in a manner that the individual splash patterns produced on the sampler by the retardant rain droplets at any instant were continually covered and thus protected from exposure to further droplet impact during the subsequent settling of the droplet cloud.

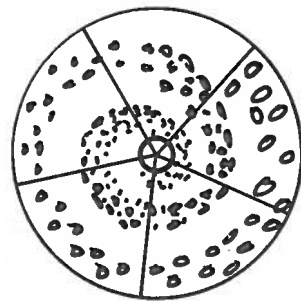
The rotating samplers were configured as an approximately 4 ft diameter rotating collector (sampler) table covered by a lid panel with a 45° sector cutout through which the falling droplets impacted with the sampler table (see Figure 24). The sector cutout was closed by a spring-loaded, solenoid-actuated metal shutter. The whole assembly was fabricated as a sturdy flat box-like structure on skids, containing the integral motor and electrical circuits. Two of the rotating samplers (No. 1 and 3) used in the field utilized a uniform sector aperture, whose shutter was closed after one revolution of the sampler table. The sector aperture of the other sampler (No. 2, located adjacent to the camera) was fitted with an additional 4 inch wide curved slit which moved slowly radially inward by means of a pulley drive to give a spiral drop pattern on the rotating collector table. The shutter was closed after approximately 4 revolutions. The dimensions were chosen to minimize the droplet splatter on the collimating edges. The mechanism was covered on the top and sides as much as possible for protection from the dropped retardants.

The power for the samplers was provided by a set of 12 volt storage batteries that activated the collector table motor when a relay was switched on at the same time as the camera circuit was activated, Figure 25.



A - Uniform Pattern

Time Resolved  
Exposed Sampler  
Area



B - Spiral Pattern

Figure 24. Rotating Impact Sampler Schemes Used to Prevent Overloading of Target and Provides Time Resolution of the Droplet Sizes.



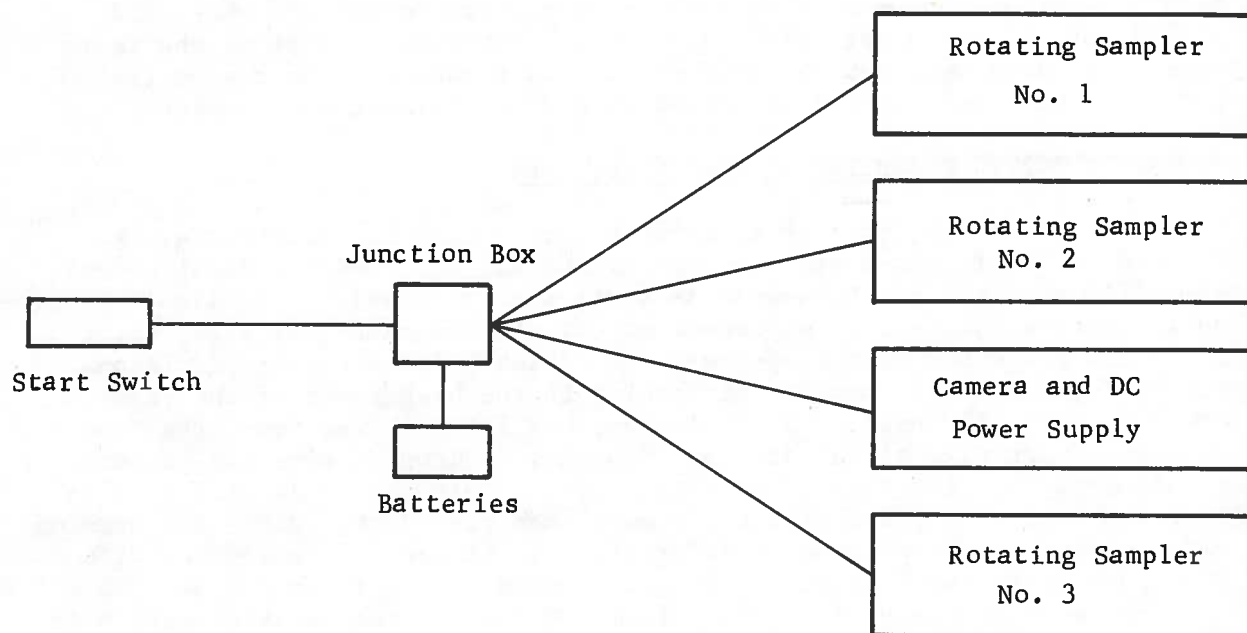


Figure 25. Schematic of the Camera and Rotating Sampler Controls.

The circuit was activated manually by an operator prior to the time that the first falling droplets reached the ground. The speed of rotation of the collector table could be varied by means of a rheostat in the power circuit from about 7 to 32 seconds per revolution. However, in the field tests it proved convenient to utilize speeds of only about 7-10 sec/rev. The drops were collected on the glossy side of five sector-shaped sheets of white Mead Mark 1 cover paper about 18 inches wide that were taped to the rotating table. This paper is essentially the same as Printflex cardboard paper and is of 10 pt. weight. One side of the paper is glossy, and the other side has a matte finish. The paper is similar to that used by the Forest Service in their studies of droplet impact. The circular sheet assembly was dried on flat masonite racks after the tests.

In general the rotating samplers worked as designed and gave good results. However, in a small number of cases, some overloading of localized regions of some of the samplers occurred, and this may have been due in part to wind conditions. There were also instances when the shutters did not close properly. After the tests the rotating samplers were turned over to the Forest Service as government property.

### 3.2.3 Impact Sampler Cards

The 29 impact sampler cards were used to sample the droplet sizes in various regions of the ground pattern where (for an idealized ground hit) the droplet concentration would be sufficiently small that overloading would not occur. The sampler cards were 10x13 inches in cross-section and made from the same cardboard paper as used for the rotating samplers (glossy side up). The cards were taped flat on the top of pipe-supported masonite boards located about two feet off the ground. After a test the cards were placed horizontally in a rack for drying.

The impact cards functioned as desired and provided some information regarding droplet size in regions of the ground pattern where the liquid concentration was relatively light. However, in most of the tests splash patterns were not obtained on all the cards, for the reason that the cards were either over-saturated or did not collect any droplets.

#### 3.2.4 Reduction of the Camera Data

The films from the tests were each viewed in its entirety, and the best film of each test matrix condition was selected for data reduction (both films of the 1.6 Phos-Chek XA tests were reduced). The films were projected onto a wall screen at approximately 2:1 image-to-real size, using a medical projector with stop-frame and variable framing rate provisions. The grid pattern with known line spacing in the background of the viewed area was initially used as a calibrator, but later it was found that the apparent image size of the droplets depended on droplet size and it was consequently necessary to correct the data on this basis, as will be discussed. Each of the selected films were then viewed at a very slow framing rate to determine the frame where droplets first appear ("zero frame") and the approximate duration of the droplet shower. The latter was used to select the frames to be measured for each film. Generally the useable portion of the films lasted approximately 600 frames, with six frames chosen for measurement. This duration ( $\sim 3$  sec) was less than the total duration of the rain, but for the Phos-Chek solutions generally contained a dominant portion of the total mass. The measured duration was limited by various factors including termination of the film, difficulty in film reading due to droplet size reduction, and smearing of the grid by the falling droplets. Because the larger and more interesting droplet sizes occurred early, the frame sampling sequence used was not equilateral, but rather, more frequent at the outset.

Each measured frame was marked, and its relative number (from zero) noted. The spacing of the fiducial lines on the background grid was measured to scale all measured dimensions to true dimensions. The apparent diameter of each droplet was measured. Advancing or retreating the film by one frame enabled the measurement of the fall distance of a representative number of drops, prior to impact, which was used in the calculation of droplet impact velocity. Finally, the framing rate of the film at each measured frame was determined by measuring the on-film signature length of a timing light flashing at a known frequency and duration.

The data taken from the film consisted of a relative frame number, framing rate, droplet diameter, droplet fall distance, and scaling factor. The true droplet diameter, droplet impact velocity and details regarding droplet distribution on each frame and on cumulated frames were then computed using an electronic computer. The time placement of each frame was determined from a plot of the reciprocal of the framing rate, i.e.,  $f^{-1}$ , vs the frame number,  $f$ , since the area under this function to a particular  $f_0$  yields to time  $t_0$ . A trapezoidal approximation of the integral was used with the data to determine the times.

The major cause of uncertainty in reading the films was the large film magnification ( $\sim 100$  to 1) required to make the droplets visible. The magnification produced a loss of contrast and indistinct boundaries between

the droplets and the background, leading to an uncertainty in the measurements that was found to depend on droplet size. Furthermore, the grain in the background made the discrimination of drops with apparent diameters smaller than about 2 mm (1 mm real diameter) virtually impossible. It was thus necessary to include a correction factor,  $F$ , for the effect of apparent image size on real droplet size in the data reduction. Figure 26 shows the experimental relation between  $F$  and apparent image size,  $d_{app}$ . Real droplet diameter,  $d$ , is related to apparent image size by,  $d = Fd_{app}$ . The reference

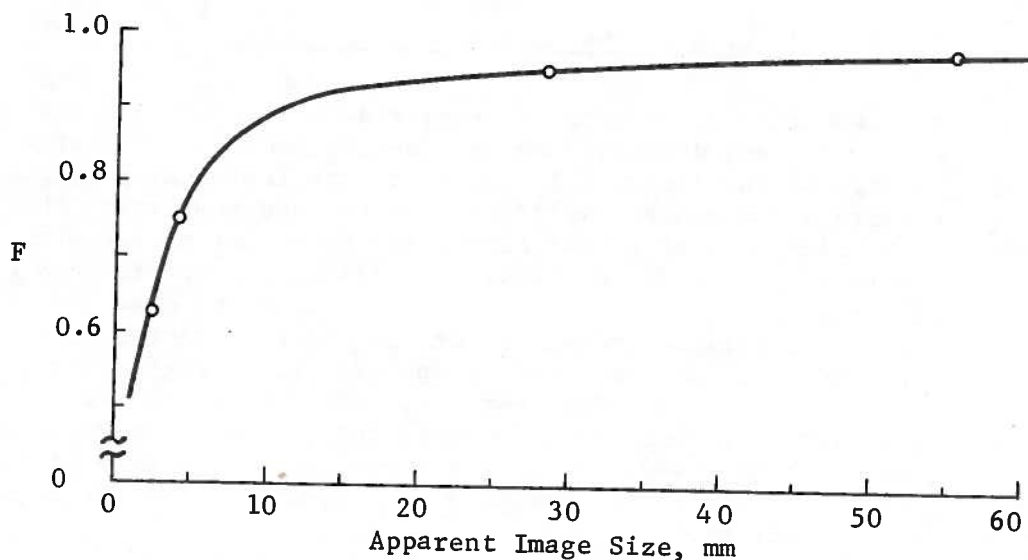


Figure 26. Experimental Correction Factor versus Apparent Image Size.

marks used in obtaining the experimental points in Figure 26 consisted of the 1.5 and 3 mm wide black tape used in making the grid lines, and the external boundaries between the 1" and 2" grid lines. It would have been desirable to have some data in the range of 7-25mm, but it was not available. Future grids for studies of this nature should contain a series of absolute calibration widths of various sizes in the region of interest. Nevertheless it is believed that the curve in Figure 26 is sufficiently reliable for the present purposes.

The films showed that the droplets were in general roughly spherical, except that the larger droplets were often flattened. There was no evidence of droplet smear due to incorrect exposure time. In some cases the droplets were roughly dumb-bell in shape or (for Phos-Chek XA) contained a ligament between two particles. Some ligaments by themselves were also sometimes present for the Phos-Chek XA solutions.

As discussed before, a large blow-up of the test film was necessary for the droplet measurements. This generally prevented the printing of satisfactory pictures that show the falling droplets in detail, except for the largest droplet retardants. It was originally planned to reduce the film data by making enlarged photographs of individual frames and measuring the droplet sizes from the photographs. This technique was not in general satisfactory however, making the screen blow-up technique necessary. Figure 27 shows a print of two film frames of the falling droplets for normal Phos-Chek XA (DN 147 - this film was not reduced). It can be seen that several of the larger droplets are flattened and appear to be possibly getting ready to undergo bag formation.

### 3.2.5 Reduction of the Impact Sampler Data

The reduction of the impact sampler data - both the rotating samplers and cards - was accomplished by visually measuring the average circular diameter of the individual droplet splash (splotch) patterns on the samplers with a transparent millimeter ruler, and converting the measured splash diameters to spherical droplet diameters using experimentally calibrated spread factor data. The latter calculations as well as those for the consequent droplet size distribution and mass mean diameter on each of the various individual and cumulated impactor sectors and cards were made with an electronic computer. In a large fraction of the cases all the individual splash patterns on the rotating sectors and cards were measured. In some cases however, only representative areas of a sector or card were measured, and in these cases, the data was weighted according to the actual measured area compared with the total covered area when necessary.

Figure 28 illustrates the general appearance of the splotch patterns produced by the impacting droplets of the various retardants on the target paper of both types of rotating impact samplers used in the tests. The general appearance of the splotches on the impactor cards was similar. The difference in the splotch patterns on the various targets are not all necessarily directly comparable, since the ground concentration of liquid was not always the same, and the data suggested (next section) larger droplet sizes for heavy ground concentration. Nevertheless the differences give a qualitative measure of the differences in the droplet sizes of the retardants, and are of some interest. The location of the samplers with respect to ground concentration is given in the next section.

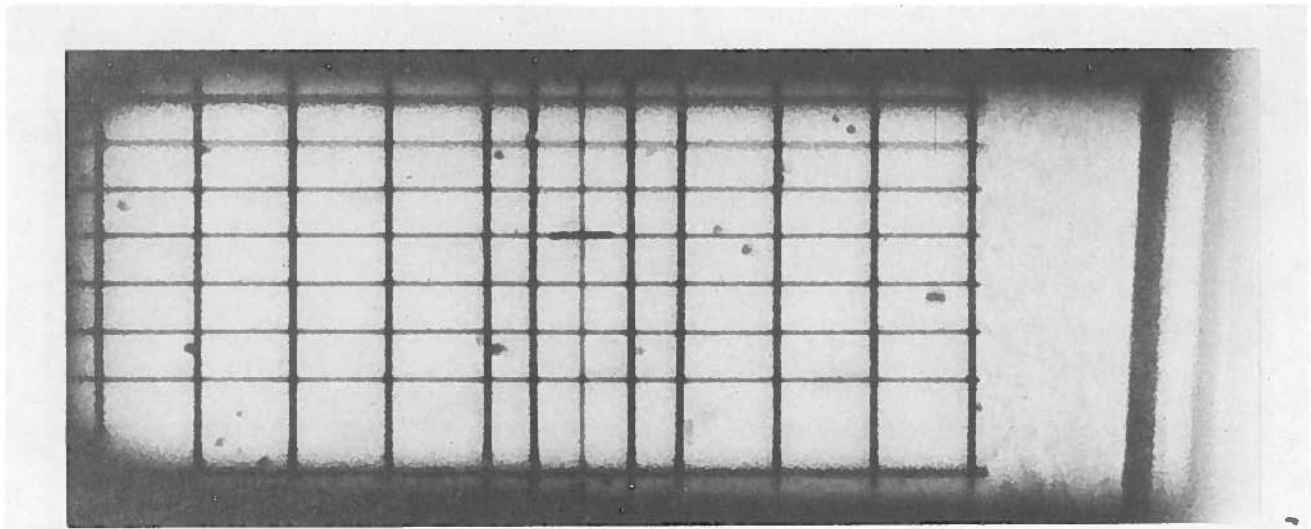
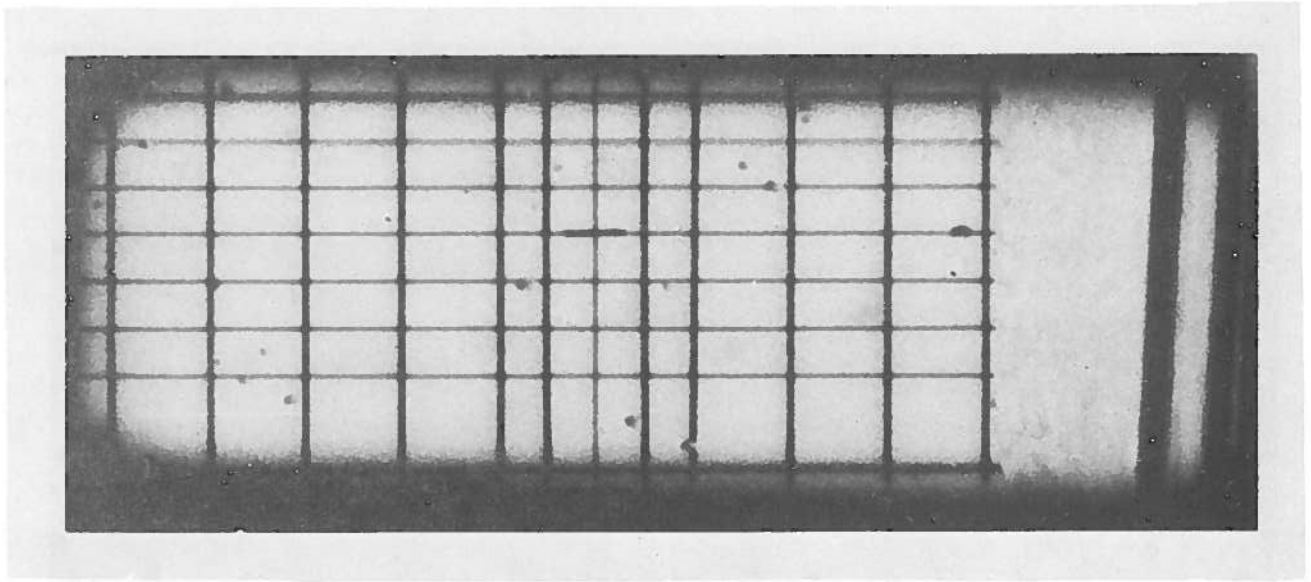
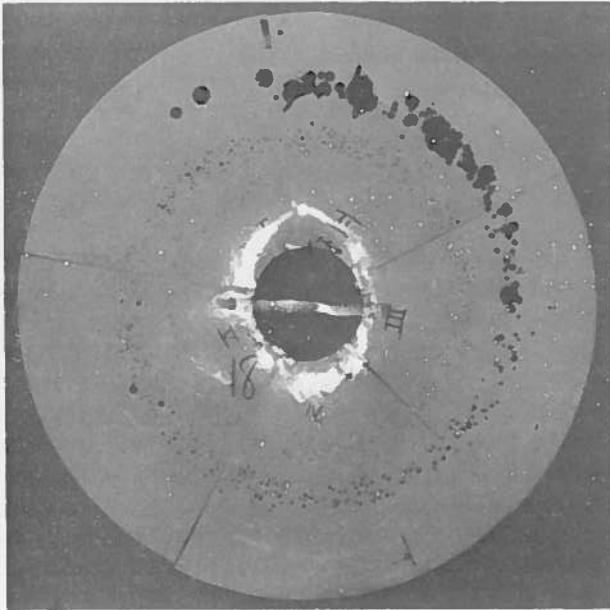
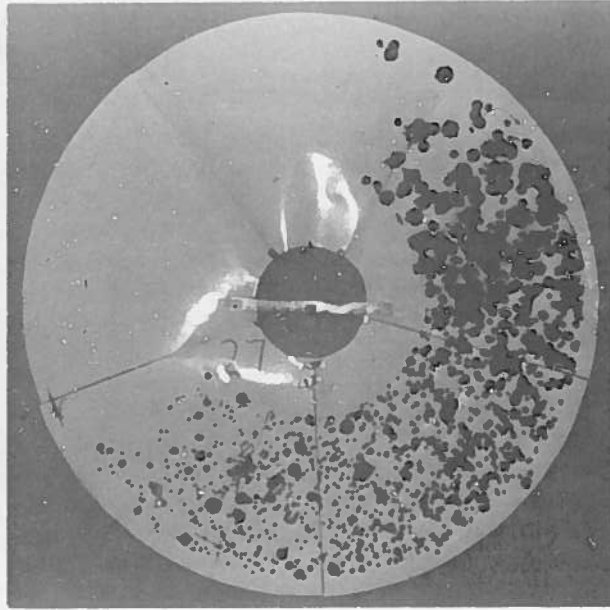


Figure 27. Two Frames of the Camera Film Obtained for Phos-Chek XA (Drop Test No. 147). Time Between Frames is 4.1 msec. Grid Spacing is 2 x 1 inch.

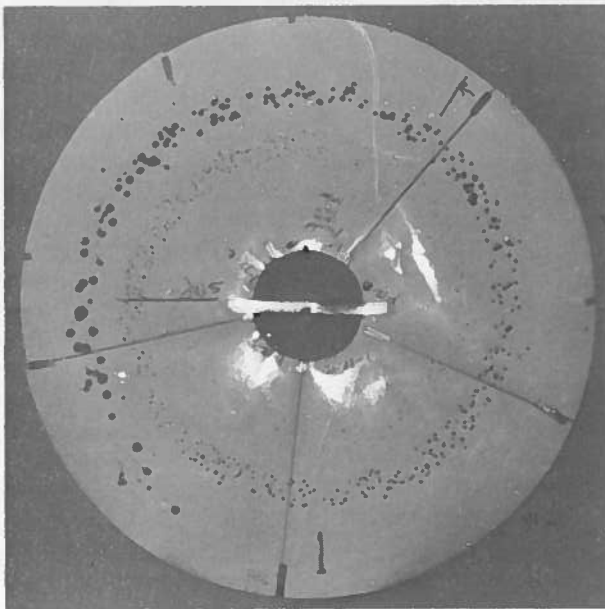
Phos-Chek XA (DT-155)  
SII,  $V_a = 134.5$  knots



Phos-Chek XA (DT-147)  
SIII,  $V_a = 127$  knots



Phos-Chek XA (DT-161)  
SII,  $V_a = 186.4$  knots



Water (DT-162)  
SI,  $V_a = 128.4$  knots

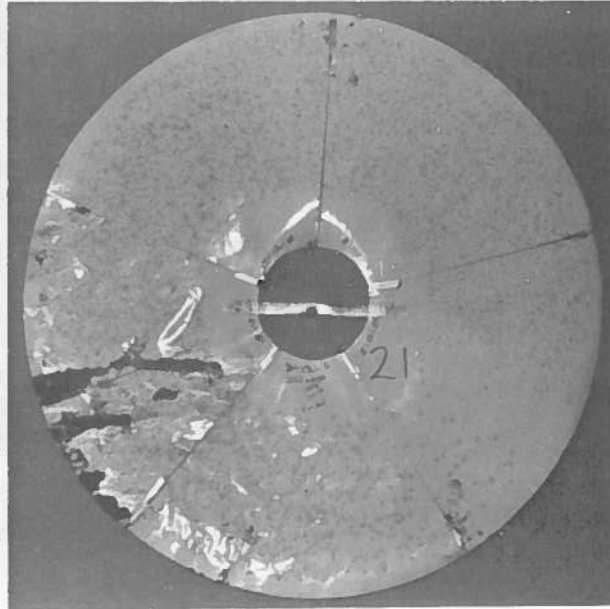
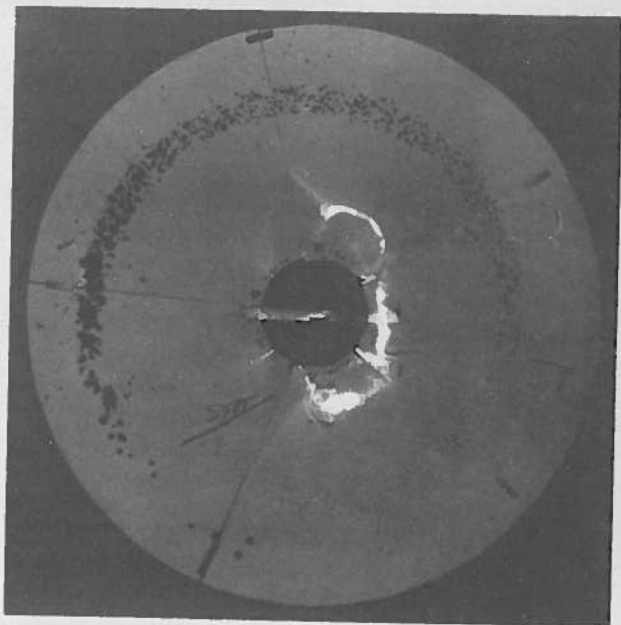
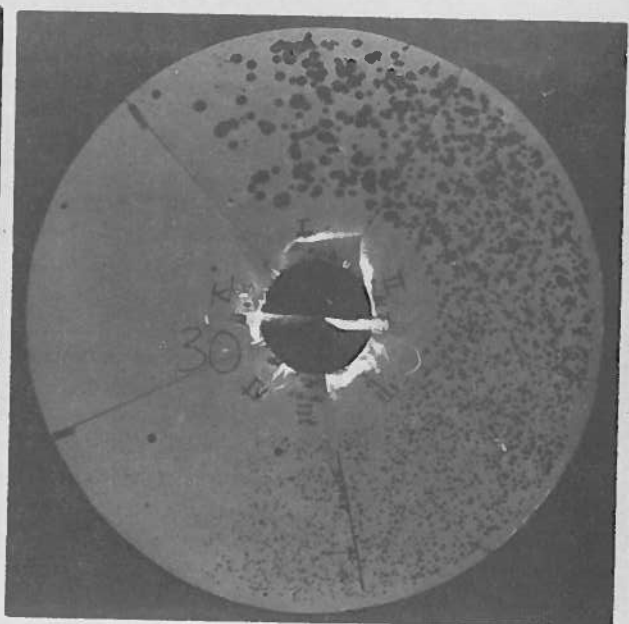


Figure 28. Typical Droplet Splotch Patterns Obtained by the Rotating Impact Samplers.

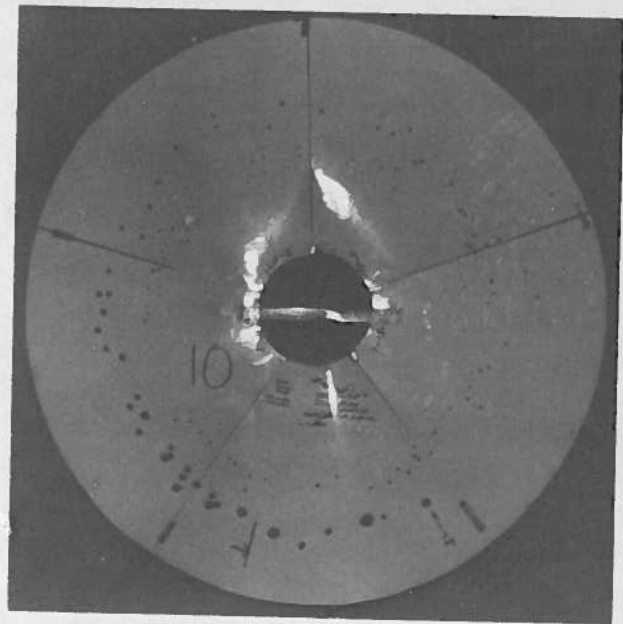
0.42 Phos-Chek (DT-163)  
SII,  $V_a = 129.2$  knots



0.42 Phos-Chek (DT-163)  
SIII,  $V_a = 129.2$  knots



1.6 Phos-Chek (DT-168)  
SII,  $V_a = 137.5$  knots



1.6 Phos-Chek (DT-169)  
SIII,  $V_a = 133$  knots

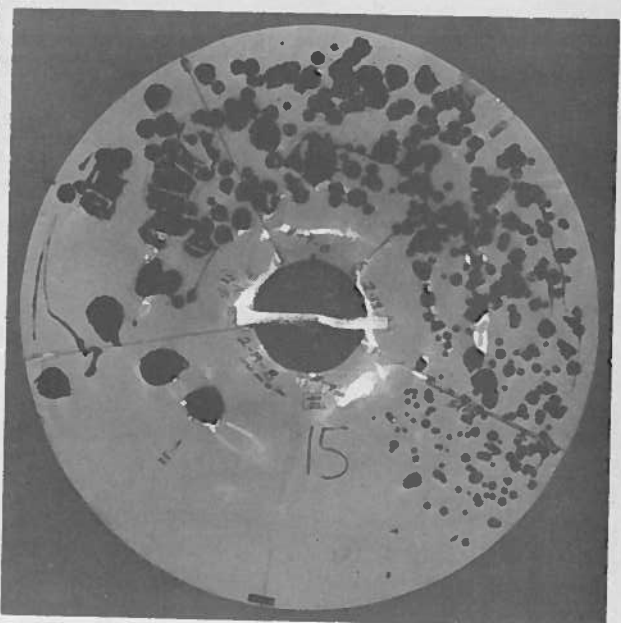
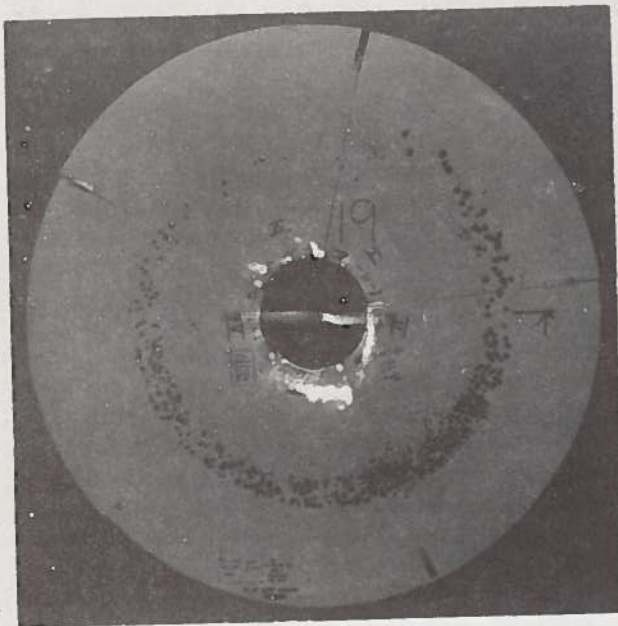
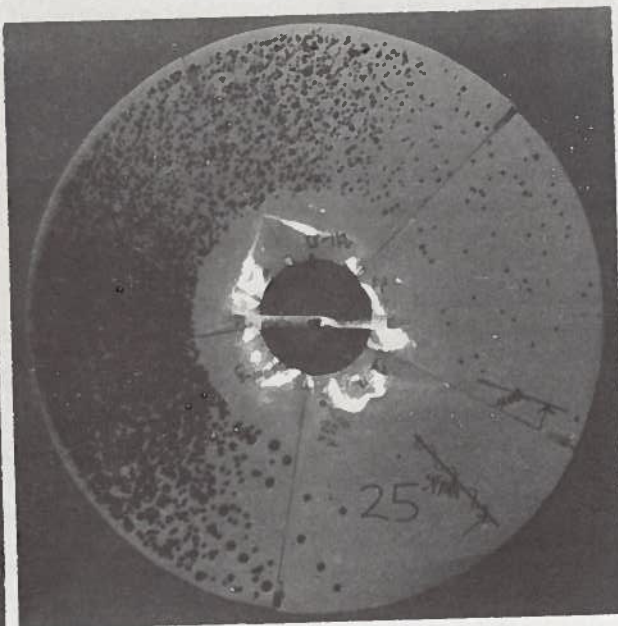


Figure 28. (continued)

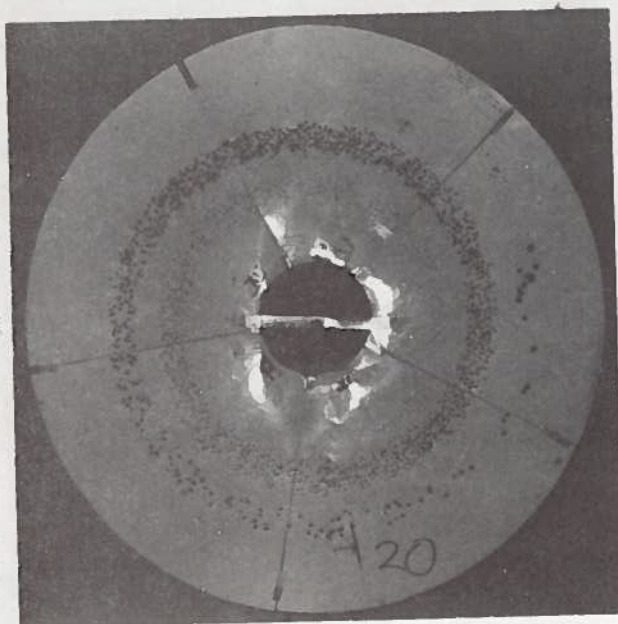
Fire-Trol 100 (DT-160)  
SII,  $V_a = 130.9$  knots



Fire-Trol 100 (DT-160)  
SIII,  $V_a = 130.9$  knots



Fire-Trol 931 (DT-166)  
SII,  $V_a = 133.9$  knots



Fire-Trol 931 (DT-165)  
SI,  $V_a = 124$  knots

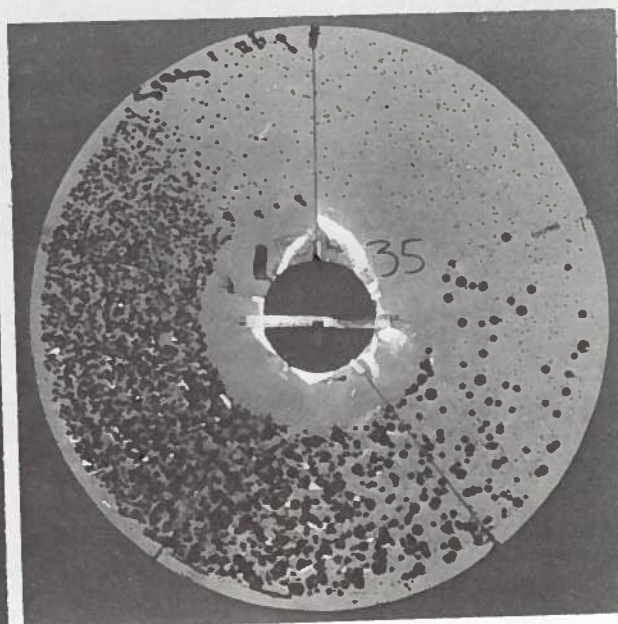


Figure 28. (concluded)



### 3.2.5.1 Spread Factor Calibration Procedure

The spread factors of the droplets of the various retardants were obtained as a function of droplet size by dropping individual drops of the retardant from a 40 ft. drop tower and measuring the average circular diameter of the splash pattern produced on the same cardboard paper as used in the field tests. This height is sufficient to produce essentially full terminal velocity for droplets 4-5 mm in diameter and smaller. Subsidiary measurements showed that for larger droplets where full terminal velocity is not necessarily attained, the spread factor is relatively insensitive to impact velocity above values that are attained by the tower. Thus, the calibration experiments could be conducted directly using the drop tower.

The droplet sizes used in the calibration experiments were produced in two different ways. Droplets larger than about 2.9mm were made with various diameter orifice eyedropper designs. Each different size eyedropper was calibrated for a particular retardant by weighing individual drops with a sensitive balance.

For smaller diameter droplets the preceding technique was not suitable due to clogging, tip breakage, non-reproducibility in size or non-generation of small droplets, and a different technique was used. It was found that the impact of a larger droplet with a coarse screen produced a series of small droplets of the size range desired. Because these droplets of different sizes could not be weighed conveniently to determine their diameters, they were photographed in flight in front of a fiducial grid. A two unit sequential flash system permitted the velocities of the droplets to be determined at the same time.

The small droplet testing sequence was conducted as follows. A 4 to 5mm drop of retardant was released at the top of the 6" diam. drop tube (on the drop tower) and allowed to fall 40 ft. before striking a #18 mesh screen positioned over an 18" x 19" x 33" observation chamber which contained a droplet sample card which was positioned 34 inches below the screen. A model 110A Polaroid camera with a close-up lens was operated in the open-shutter mode and positioned 9" from the droplet plane to record the falling droplets. Lighting was provided by a General Radio Model 1541 dual flash system with a 2 msec delay between flashes. This interval gave two images for each droplet over a known time period and this yielded the individual droplet velocities. A microphone triggered the flash sequence by sensing the impact of droplet spray following screen impact. A droplet mask 1.5" wide x 4" long was positioned above the sampler card and fiducial grid to intercept off-axis spray so that only droplets falling within the camera's proper depth of field would be recorded. Individual droplet-to-camera and fiducial-to-camera distances were used in converting the photographic image size to true droplet size. A 5X magnifier with integral metric scale of 0.1mm resolution was used to measure the photographic image sizes and sampler spot diameters.

### 3.2.5.2 Reduced Spread Factor Data

Figure 29 shows the experimental values of droplet diameter vs the average diameter of the splotch patterns they produce at terminal velocity (some of the larger data points are not shown). The following procedure was used to obtain calibration formulae relating droplet diameter with its corresponding splotch diameter.

For respective retardants, the data were plotted with the splotch diameters along the x-axis and droplet diameters along the y-axis. The lay of the data suggested a monotonically increasing function crossing the origin. Inverting the axes, the data appeared to accommodate one leg of a parabola whose minimum lay in the (new) third quadrant. In this orientation, the fitting function used was

$$(x + x_0) = a(y + y_0)^2 \quad (15)$$

for a parabola minimum at  $(-y_0, -x_0)$ . The fitting parameters  $a$ ,  $x_0$ , and  $y_0$  were calculated using standard least-squares regression techniques coupled with the requirement  $x(y=0) = 0$ . Once these constants were determined, the function was inverted again to its final form

$$y = -y_0 + [(x + x_0)/a]^{1/2} \quad (16)$$

In this equation,  $y$  is the spherical droplet diameter that corresponds to a splotch pattern having an average circular diameter  $x$ . Table VI shows the values of  $x_0$ ,  $y_0$  and  $a$  for the various retardants.

TABLE VI. EXPERIMENTAL VALUES OF THE SPREAD FACTOR CONSTANTS

Retardant	$x_0$ mm	$y_0$ mm	$a$ (mm) <sup>-1</sup>	$\sigma^*$
Fire-Trol 931	1.141	1.100	0.942	0.057
Water	2.647	1.857	0.770	0.090
Fire-Trol 100	3.159	2.484	0.519	0.063
Phos-Chek XA	7.025	5.004	0.281	0.160
1.6 Phos-Chek XA	7.078	5.508	0.233	0.027
0.42 Phos-Chek XA	29.736	14.344	0.145	0.018

\* Standard Deviation of the Experimental Points from the Least Squares Curve of the Data

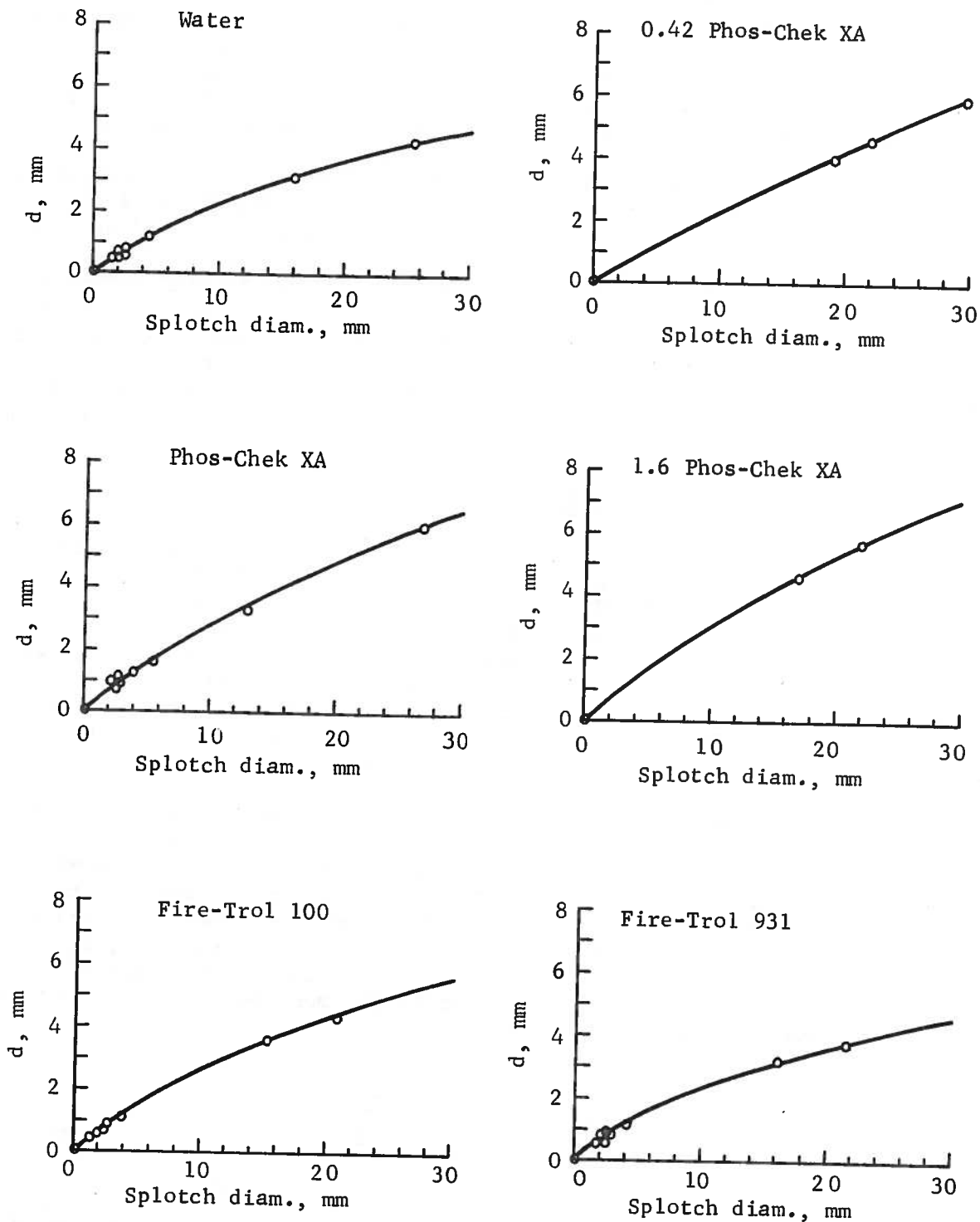


Figure 29. Experimental Relation Between Droplet Diameter and Splotch Pattern Diameter of the Retardants.

The values of the constants for 0.42 Phos-Chek appear out of line with the others and are the result of the near linearity of the curve at the smaller values of  $x$  shown in Figure 29 (no experimental data was obtained in this region). A slightly more non-linear curve in this region (as for the other retardants) would give constants for this fluid whose values lie between those of Fire-Trol 100 and Phos-Chek XA. However, the constants given in the table are valid for the curve for 0.42 Phos-Chek given in Figure 29.

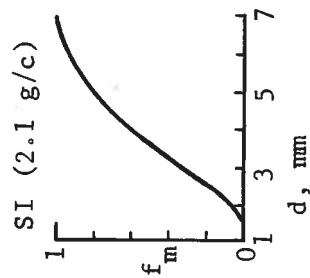
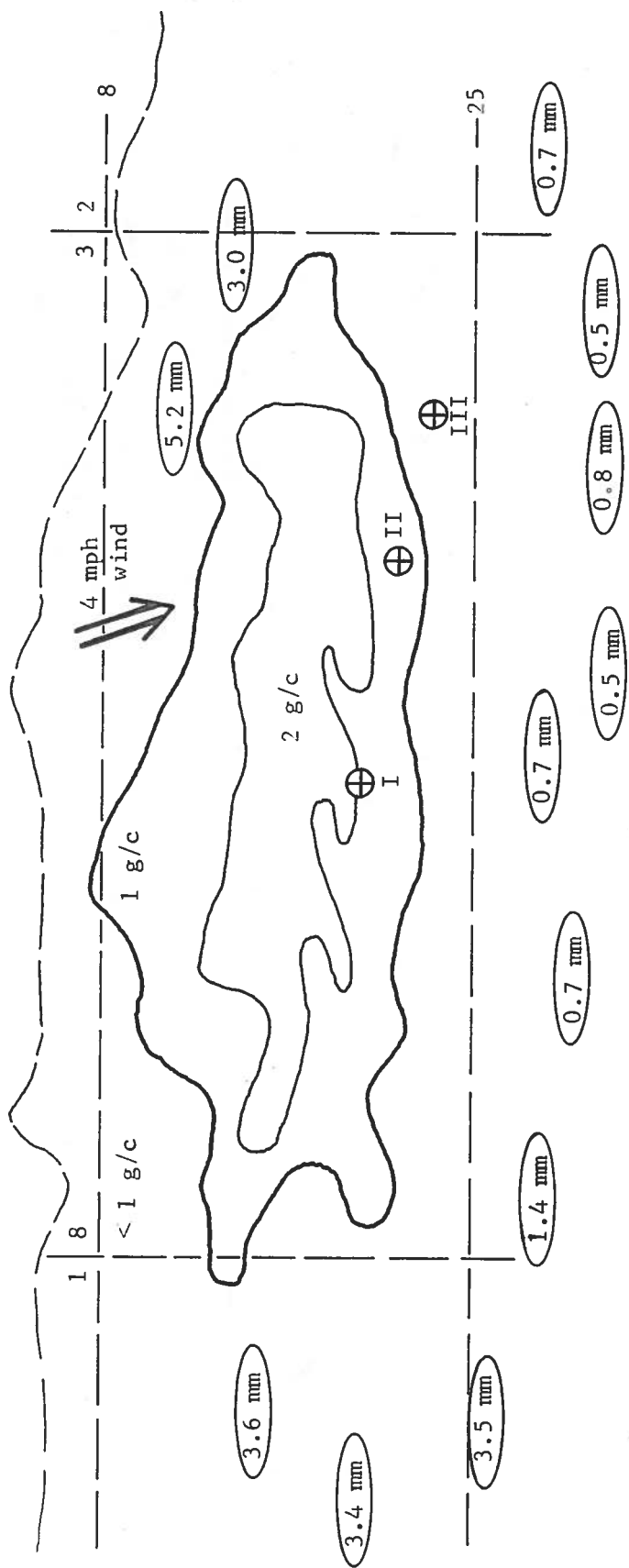
It should be mentioned that the largest splotch patterns obtained in the field tests for some of the retardants were significantly larger than the patterns obtained in the calibration tests, i.e., some of the droplet sizes in the field were much larger than covered by the calibration tests. The sizes used in the calibration tests were limited by time and ease of formation. As a consequence, any deviation of the calibration curves from the real values would be reflected largely in the values of the droplet size the curves predict by extrapolation to large droplet size. It should also be mentioned that the idealized, carefully mixed solutions used in preparing the calibration curves may differ to some degree from those used in the field.

#### 4. EXPERIMENTAL RESULTS

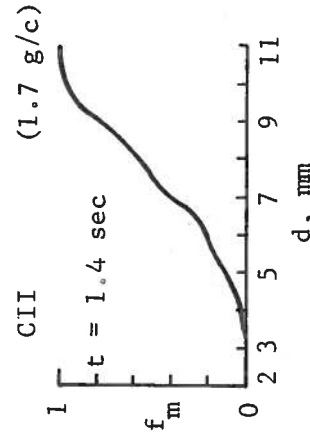
The results of the experimental droplet size measurements on the various retardants are summarized in Figures 30-44. These figures show the droplet size measured by the various sensors, and the location of the sensors with respect to the ground concentration pattern of the disseminated liquid (some identifying grid lines of the pattern are noted). The ground patterns were obtained from the Forest Service. For clarity they show only a rough grouping of the liquid concentration levels and have been smoothed to some extent. However, the actual averaged measured concentration in the vicinity of the rotating samplers and camera is given in parenthesis in gallons per 100 ft<sup>2</sup>, (g/c). The drop pattern runs from left to right, and the magnitude and direction of the wind is also shown. The three rotating impact samplers are denoted by S, and the camera by C. The plots of  $f_m$  vs  $d$  are the droplet size distributions based on liquid mass, as obtained from the rotating samplers and camera.  $f_m$  is the cumulative mass fraction of the liquid at the sensor and  $d$  is droplet diameter. The mean (average) diameter of the droplets based on mass is called the mass mean diameter,  $d_m$ , and its computed value based on the drop size distribution is shown below the distribution curves. The mass mean diameter is the most meaningful average value for most purposes, and is given by

$$d_m = \frac{\sum m_i d_i}{\sum m_i} = \frac{\sum d_i^4}{\sum d_i^3} \quad (17)$$

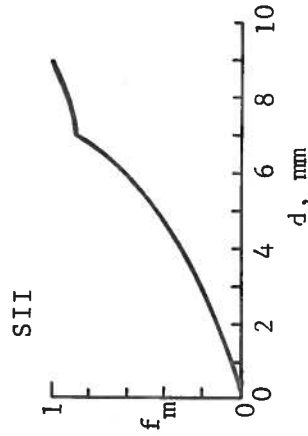
where  $m$  is particle mass. The mass median droplet diameter corresponds to the point  $f_m = 0.5$  on the curves. Also shown in the figures (by a number) is the mass mean diameter of the droplets on the impactor cards and their location in the pattern.



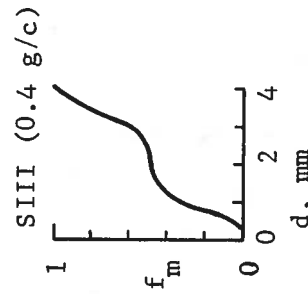
$d_m = 3.9 \text{ mm}$



( $d_m = 7.7 \text{ mm}$ )



$d_m = 5.2 \text{ mm}$



$d_m = 2.3 \text{ mm}$

Figure 30. Measured Droplet Sizes: Phos-Chek XA (Drop No. 155),  $V_a = 134.5 \text{ knots}$ ,  $DH = 369 \text{ ft}$ .  
( $1 \text{ cm} \approx 18.85 \text{ ft}$ )

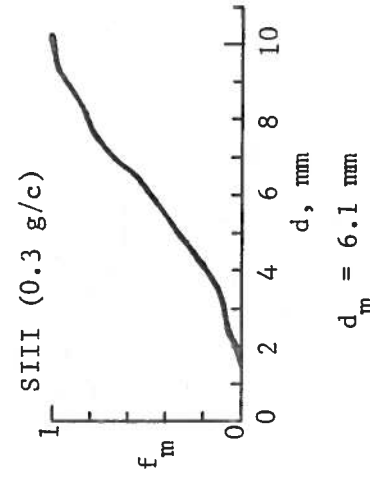
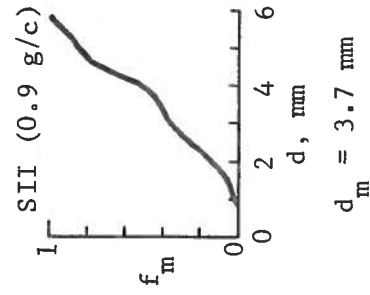
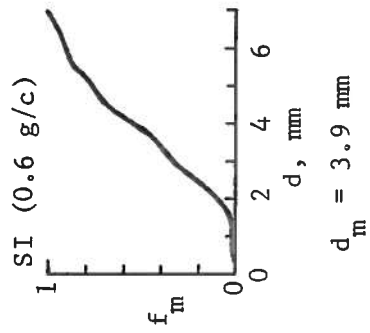
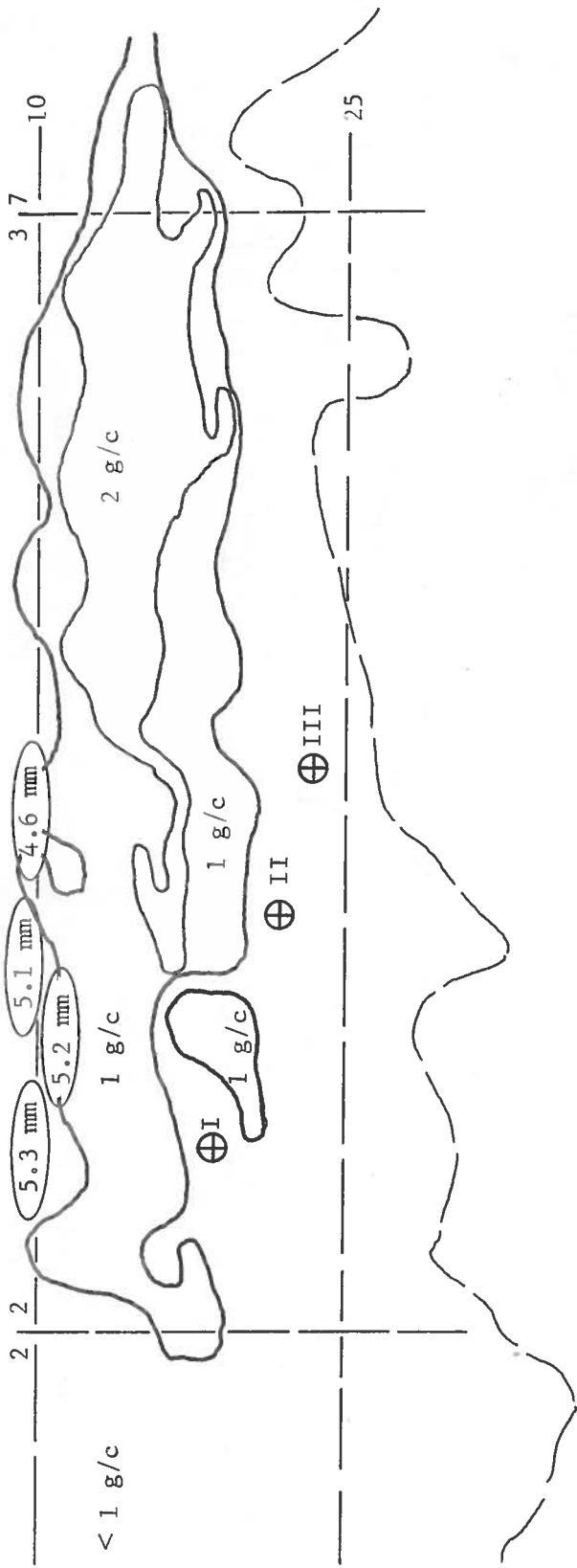


Figure 31. Measured Droplet Sizes: Phos-Chek XA (Drop No. 147),  $V_a = 127$  knots,  $DH = 342$  ft.

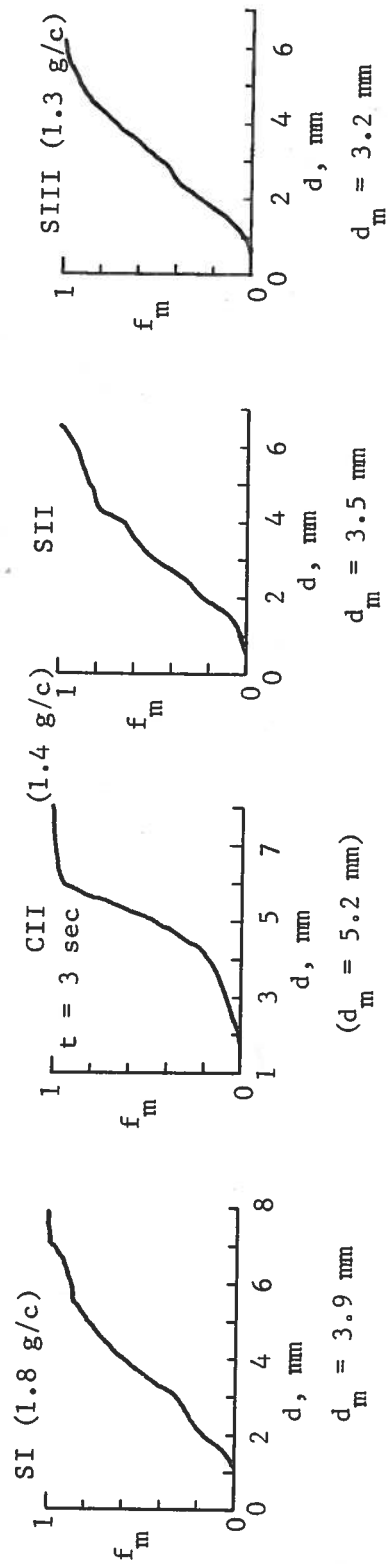
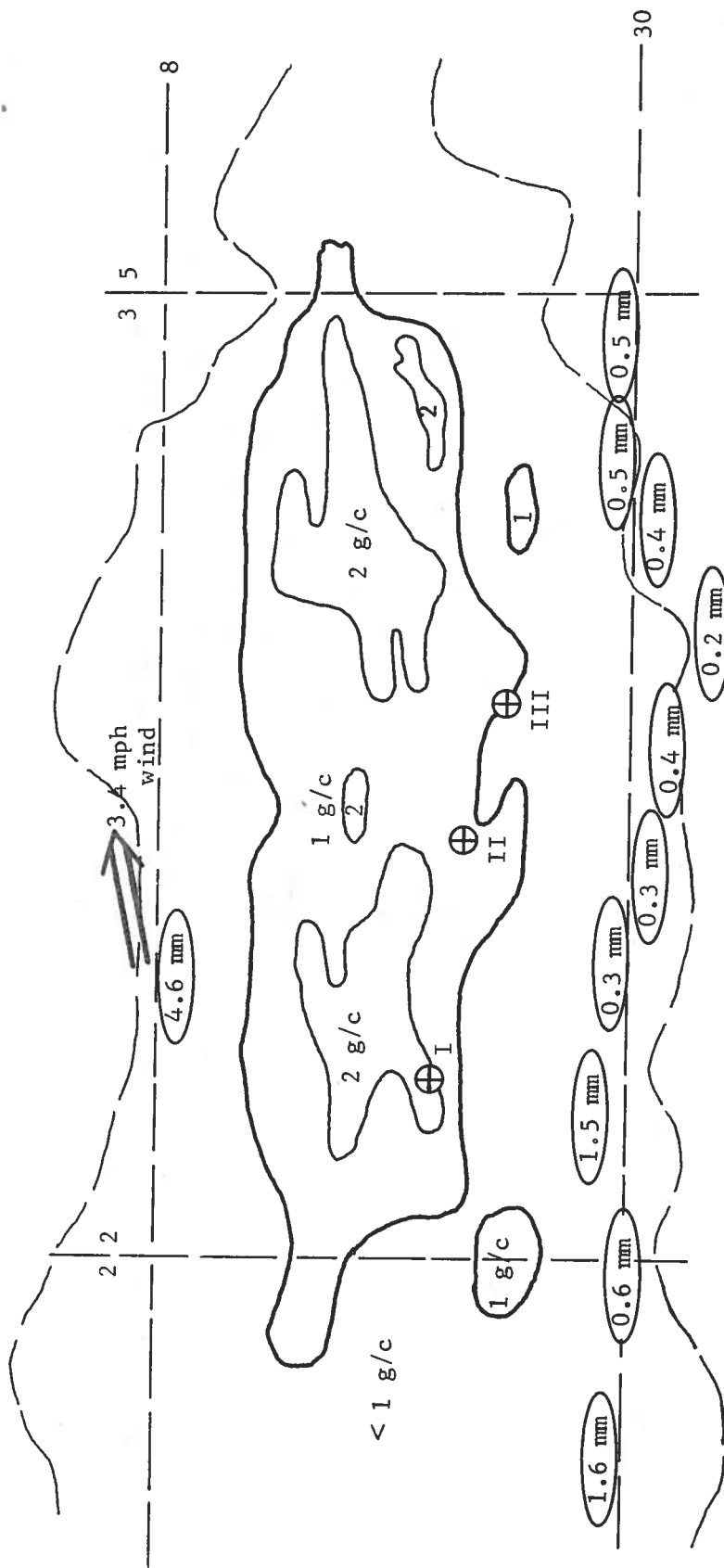


Figure 32. Measured Droplet Sizes: 0.42 Phos-Chek XA (Drop No. 163),  $V_a = 129.2$  knots,  $DH = 335$  ft.

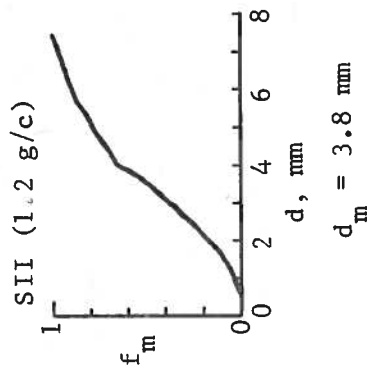
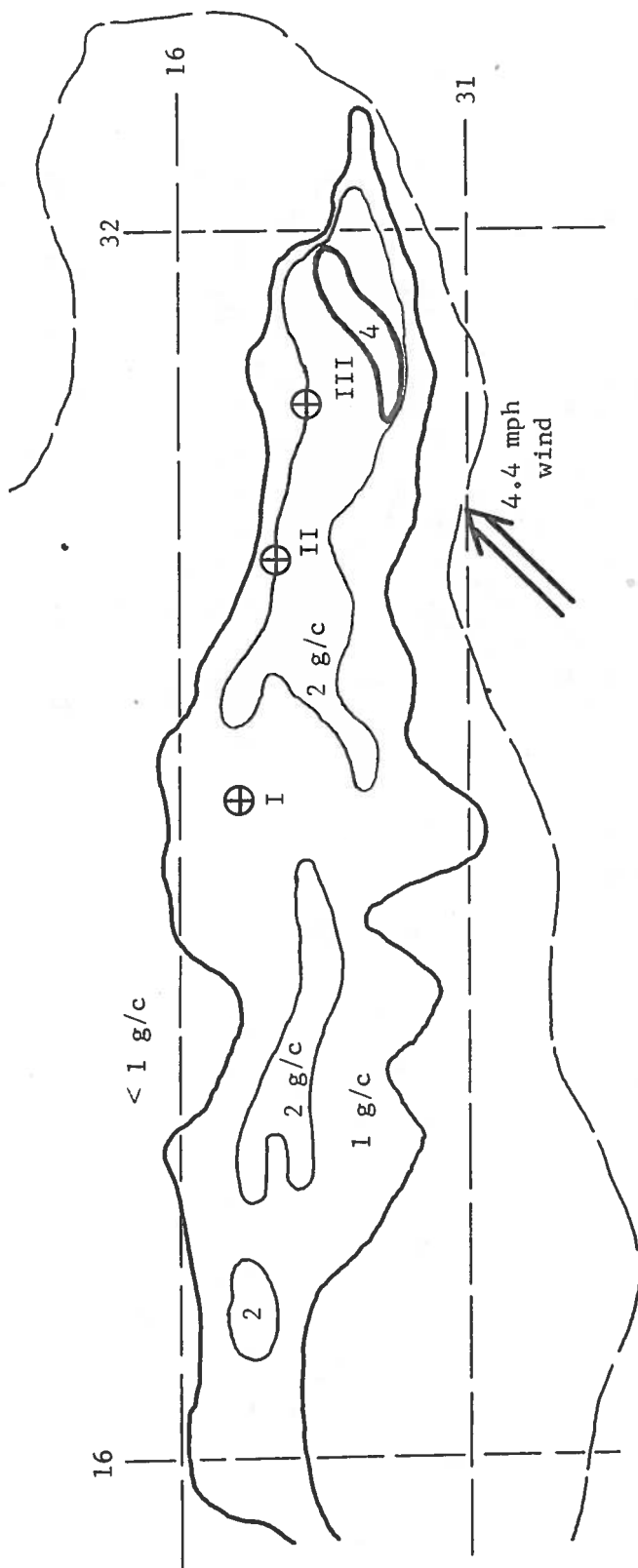


Figure 33. Measured Droplet Sizes: 0.42 Phos-Chek XA (Drop No. 164),  $V_a = 122.9$  knots,  $DH = 314$  ft.



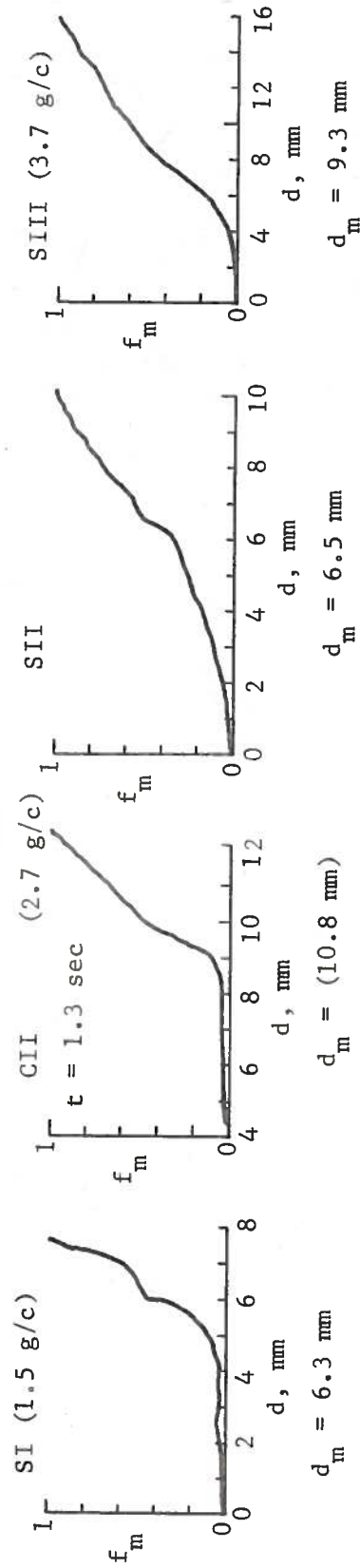
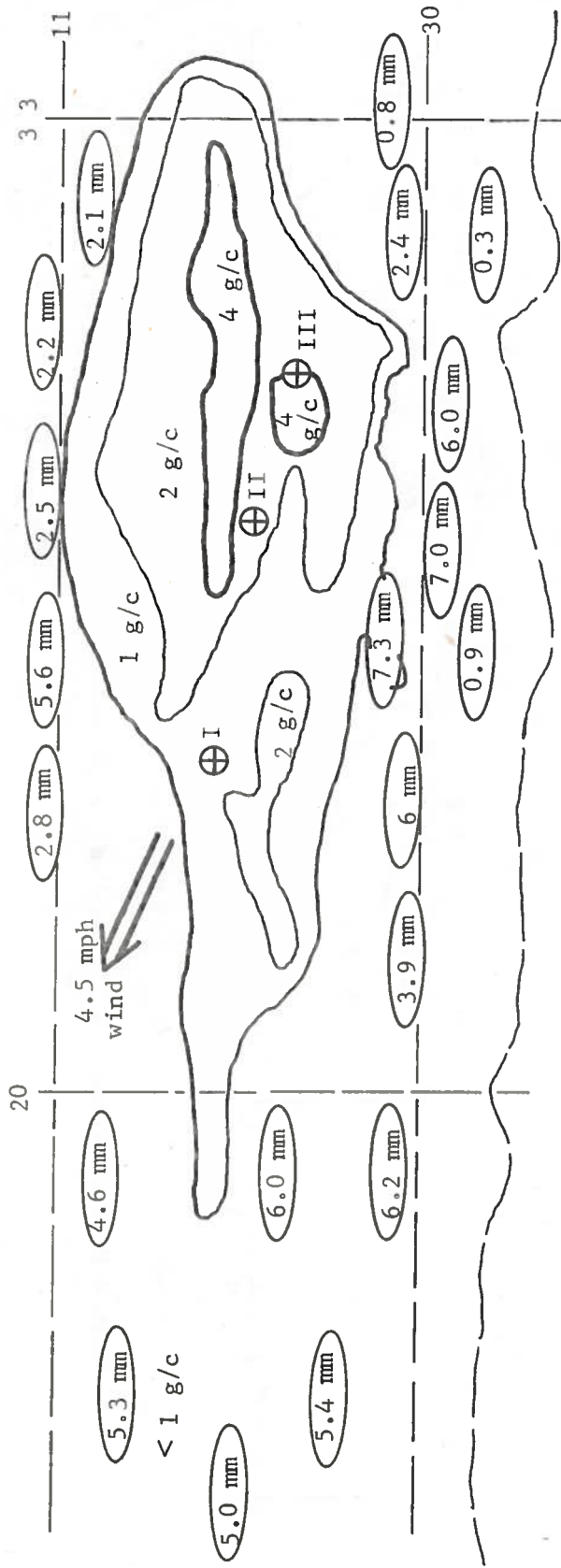


Figure 34. Measured Droplet Sizes: 1.6 Phos-Chek XA (Drop No. 169),  $V_a = 133$  knots,  $DH = 341$  ft.

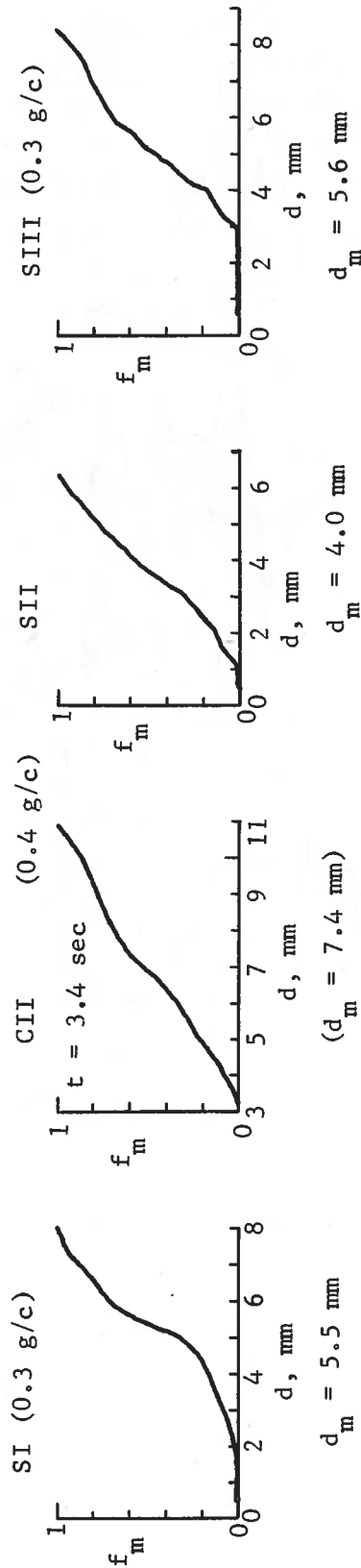
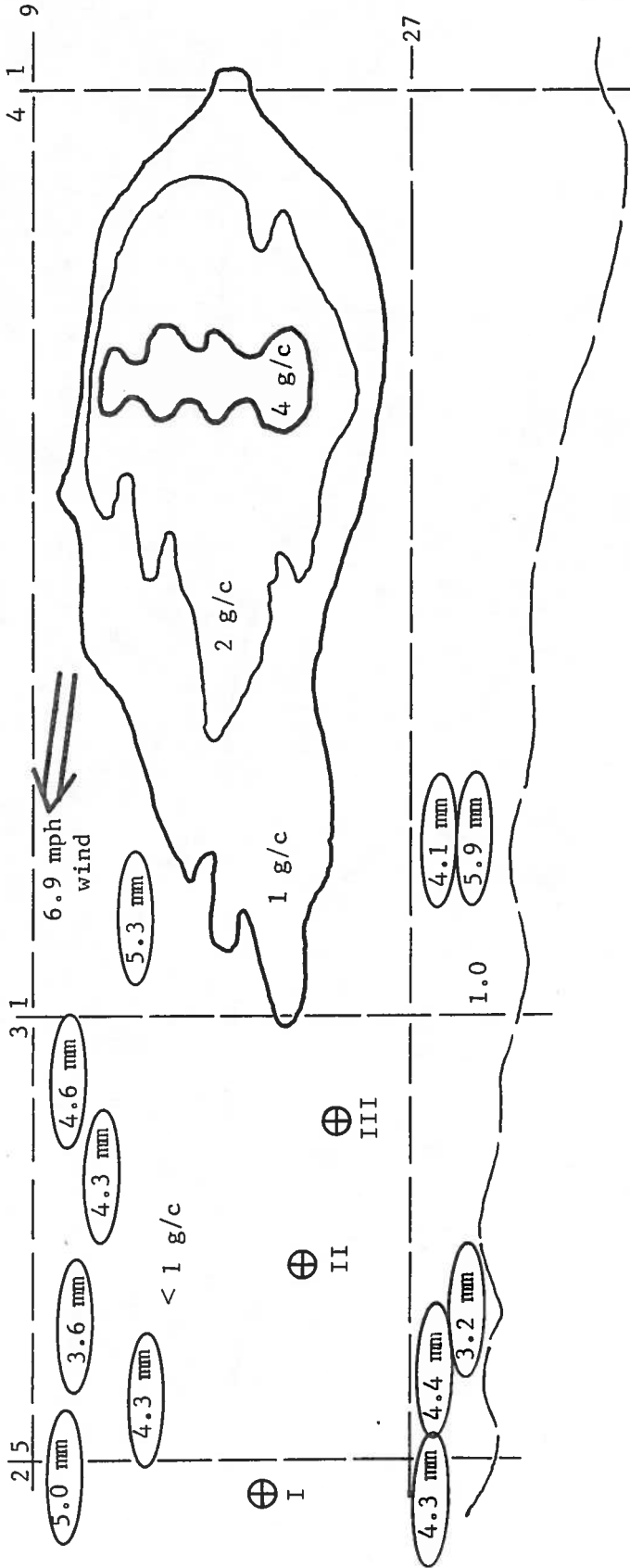


Figure 35. Measured Droplet Sizes: 1.6 Phos-Chek XA (Drop No. 168),  $V_a = 137.5$  knots,  $DA = 318$  ft.

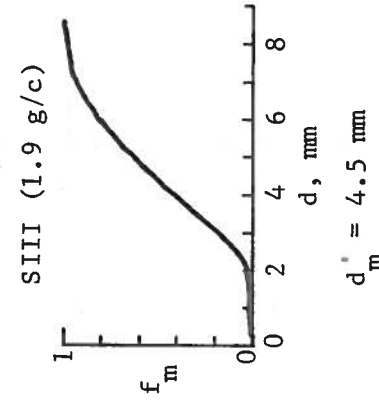
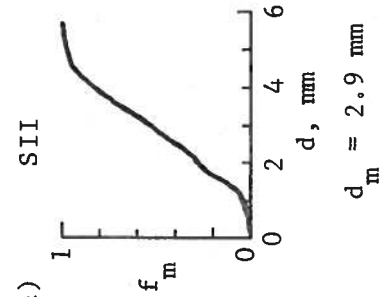
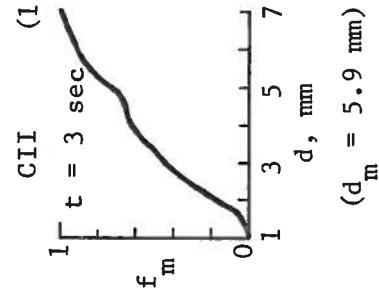
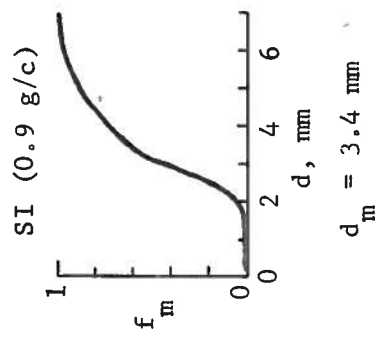
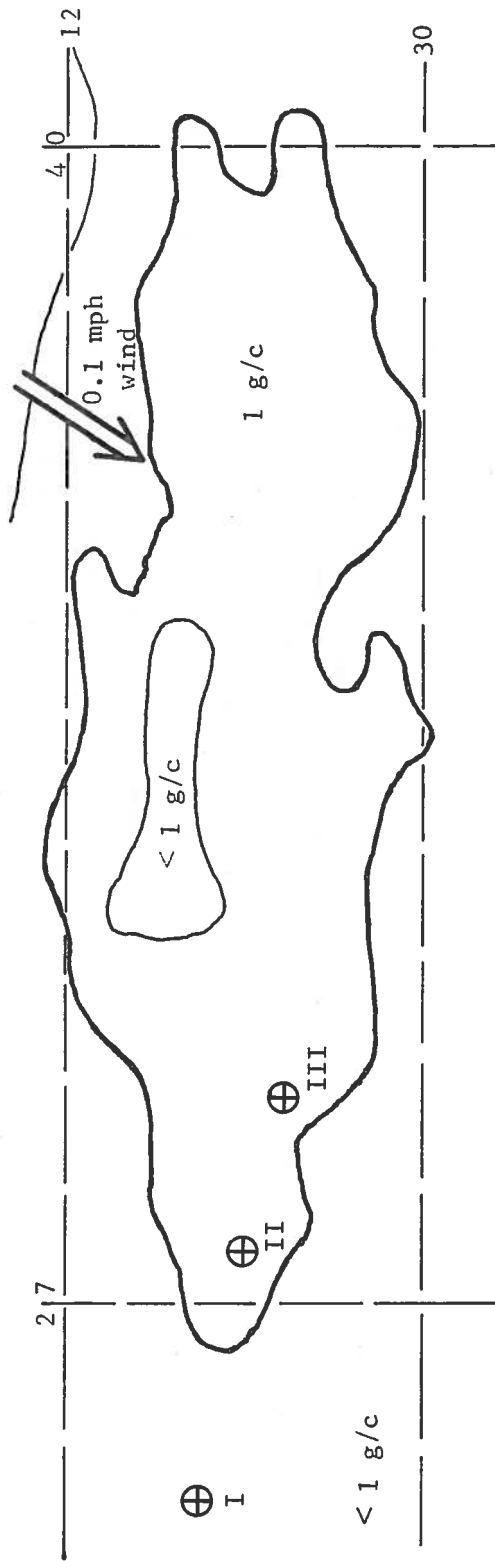
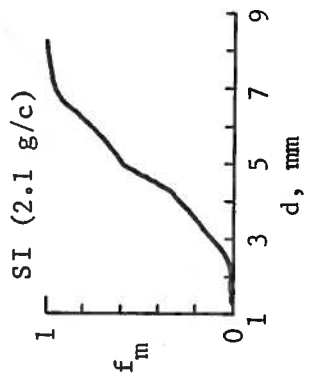
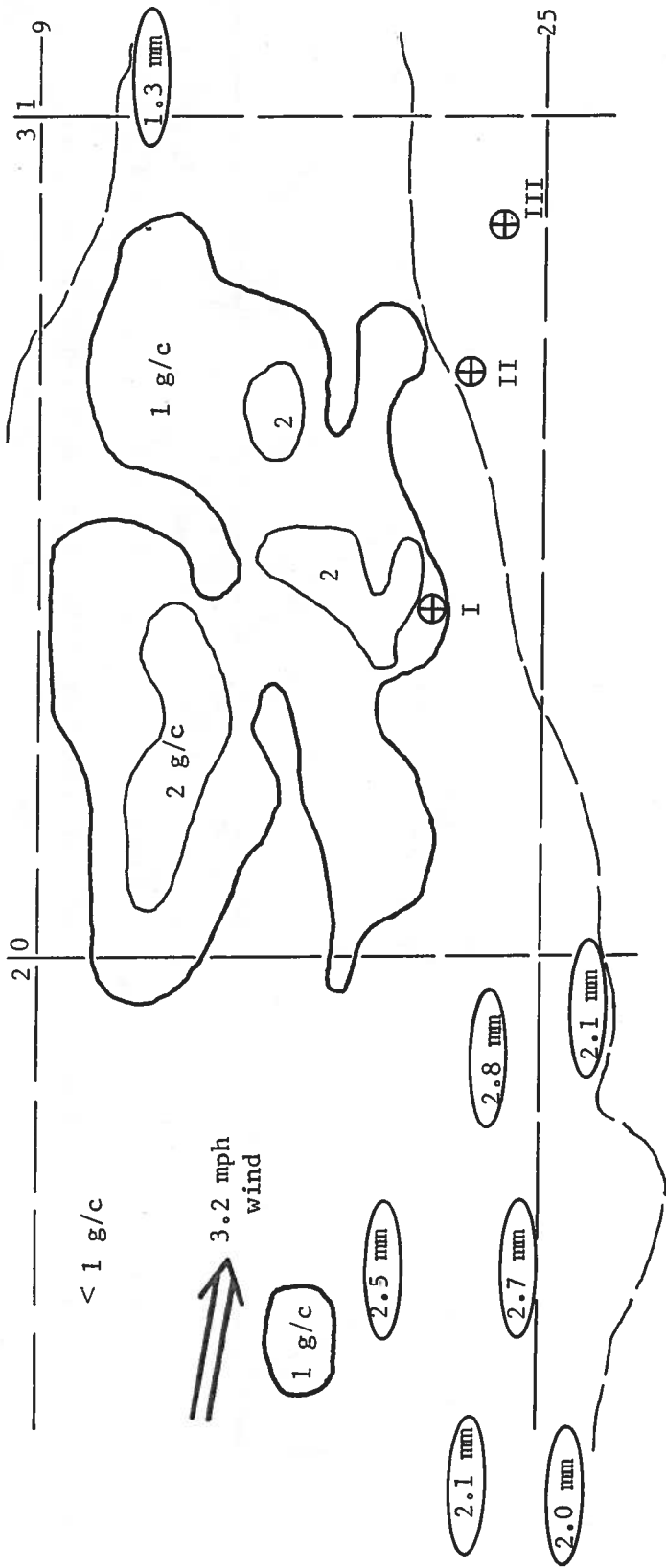


Figure 36. Measured Droplet Sizes: Phos-Chek XA (Drop No. 161),  $V_a = 186.4$  knots,  $DH = 337$  ft.



$d_m = 4.9 \text{ mm}$

Figure 37. Measured Droplet Sizes: Phos-Chek XA (Drop No. 157),  $V_a = 187.7$  knots,  $DH = 409$  ft.

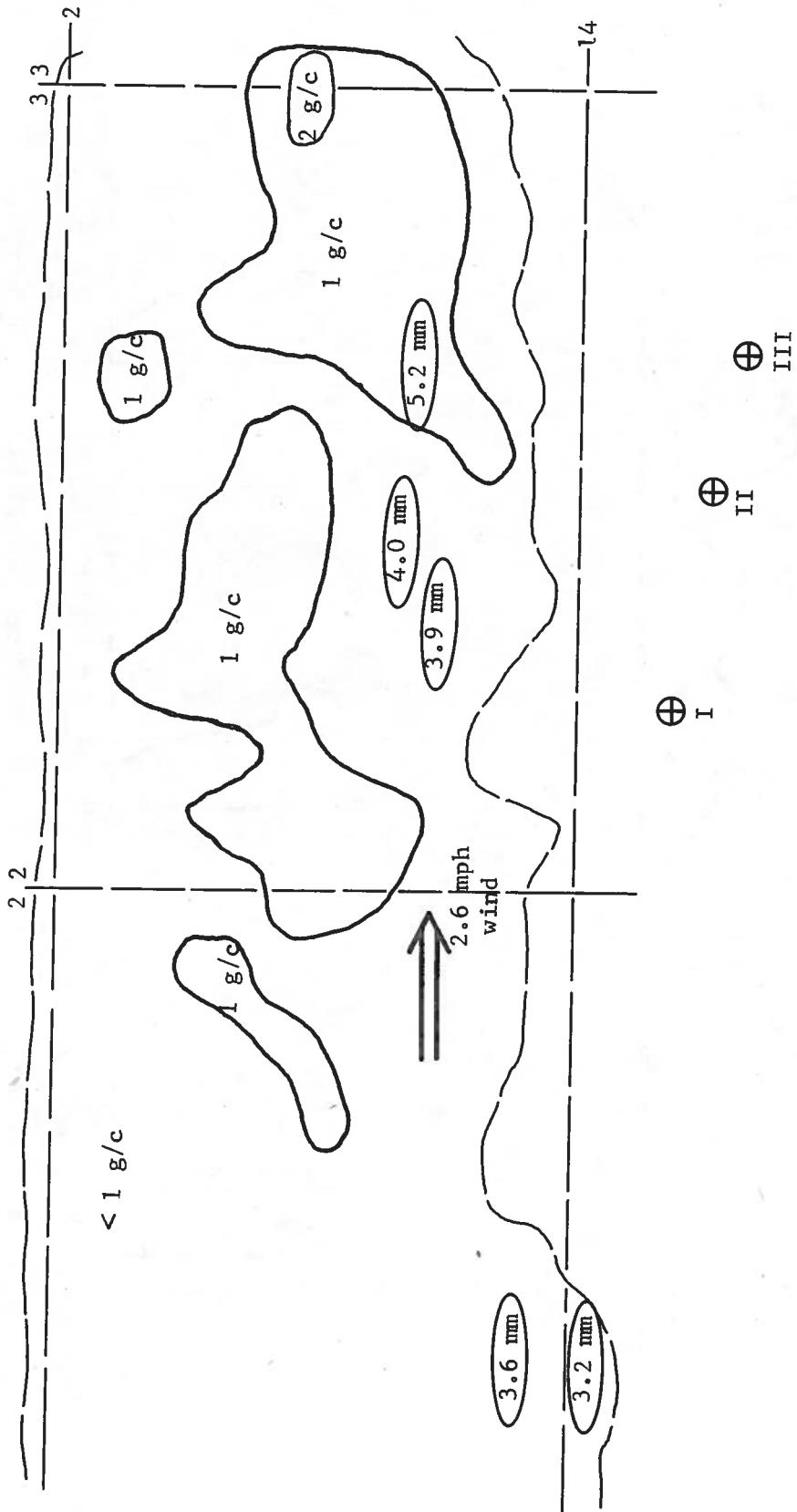


Figure 38. Measured Droplet Sizes: Phos-Chek XA (Drop No. 158),  $V_a = 187.1$  knots,  $DH = 370$  ft.

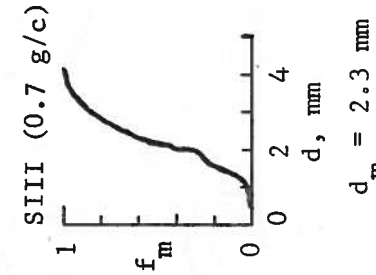
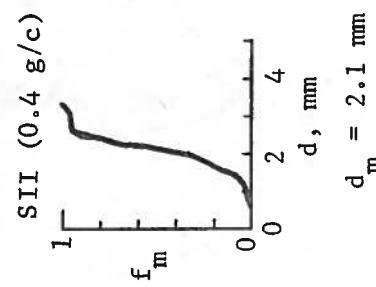
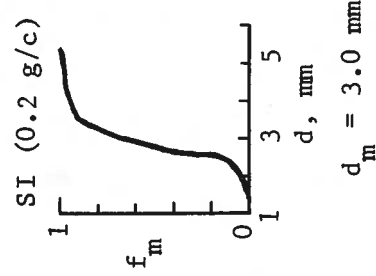
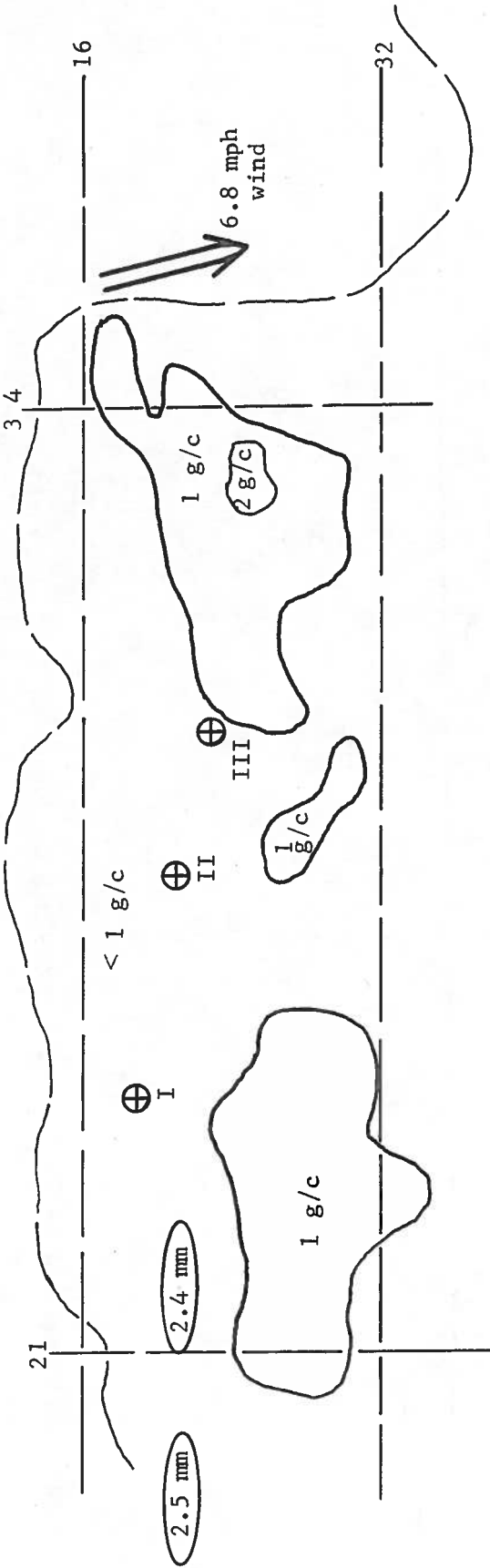


Figure 39. Measured Droplet Sizes: Fire-Trol 100 (Drop No. 160),  $V_a = 130.9$  knots,  $DH = 304$  ft.

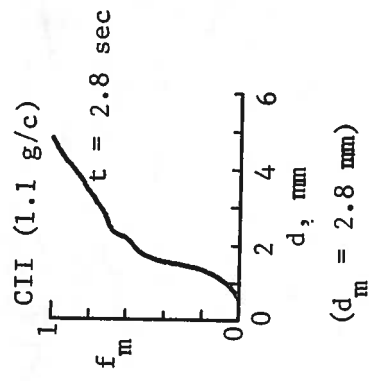
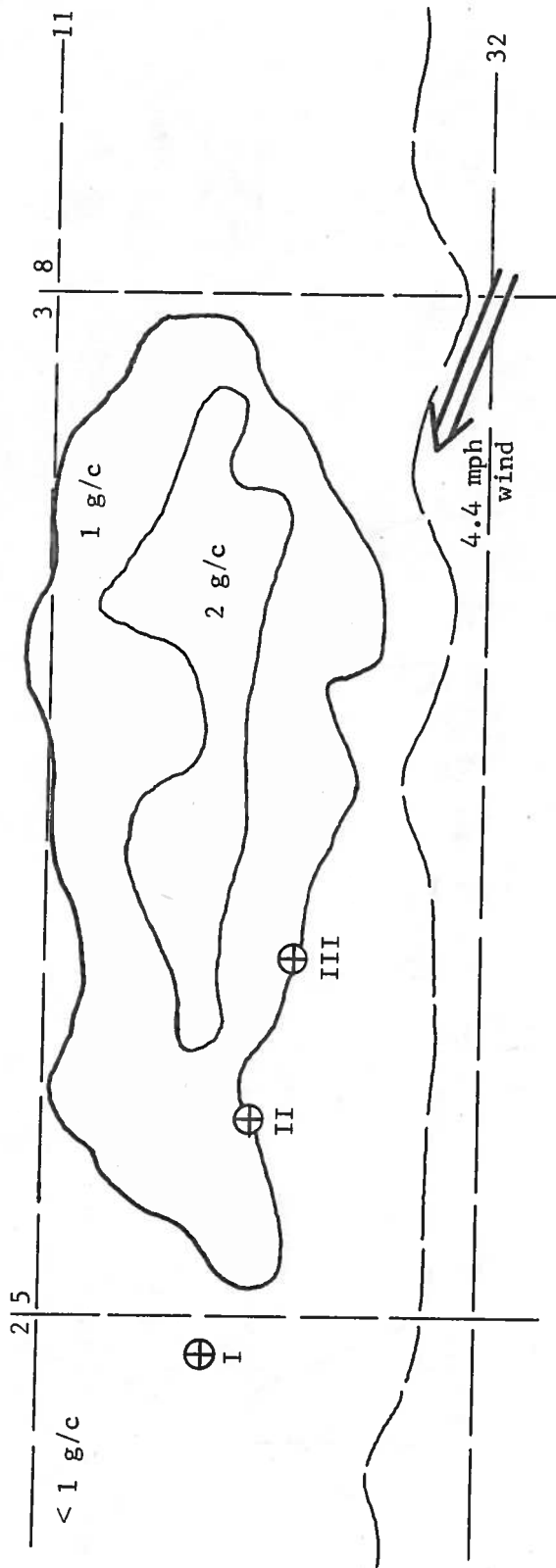


Figure 40. Measured Droplet Sizes: Fire-Trol 100 (Drop No. 240),  $V_a = 131.6$  knots,  $DH = 350$  ft.

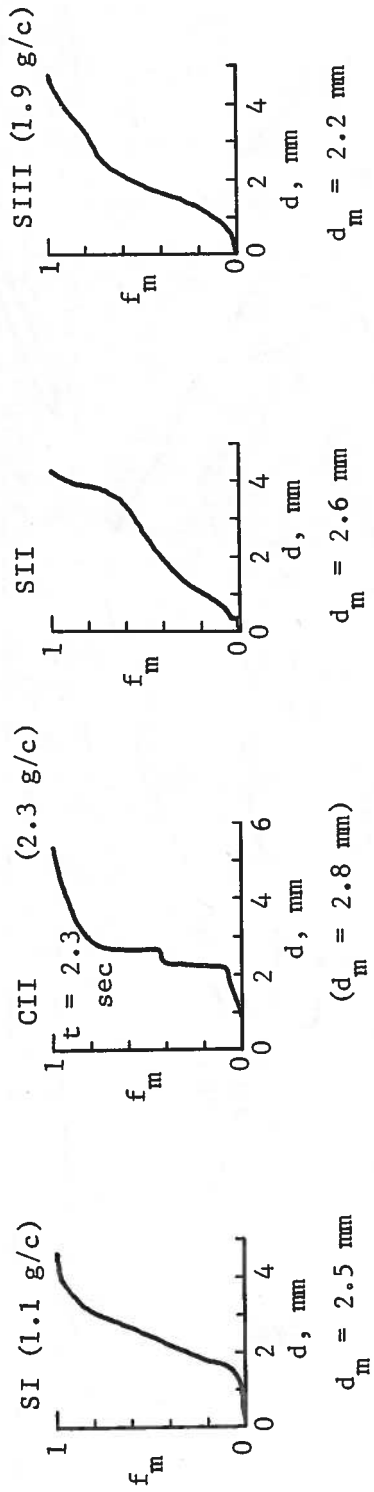
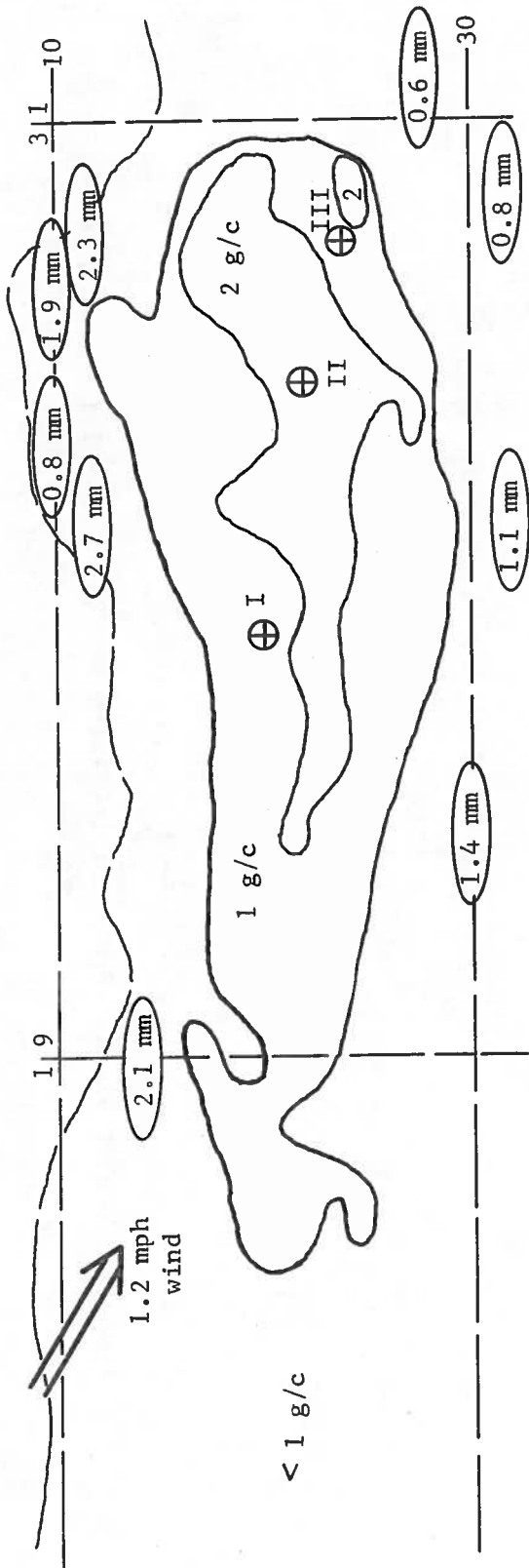


Figure 41. Measured Droplet Sizes: Fire-Trol 931 (Drop No. 165),  $V_a = 124$  knots,  $DH = 351$  ft.



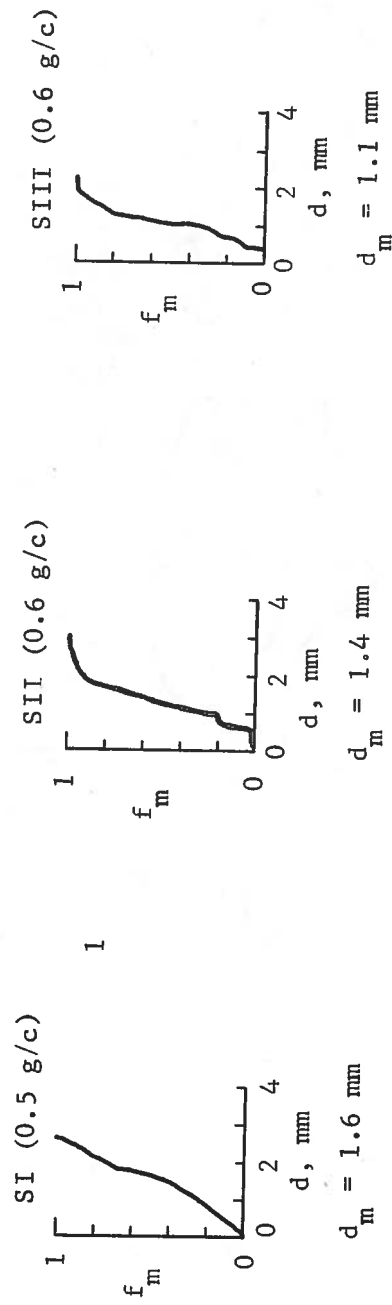
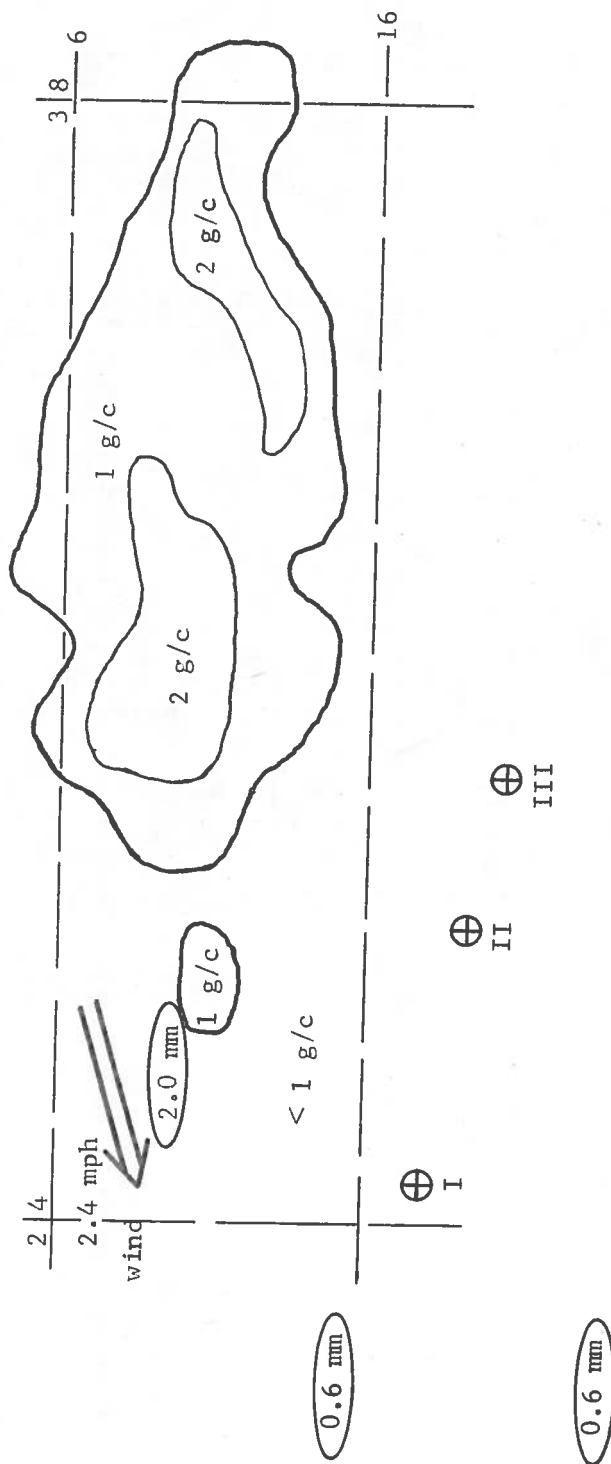
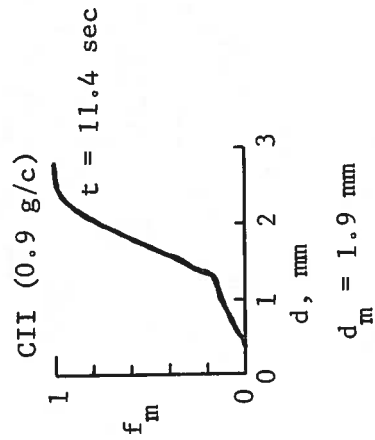
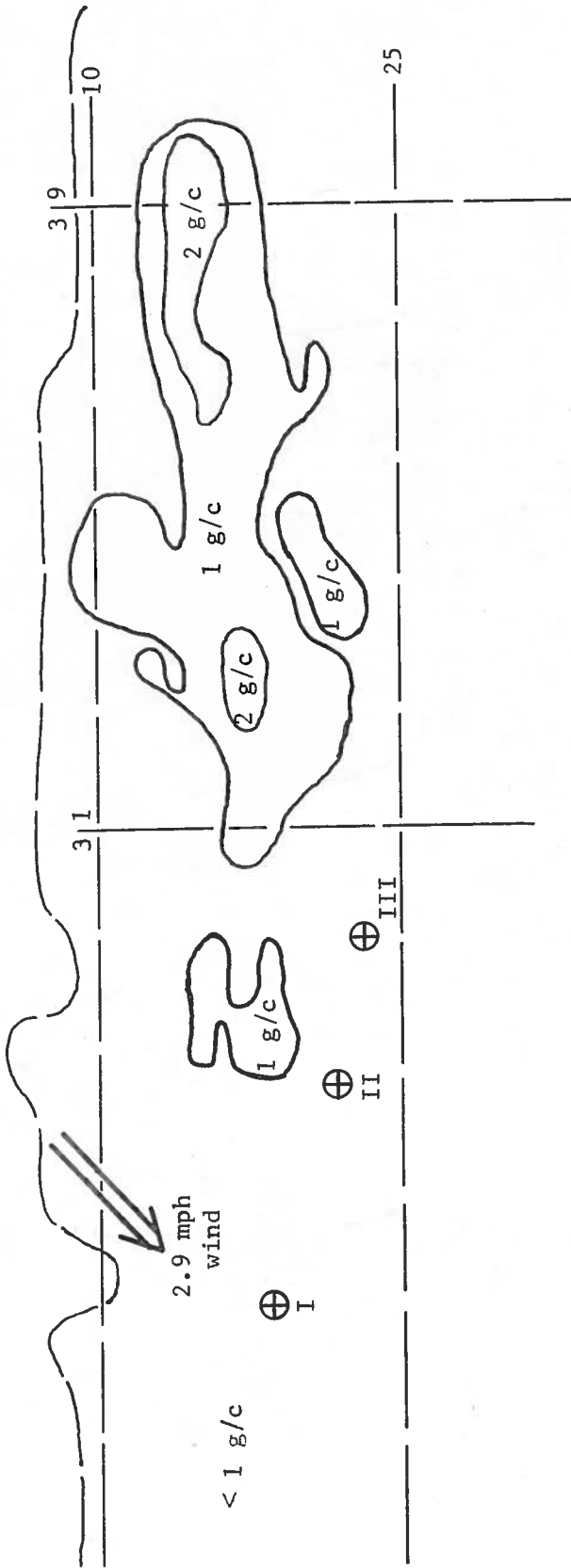


Figure 42. Measured Droplet Sizes: Fire-Trol 931 (Drop No. 166),  $V_a = 133.9$  knots,  $DH = 342$  ft.



$$d_m = 1.9 \text{ mm}$$

Figure 43. Measured Droplet Sizes: Water (Drop No. 151),  $V_a = 137$  knots,  $DH = 306$  ft.

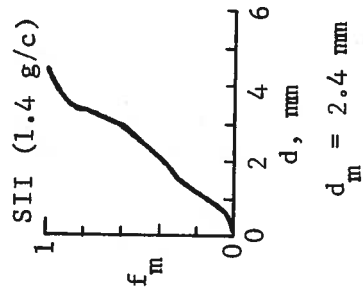
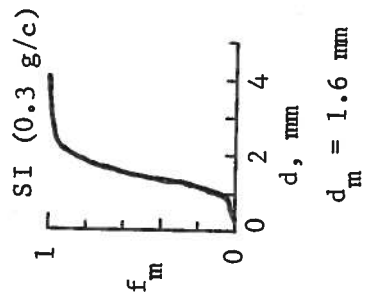
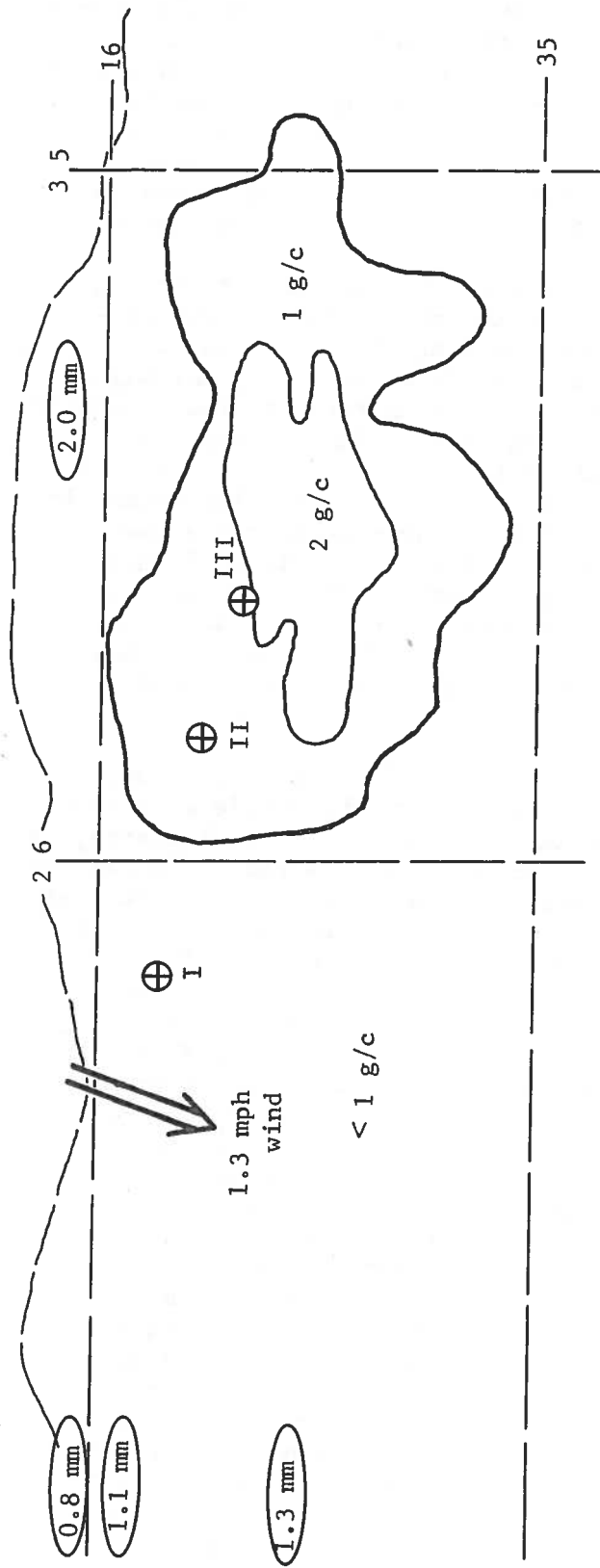


Figure 44. Measured Droplet Sizes: Water (Drop No. 162),  $V_a = 128.4$  knots,  $DH = 301$  ft.

In examining the data given in the Figures 30-44 it should be noted that the droplet sizes obtained from the camera film generally represent only a limited portion of the retardant rain, and thus are usually not directly comparable with the sampler data. The sampler data to good approximation represents the entire rain cloud-especially sampler II which had a very long sensing duration. In the figures, the measurement time of the camera is shown near the cumulative droplet size distribution obtained in that time period, and the mass mean diameter of the droplets obtained in the same time period is given below the distribution curve in parenthesis.

The general uncertainty of the measurements and data reduction techniques should also be kept in mind. For the camera data it was previously noted that droplets smaller than about a millimeter could not be measured, and image distortion imposed an uncertainty whose general magnitude increased with decreasing droplet size. This uncertainty was accounted for insofar as possible in the data reduction, but was not necessarily eliminated completely. With regard to the data reduction, only a limited number of frames on each test film were reduced (usually 6). The manner in which the frames were selected may have affected the results but a basis for a completely valid procedure could not be determined. It would have been desirable to reduce the data on a much larger number of frames, and this would reduce the possible error due to frame selection. The number of droplets on which the camera data is based is generally considerably smaller than for the rotating impact samplers (whose droplet statistics should be quite good).

For the impact sampler data the main source of error possibly related to the measurement of the splotch patterns of the droplets, although the calibration curves may also contain some error at large droplet size, as noted previously. Since many thousands of spots were measured there was not time to dwell on making detailed measurements on every single spot, and most measurements were quickly and roughly made to the nearest 1/2 mm without recourse to check. For the large spots the measurements could only be made to the nearest 1 or 2 mm at best (sometimes several mm), since they were not always circular (especially for the Phos-Chek solutions). In these cases a measurement was either made in two directions and averaged, or an average diameter merely estimated on the basis of a single measurement and the general shape of the spot. In some cases with the larger Phos-Chek spots a localized group of large spots would be clumped together, and it was difficult (or impossible) to ascertain whether the clump represented several individual drops or a single large glob. In these cases, the clumped spots were usually considered to represent individual drops that had interacted on impact, and the spots were separated for measurement as best as possible. The Phos-Chek spots also often contained small air pockets, presumably as the result of air incurred by the liquid during its preparation (mixing of the retardant powder with water), and subsequent pumping into the tank of the aircraft (the disseminated liquid was often frothy). These pockets were not present in the liquid used for the calibrations (the calibration spots of all the retardants were usually more idealized and perfect than generally found in the field). Some of the retardants, especially the Phos-Chek solutions, also sometimes contained a density gradation at the periphery of the spot (often nonuniform in direction) which imposed further uncertainty on where the measurements should be made. In addition, the Fire-Trol 100 spots usually contained small

instabilities or jets at the periphery which were roughly accounted for in the measurements. In general each retardant and drop size range (and sometimes the different samplers) posed its own particular problems with regard to the uncertainty in the measurements (even though they were often small) and it would be hoped that statistically these uncertainties would be largely averaged out in the measurements. The uncertainties also include personnel differences in making the general measurements and correcting for spot imperfections since more than half a dozen people participated to some extent at various times in the reduction of the rotating sampler and impact card data.

#### 4.1 CORRELATIONS OF DROPLET SIZE

##### 4.1.1 Comparison of Camera and Sampler Data

Since the camera and Sampler No. II (the spiral sampler) were at the same general location in the ground pattern in the tests, it would be expected that the droplet sizes they measure should be roughly the same. Unfortunately the camera measurements were usually for a shorter time period than the sampler, as discussed previously. The sampler measurement should represent essentially the droplet size distribution of the entire rain duration at that location, but the camera represents only the initial (but usually the most significant) portion of the rain. However, it is possible to compare the maximum droplet size measured by both the camera and sampler during the measurement time of the camera, as well as the mass mean diameter of the droplets measured during this period. Table VII shows a comparison of the data. It may be seen that the maximum size of the droplets

TABLE VII. COMPARISON OF THE DROPLET SIZES MEASURED BY THE CAMERA AND CORRESPONDING ROTATING SAMPLER (NO. II) DURING THE CAMERA MEASURING TIME

Fluid	Drop Number	Maximum Diameter		Ratio	Mass Mean Diameter		Ratio
		Camera (mm)	Sampler II (mm)		Camera (mm)	Sampler II (mm)	
1.6 Phos-Chek	169	12.3	10.1	1.22	10.8	8.4	1.29
1.6 Phos-Chek	168	10.9	6.3	1.73	7.4	4.6	1.61
Phos-Chek XA	155	11.3	9.0	1.26	7.7	6.0	1.28
Phos-Chek XA (180 knots)	161	7.1	5.7	1.25	5.9	3.8	1.55
0.42 Phos-Chek	163	8.1	6.5	1.25	5.2	3.5	1.49
Fire-Trol 100	240	4.8	*	*	2.8	*	*
Fire-Trol 931	165	5.3	4.3	1.23	2.8	3.1	0.9
Water	151	2.8	*	*	1.9	*	*

\* No data was obtained on Sampler No. 2

as measured by the camera is roughly 25% greater than the corresponding sampler measurement, except for the one test of the thick Phos-Chek XA solution for which it is much greater (73%). The mass mean diameter of the droplets as measured by the camera are likewise significantly larger than by the sampler except for the Fire-Trol 931 for which the measurements are roughly the same. No sampler data was obtained near the camera for Fire-Trol 100 and water, but comparison with the other sampler data suggests that the maximum droplet sizes are roughly the same for both measurement techniques in these cases. Moreover, the mass mean diameter of water obtained by the camera over a long time duration (11 sec) was roughly the same as measured by the samplers. This suggests that the camera and impact samplers may actually be in rough agreement for the smaller droplet fluids (water and the two Fire-Trol solutions), and the largest discrepancy occurring for the larger droplet fluids (the Phos-Chek XA solutions). There is no firm data for this hypothesis however.

The reason for the general discrepancy between the results for the two techniques could not be determined, in spite of extensive effort to do so. It is possible that a more reliable correction curve for image size than that given in Figure 26, or the reduction of more of the film frames, could result in better agreement between the two techniques. Likewise the acquisition of more impact sampler calibration data at larger droplet size than used in Figure 29 may also result in improvement (a linear fit to the data may be preferable to the parabolic form used). For the present however, the problem has not been resolved. In the following general comparison of the droplet sizes of the various retardants, emphasis is placed on the rotating impact sampler measurements since they represent most of the rain droplets; whereas the camera measurements represent only the initial portion of the rain. However, it should be kept in mind that the absolute values of the droplet sizes as given by the samplers (especially for the Phos-Chek XA solutions) may possibly be larger (e.g., by 25%) as suggested by the camera measurements.

#### 4.1.2 Effect of Ground Concentration

An inspection of Figures 30-44 shows that the droplet size in the field depends to some extent on the location in the ground pattern, i.e., on the ground concentration. It is to be expected that the droplet size should generally be smallest on the periphery of the pattern since small droplets, in the settling droplet cloud, will undergo greater spreading than larger droplets due to (turbulent) diffusion. The general effect will be modified (directionalized) and amplified by wind, and is especially evident in Figures 30 and 32.

The droplet size upstream of the heavy (effective) concentration pattern (1-2 g/c)\* should in principle be smaller than that in the heavy pattern. This is because the dropped liquid initially undergoes surface stripping (erosion) while traveling at essentially the full aircraft velocity

---

\* The symbol (g/c) represents the ground concentration of retardant in gallons per 100 square feet of ground area.

but after the subsequent breakup of the bulk liquid into smaller particles by Taylor instability, the particle stripping occurs at a lower velocity.<sup>4</sup> This effect is generally supported by the data given in the figures (other card data further upstream of that shown in the figures is also available), and will be discussed further later. Finally, it may be noted that some of the data suggests that the droplet size often tends to increase with increased ground concentration, especially in localized areas where the liquid concentration increases significantly. The latter is the case for example in the data given by SI(DN-163) (DN is drop number), SIII(DN-169), SIII(DN-161), SI(DN-157), and SIII(DN-162). For the DN-162 water test, sampler III was in a high concentration region (1.9 g/c) and was oversaturated in several sectors so that the droplet size distribution could not be measured. Nevertheless the mass mean diameter of the largest drops of the first sector (3.2 mm) were significantly larger than the measured values in regions of lower concentration.

The preceding trend of larger droplets in higher concentration regions was not always consistent however (e.g., SIII, DN-147). This could be due to the particular liquid that fell on the samplers, or error in the measurement of the droplet size or the localized ground concentration (the concentration gradients were sometimes relatively large in the vicinity of the samplers). Nevertheless it is believed that the data generally do suggest that the droplet size depends to some extent on ground concentration (the general effect may depend on both the retardant and concentration level), especially in localized heavy concentration regions of the pattern. The reason for this, if true, is not known, but is consistent with the notion that a large concentration of moving liquid particles undergoing surface erosion (the Taylor breakup particles) will set the air in motion. Consequently the erosion of a portion of the particles will occur at a lower relative air velocity than for stagnant air which will tend to increase droplet size.

#### 4.1.3 Comparison of Retardants

A comparison of the droplet sizes produced in the various tests (Figures 30-44) shows definite trends in droplet size for the various retardants, i.e., different droplet sizes are produced by the different retardants for the same drop conditions. However, the general scatter in the experimental measurements together with the potential effect of ground concentration on droplet size makes it difficult to assign a mean value for droplet size of a retardant that is either valid statistically or that has meaning with respect to all the pattern. The degree of scatter in the measurements is not surprising, all things considered, and in general is quite reasonable considering the field nature of the measurements and the exploratory nature of the program. Measurements on the droplet sizes produced by the breakup of small jets under carefully controlled laboratory conditions in the literature have often yielded even less consistent results.

With regard to ground pattern, one means of treating the data would be to assign droplet sizes to various concentration regions of the pattern on the basis of experiment, and average over the entire pattern. This procedure, while possibly correct in principle, did not appear useful for the present program since the droplet size was not obtained at all concentration levels for all retardants, and it was not possible to determine an

unique dependence of droplet size on pattern concentration. It would also entail significant effort which, without the use of proper data for the averaging process, would be of little value and may possibly lead to confusing results.

For the present purposes then, it appears most useful to consider the general magnitude of the droplets produced in and near the high (effective) concentration pattern of the various retardants, keeping in mind the various factors regarding concentration and pattern effects discussed previously. This size then may be considered to be representative of the droplets that are on the average present in and near the most useful portion of the ground pattern, but some fluctuation within the pattern would be expected (probably accompanying concentration fluctuations to some extent). As to whether these sizes are valid under drop conditions that produce very large ground concentration levels, e.g., 2-6 g/c, is not known but the relative values determined under the present test conditions should be indicative of the relative values of the different retardants under higher concentration dissemination conditions.

The determination of a mass mean droplet size that roughly represents the effective ground pattern cannot be made directly however, and requires the use of assumptions. The simplest assumption is that the droplet size distribution in and near the particle cloud that produces the effective ground pattern is constant (uniform), and was measured to various degrees of accuracy by all of the sensors. In this case the mass mean diameter of the droplets measured by the three rotating impact samplers can be obtained directly by evaluating the combined data of the samplers of each test matrix condition using Eq. (17) (the camera data is not used in obtaining the mean diameter since it only measured the initial portion of the rain flow). The first droplet size column in Table VIII (denoted by Eq. (17)) shows the results of these calculations. In some cases difficulty was encountered

TABLE VIII. EXPERIMENTAL MASS MEAN DROPLET DIAMETER OF THE RETARDANTS IN AND NEAR THE EFFECTIVE GROUND PATTERN

Retardant	Drop Speed (knots)	Mass Mean Droplet Diameter (mm)		
		Eq. (17)	Direct Average	Normalized Eq. (17)
1.6 Phos-Chek	130	8.7	6.4±1.5	8.2
Phos-Chek XA	130	5.2	4.8±0.9	5.2
Phos-Chek XA	180	4.6	4.0±0.9	4.5
0.42 Phos-Chek	130	3.4	3.6±0.4	3.5
Fire-Trol 100	130	2.6	2.5±0.4	2.5
Fire-Trol 931	130	2.3	2.3±0.2	2.2
Water	130	1.6	2.0±0.4	2.0



in determining what data should be used in the computations so that the results would be indicative of the effective ground pattern and also be essentially directly comparable. The mean sizes given in the table were obtained after some consideration. The values for 1.6 Phos-Chek XA, Phos-Chek XA at 180 knots, 0.42 Phos-Chek XA, Fire-Trol 100 and water represent the mean of the data obtained from all the rotating impact samplers for both tests of each of these retardants. For Fire-Trol 931 the value is the mean of the impact sampler data for drop test no. 165 only, since for test 166 the main pattern was at some distance from the sensors. The data for normal Phos-Chek XA is the average of all impact samplers for both tests except for SIII(DN-155) which was at low ground concentration and whose mean value was low by more than  $2\sigma$  from the computed mean.\* The experimental drop sizes were normalized to constant velocity by assuming that the droplet diameter varies inversely with the aircraft speed.

The preceding assumption that the droplet size distribution is the same everywhere in the effective portion of the particle cloud is probably only an approximation. It is more likely that it varies to some extent in the cloud depending on certain factors such as particle concentration (wind and cloud diffusion will also affect the distribution). The evaluation of mean droplet size in this case cannot be made rigorously. The most simple and direct approximate method is to merely average the experimental mean diameters obtained from the various samplers (Figures 30-44). The second column in Table VIII shows the results of this calculation, together with the uncertainty (standard deviation) of the computed values. The same samplers as before were used in these calculations, and in addition a value of 5.2 mm from the cards was entered twice in the weighting for Phos-Chek XA (130 knots) since several good cards filled with many droplets whose average size was about 5.2 mm were obtained in these tests.

Another method of estimating the mean droplet size of the particle cloud, assuming it to be slightly non-uniform as just discussed, is to use Eq. (17) as done initially. In this case however, it is necessary to weight (normalize) the data obtained by the spiral impact sampler (No. II) when combining it with the other samplers, since it had a much smaller collection area than the other samplers. The droplets obtained after the first revolution of this sampler were also ignored in this calculation for simplification purposes (samplers I and III only underwent one revolution). The results are shown in the last column of Table VIII.

It may be seen from Table VIII that a definite trend in mean droplet size was obtained for the various retardants, and this trend is independent of the method used to average the experimental data. The absolute magnitude of the values depends to some extent on the averaging method but the effect is relatively small for the small drop size retardants. With regard to the absolute values obtained, the general difference between the values obtained by the camera and the rotating samplers should also be kept in mind. There is no obvious reason for preferring the values of any of the three methods of computing the averages, but the values obtained using the normalized Eq. (17) procedure generally lie between those of the other two procedures.

---

\*  $\sigma$  in this expression is the standard deviation.

It may be seen from the table that the droplet sizes of the higher effective viscosity (gum thickened) fluids (the Phos-Chek XA solutions) are greater than those of the lower viscosity liquids (the Fire-Trol solutions and water). The droplet size of the Phos-Chek XA solutions increases with increase in gum thickener concentration, as shown in Figure 45. The values extrapolate in a normal manner to the water value at zero gum thickener concentration.

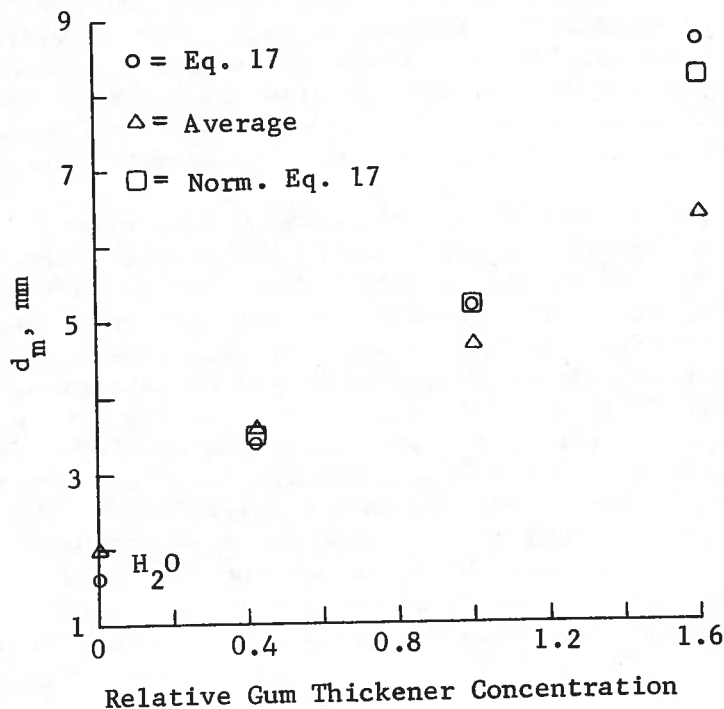


Figure 45. Experimental Effect of Gum Thickener Concentration on the Mass Mean Droplet Diameter of the Phos-Chek XA Solutions.

The mean values of droplet size for the various contemporary retardants given in Table VIII are consistent with retardant experience in the field. Thus from ground recovery experiments (evaporation effects), cloud settling times and wind-drift and other observations it has been determined qualitatively that the droplet size of Phos-Chek XA is significantly larger than those of Fire-Trol 100 and Fire-Trol 931, which are roughly comparable, which in turn are a little larger than that of water. Table VIII substantiates these observations on a quantitative basis. It should also be noticed from Figures 30-44 that the size distribution of the droplets for the gum thickened retardants covers a much wider range than for the other retardants with lower effective viscosity.

#### 4.1.4 Effect of Air Speed

A comparison of the mean droplet sizes of Phos-Chek XA at 130 and 180 knots shows that the droplet size decreases with increase in drop velocity. This effect will be discussed in more detail later.

#### 4.1.5 Temporal Aspects of Droplet Impaction on the Ground

The droplet size data summarized in Figures 30-44 for the rotating impact samplers represent essentially all the droplets in the particle cloud (except those blown to the side by wind), while the camera data represents the first several seconds of droplet fall. However, since larger droplets fall faster than smaller ones, the size distribution of the droplets that fall on the fuel at any time during cloud settling is not the same as that of the final (total) distribution, but rather is a distribution that contains the effects of the fall rate of the droplets. Figure 46 shows the mass mean diameter of the impacting droplets vs time as obtained from the high speed camera measurements (zero time corresponds to the first frame measured). It will be observed that the larger drops reach the ground first, and that the average size of the falling droplets decreases with increasing time. The rate of decrease of droplet size with time is larger for fluids with larger droplet size. Thus the droplet size of the Phos-Chek XA solutions falls off rapidly with time, but the size decreases only very slowly for the Fire-Trol solutions and water.

Figure 47 illustrates the entire size distribution of the impacting droplets vs time, as measured by the rotating impact samplers. As discussed previously these samplers revolved at the rate of about 7 to 10 sec/rev, and contained a sampler wheel made up of 5 sectors of paper. The times given in the figure represent the distributions on the various paper sectors (zero time is the first sector hit by the droplets). Sampler II produced a spiral which allowed more than a complete revolution of sampling time (most of the liquid mass reached the ground within one revolution of the wheel).

Figure 47 shows in agreement with the camera data that the larger droplets reach the ground first. However, the earlier impacting mass also contains some smaller droplets, i.e., a distribution of sizes is present at all times in the impacting liquid. The droplet size range becomes more narrow as the mean droplet size becomes smaller with increasing time. Likewise, the size distributions of the retardants with smaller droplet size, i.e., the two Fire-Trol solutions and water, are more narrow than those of the Phos-Chek XA solutions.

#### 4.1.6 Droplet Impact Velocities

As discussed previously, by advancing or retreating the frames of the camera film it was possible to measure the distance the droplets fell in front of the grid in a known time period, and from this data to obtain the impact (terminal) velocity of the droplets. Figure 48 shows the values obtained for various sized droplets of the retardants. There is some degree of scatter in the data and this is due in part to the fact that for non-vertically falling droplets the vertical component of fall was mistakenly used as the fall distance between frames rather than the actual fall path distance. Also, in some cases, particularly when many droplets were present, it was difficult to positively identify the same particle in two adjacent frames. This latter was also the probable cause of obtaining a number of experimental velocities (not shown) that differed very significantly from the values given in the figure.

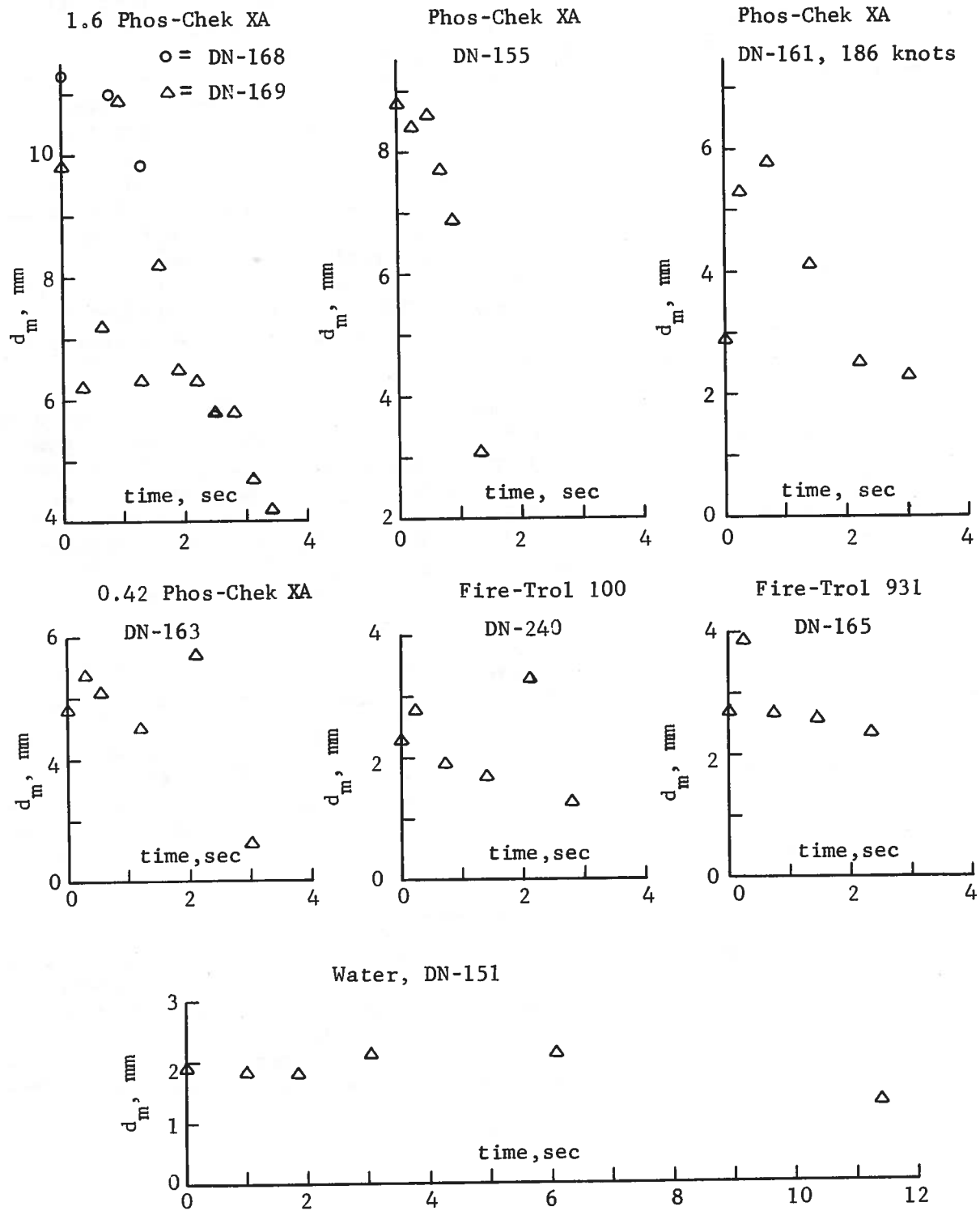


Figure 46. Mass Mean Diameter of the Impacting Droplets versus Time, as Measured by the Camera Technique.

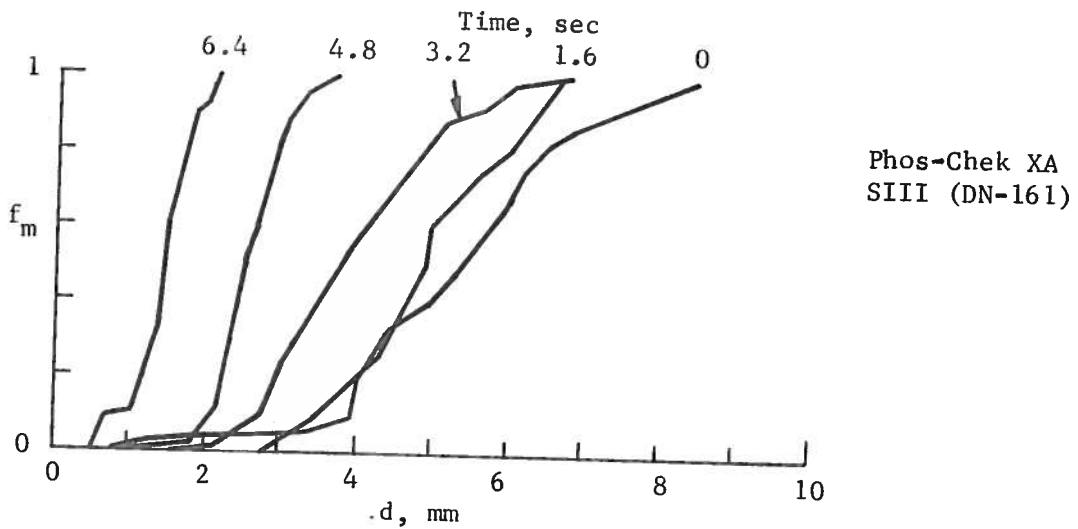
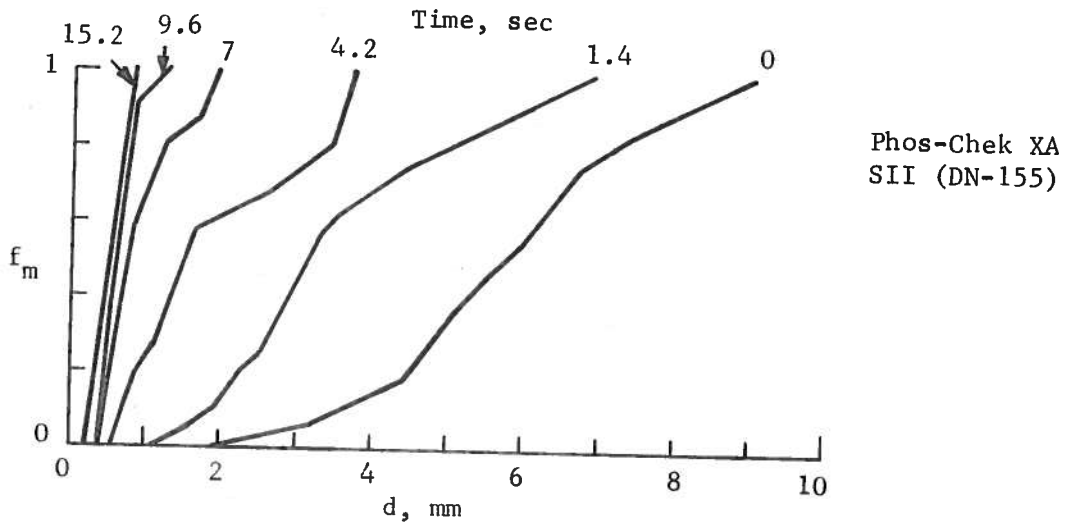
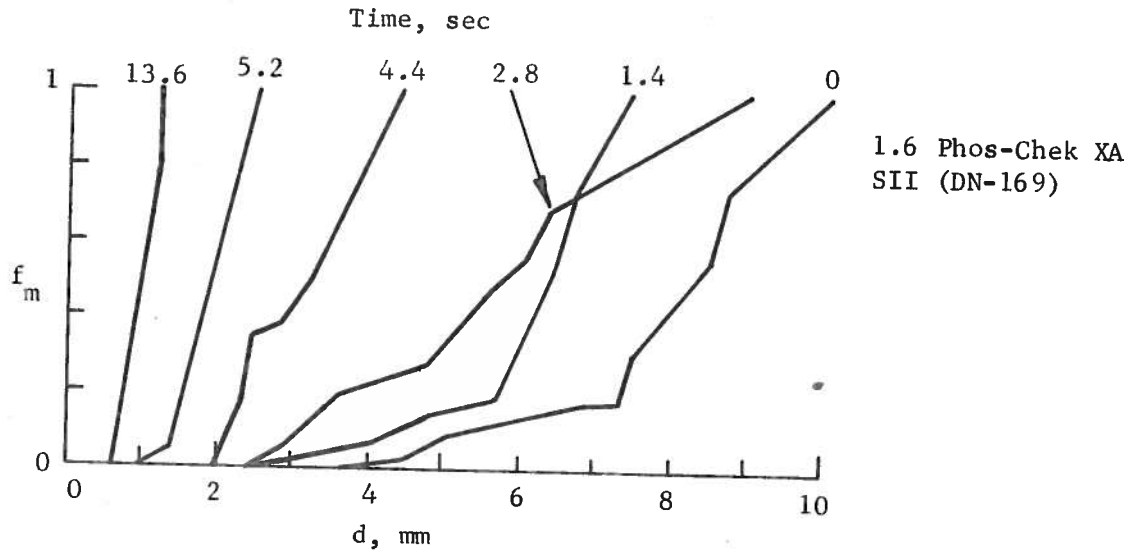
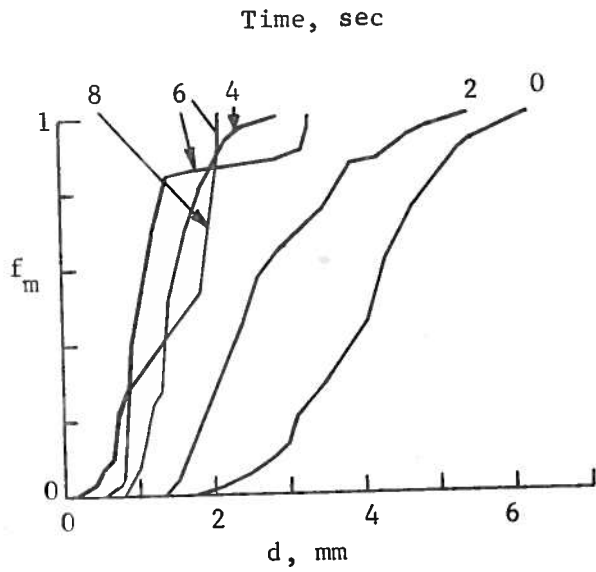
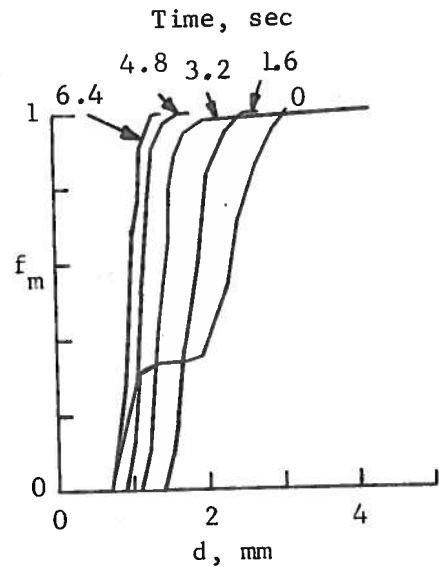


Figure 47. Droplet Size Distributions of the Impacting Droplets versus Time as Measured by the Rotating Impact Samplers.

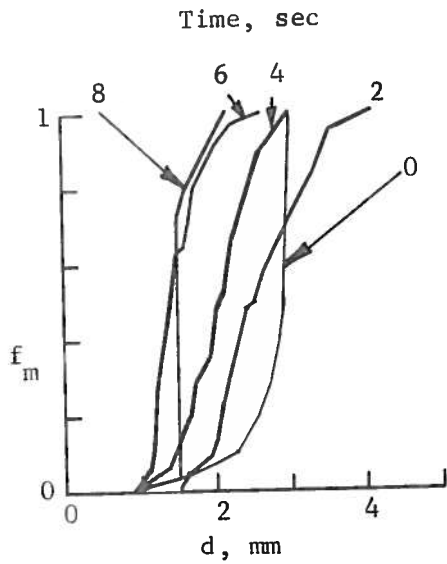
0.42 Phos-Chek XA  
SIII (DN-163)



Water  
SI (DN-162)



Fire-Trol 100  
SIII (DN-160)



Fire-Trol 931  
SIII (DN-165)

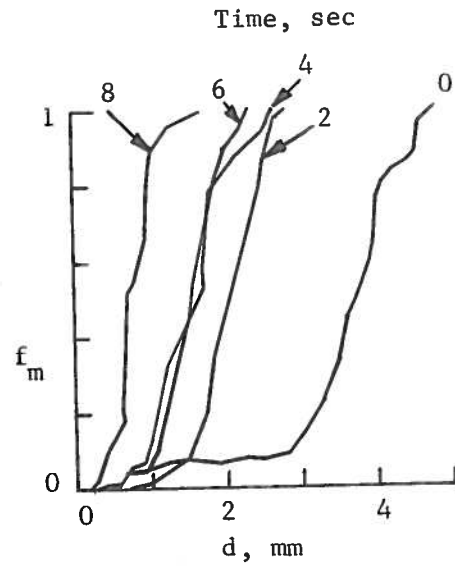


Figure 47. Concluded.

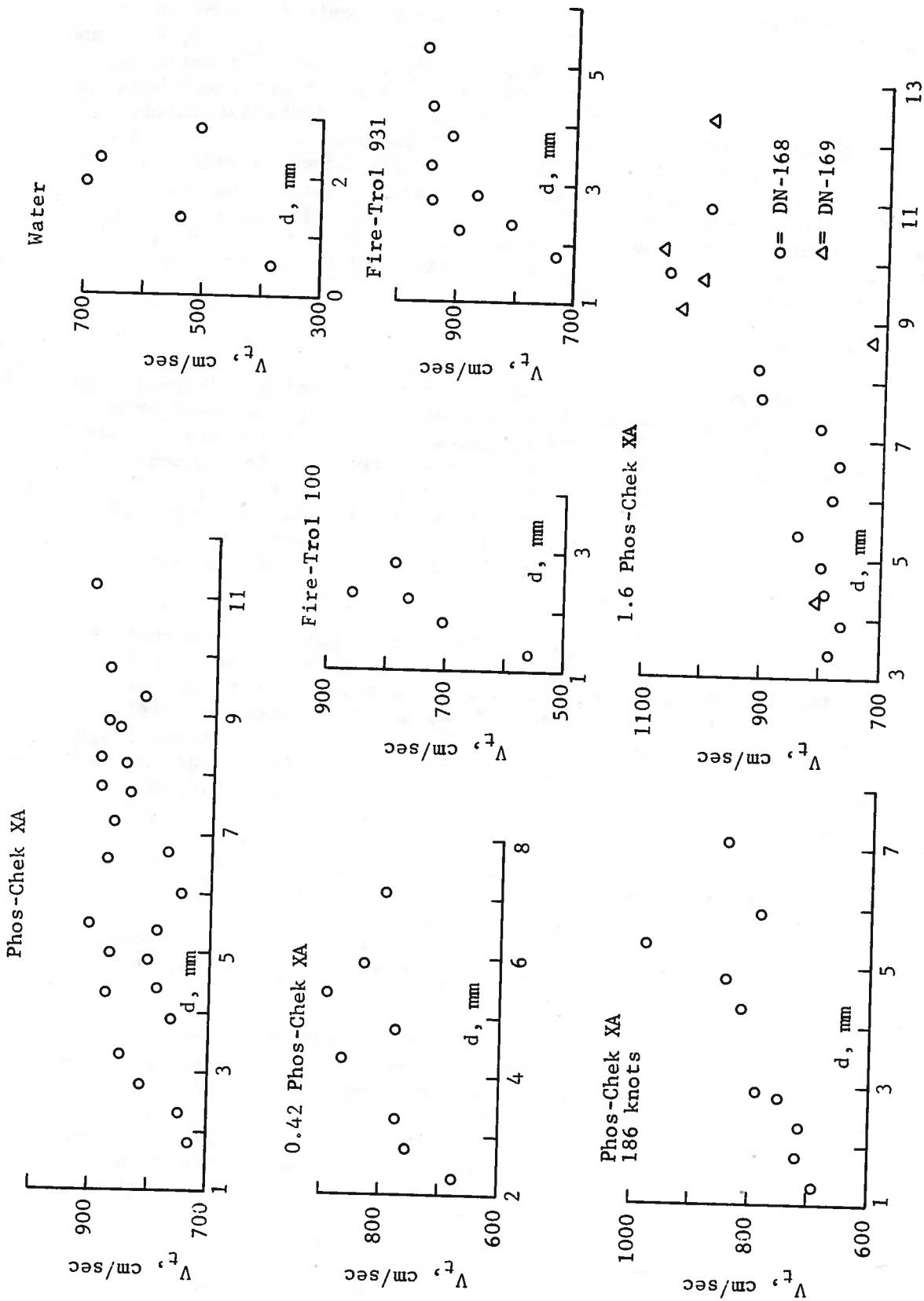


Figure 48. Terminal Velocities of the Droplets vs Drop Diameter, as Measured by the Camera Technique.

The measured velocities of the retardant droplets may be compared with those given in the literature for water, viz, for  $d = 1, 2, 3, 4, 5$  and  $6$  mm, the literature values are 403, 651, 801, 880, 914 and 923 cm/sec, respectively (Ref. 3, p. 122). In general there is rough agreement between the trend of the data in Figure 48 and these values, and the literature values suggest what points are grossly in error in the figure. Often the data given in the figure is slightly on the low side compared with the literature values. This may be due in part to the vertical component measurement mentioned previously. The density of the retardants is greater than that of water and this should increase their velocity (Eq. (85), ref. 3). However the drag coefficient may also differ and it is not possible to estimate this effect in an a priori manner.

#### 4.2 GROUND CONTOUR PATTERN

The gross ground patterns produced by the aerial dissemination of the various retardants used in the tests are shown in Figures 30-44, and the Forest Service also provided more detailed patterns of the tests. These patterns were examined in some detail with regard to obtaining information relating to the effect of retardant rheology on ground contour pattern. Unfortunately the scatter in the general patterns produced in individual identical tests together with wind effects (which often were possibly largely responsible for the scatter) precluded obtaining definite correlations, although some general trends were obtained.

As may be seen in the figures, the general pattern consisted of a very light ground concentration profile starting roughly at the initial point of door opening and increasing in surface density downstream (as more falling liquid becomes exposed to the airflow) until the dominant (effective) portion of the pattern is attained. This effective portion consists roughly of an outer  $1$  g/c ellipse which contains higher liquid density regions inside. The  $1$  g/c pattern is surrounded by a decreasing density profile, which in the forward direction usually rapidly comes to an end (in the absence of a tailwind). The light density portion of the pattern is affected strongly by wind, and its extent in any direction depends on wind direction. Retardants with small droplets (FT-100, FT-931,  $H_2O$ ) are generally affected to a greater degree than those with larger droplets, but the overall effect can be influenced by localized gusts, altitude gradients in wind and other factors. These same factors also can perturb the main pattern to various degrees depending on conditions.

The length of the  $1$  g/c pattern of the Phos-Chek XA solutions was on the average a little under 300 ft (wide fluctuations were observed), and the average length of the smaller particle retardants (FT-100, FT-931,  $H_2O$ ) was slightly shorter. The average maximum width of the patterns of all retardants was roughly the same, as was the product of length times maximum width. The actual areas of the  $\geq 1$  g/c pattern of the retardants were not measured because of wind effects on the patterns. The wind in general appeared to often have a significant effect on the general heavy pattern which not only caused distortion and twisting of the pattern in many cases, but also caused breakup of the heavier concentration patterns within the  $1$  g/c region into two or more distinct regions as well as breakup of the  $1$  g/c pattern itself. Some of this breakup and general perturbation of the heavy pattern may be due to statistical fluctuation of tank performance or aircraft path or attitude but the cause is often difficult to ascertain.



The 1 g/c pattern of the retardants generally contained a smaller concentric 2 g/c ellipse within itself (or two or more smaller regions of 2 g/c localized concentration). In some cases one or more very small localized regions of 3 g/c were present within the 2 g/c pattern. In the case of 1.6 Phos-Chek however (both tests), a relatively large 3 g/c region was present, and within this boundary one or more significant 4 g/c tracts were also present. In general the data indicated that higher effective viscosity fluids tend to produce more localized ground regions with higher liquid concentration than do the lower viscosity fluids. On the other hand the 180 knot Phos-Chek XA tests tended to reduce the number and size of the 2 g/c regions and none of the 5 tests resulted in any even very small 3 g/c regions. Thus increasing aircraft speed appears to reduce localized ground concentration levels.

#### 5. CORRELATION WITH THEORY

Over the years that aerial dissemination of liquid retardants has been used in fighting large fires it has become known that thickening the fluid, i.e., increasing its viscosity, causes the liquid to breakup into larger droplets (to various degrees), which improves its dissemination characteristics. However the mechanics of droplet formation as well as the important parameters and factors that control the droplet size were not quantitatively understood. Nevertheless it was recognized that some thickeners were preferable to others in use. In previous studies on this program it was shown that all the conventional thickened retardants are non-Newtonian in flow behavior, and in particular are shear-thinning in nature, i.e., the apparent viscosity of the retardant decreases with increase in shear rate. This demonstrates that the apparent viscosity of the liquid at the high shear rate experienced by the retardant under aerial dissemination conditions is smaller than that measured at low shear rates by conventional techniques, e.g., by a Brookfield viscometer. Thus the normally measured (Brookfield) viscosity is not a reliable basis for evaluating the potential relative breakup characteristics of various retardants. Figure 49 shows the apparent viscosity of the retardants vs shear rate obtained during the current and earlier phases<sup>3,4</sup> of this program. It may be seen that there is no obvious correlation between the apparent viscosity (at either the Brookfield or higher shear rate) and the relative ordering of the experimental droplet sizes of the retardants summarized in Table VIII.

However it was shown in the earlier experimental studies that some of the retardants are elastic in nature under high shear conditions. It was discussed in ref. 3 that the elasticity (as well as viscosity) retards the flow, and that the combined effect of the apparent viscosity and fluid elasticity on the flow behavior of a liquid is best described in terms of an effective viscosity,  $\eta_e$ , which is defined in Eq. (1) of this report. It is thus the effective viscosity which controls the droplet size of the aeri-ally-dispersed retardants. Figure 50 shows the experimental effective viscosity of the various retardants vs shear rate obtained during the current and earlier phases of the program. The recoverable shear vs shear rate curve on which the effective viscosity curve of Phos-Chek XA is based was given initially in Figure 4 of ref. 4. The units of this curve were somehow inadvertently shifted a small degree during

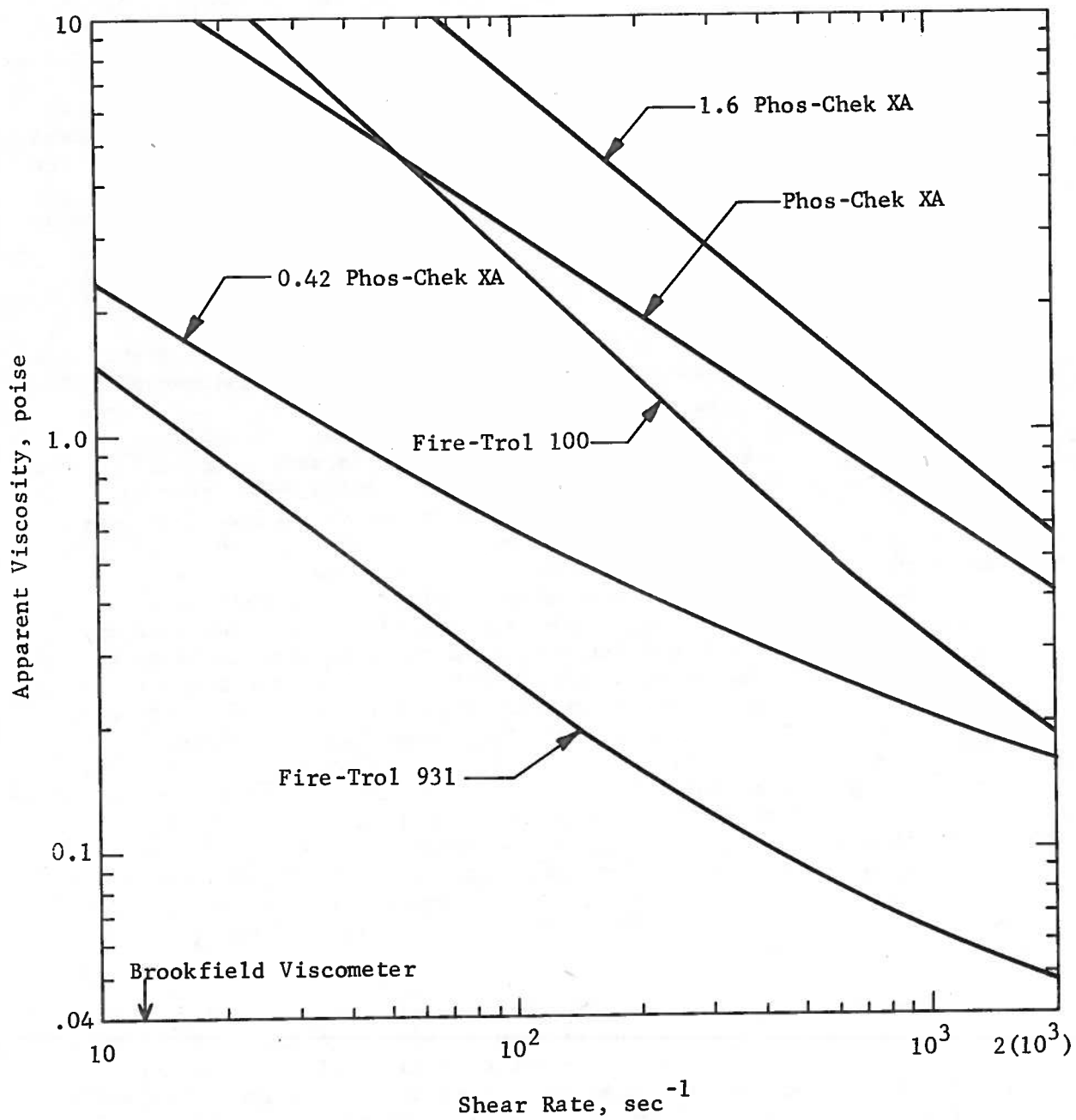


Figure 49. Apparent Viscosity vs Shear Rate of the Fire Retardant Solutions.

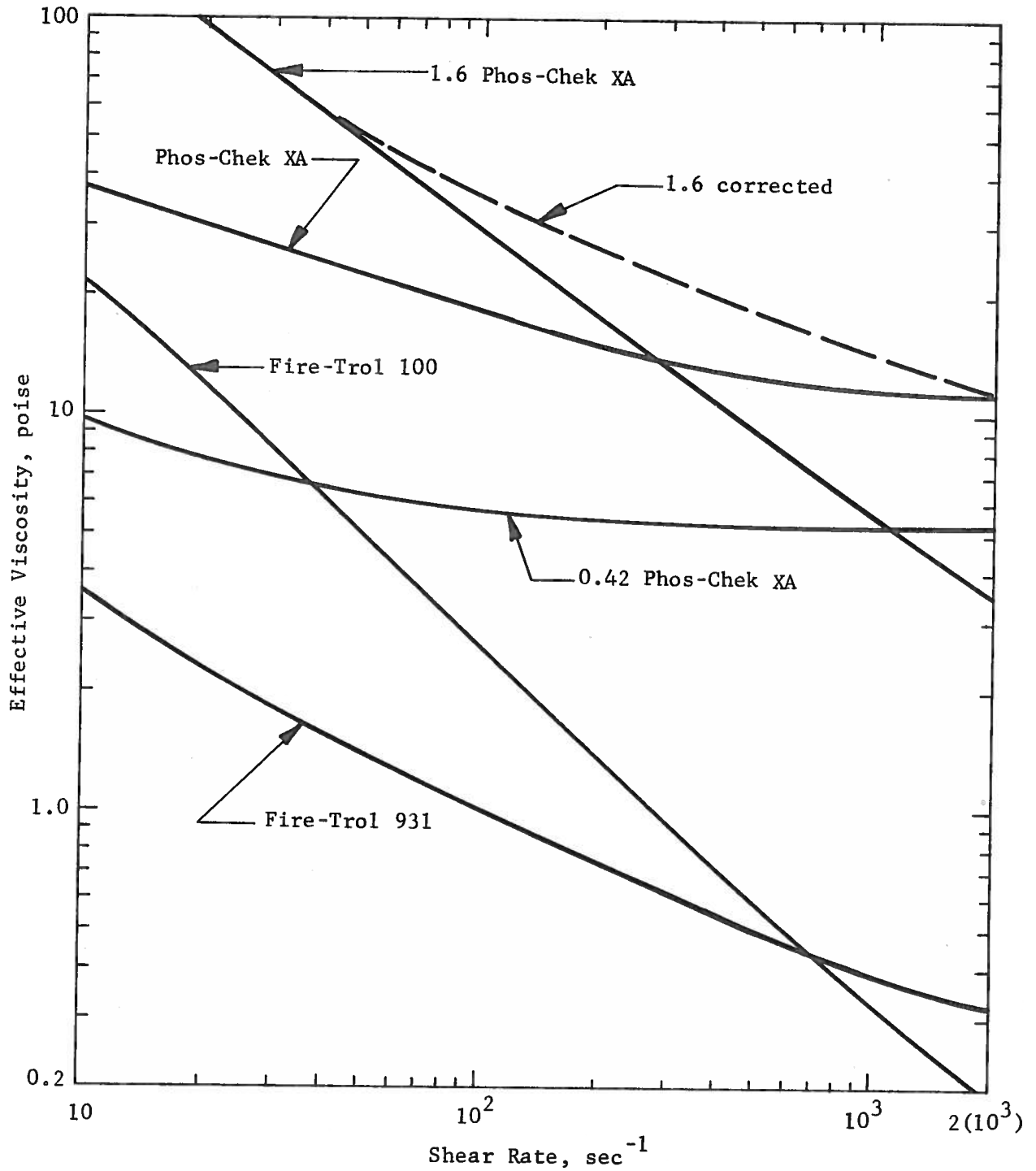


Figure 50. Effective Viscosity vs Shear Rate of the Fire Retardant Solutions.

preparation and the curve is consequently not quite correct. The correct curve is given in Figure 13 of this report. However the correct data was used in evaluating the effective viscosity curve of that reference (Eq. (5) of ref. 4). The equations for the effective viscosity of the Fire-Trols were given in Eq. (6) and (8) of ref. 4. The equation for Fire-Trol 931 was not an especially good fit of the data at the higher shear rates, and a better equation is

$$\begin{aligned} \text{Fire-Trol 931} \quad (10 \leq \dot{S} \leq 10^4 \text{ sec}^{-1}) \\ \log \eta_e = 1.6974 - 1.7974 \log \dot{S} + 0.8718(\log \dot{S})^2 \\ - 0.2567(\log \dot{S})^3 + 0.02898(\log \dot{S})^4 \end{aligned} \quad (18)$$

The equations for the 0.42 and 1.6 Phos-Chek XA solutions were given in Table IV of this report.

### 5.1 TERMINAL DROPLET SIZE

In references 3 and 4 a model was developed for estimating the terminal droplet sizes of aerially-dispersed retardants as a function of fluid properties and aircraft velocity. It was shown that the droplet size should be smaller in the initial (ineffective) portion of the ground pattern (peripheral stripping region) than in and near the subsequent heavy (effective) region which is produced as the result of the Taylor instability breakup of the bulk liquid. The reduced velocity at which the liquid surface stripping occurs after Taylor breakup is responsible for this increase in size (the initial velocity of the liquid is the aircraft velocity).

In Table III of ref. 4 estimates were made of the droplet sizes (mass mean and the entire distribution) for Phos-Chek XA, Fire-Trol 100, Fire-Trol 931 and water, and similar estimates were early made for 0.42 and 1.6 Phos-Chek XA on the current program. A comparison of the calculated droplet sizes with the experimental values given in Table VIII of this report shows rough agreement for Phos-Chek XA at 130 knots, but the values for the other retardants (also at 180 knots) differ significantly. However a modified calculation given in Table VI of ref. 4 which was based on a smaller dependence on effective viscosity shows rough agreement also with the Fire-Trol solutions. Since the time that the analysis and droplet size calculations on the present program were conducted, more extensive studies of liquid breakup have been conducted on another program. These studies together with the trend of the experimental droplet sizes obtained on the current program show the reason for the discrepancy between the previously calculated and experimental values, and indicate how the model can be modified in an approximate manner so that it is in essential agreement with experiment for predictive purposes. This modification will now be discussed.

#### 5.1.1 Mass Mean Diameter Equations

The number mean diameter,  $d_m$ , of the droplets stripped aerodynamically from liquid moving at a high velocity through air is given by the capillary wave equation discussed and used in references 3 and 4, i.e.,

$$d_m = (9/2) F(g/f)^{2/3} \quad (19)$$

$$f = (\pi/2 \rho_1 \sigma)^{1/2} \beta \rho V^2; \quad g = 8\pi^2 \eta_e / \rho_1 \quad (20)$$

where  $\rho_1$ ,  $\sigma$  and  $\eta_e$  are the density, surface tension and effective viscosity of the liquid,  $\rho$  is air density,  $V$  is the relative velocity between the liquid and the air stream, and  $\beta$  and  $F$  are parameters discussed in ref. 3. Equation 19 is for a single stage stripping process, and indicates that the mean droplet size should be proportional to the two-thirds power of the effective viscosity - which was the basis of the previous calculations. This equation is a good approximation to an equation (Eq. 14 & 17, ref. 3) whose value depends only relatively weakly on the size of the maximum wavelength excited on the stripping liquid (a wavelength distribution function can be used to obtain the droplet size distribution).

The mass mean diameter of the droplets is given by Eq. (21) of ref. 3. However unlike the equation on which Eq. (19) is based, the mass mean equation depends significantly on the value of the maximum stripping wavelength, and hence on the liquid dimensions. In the previous studies it was assumed that there was no secondary breakup of the droplets produced by the bulk stripping process (ref. 3, Section 4.1.3), and the wavelength cut-off was determined by the same fractional number criteria approximation as used in the number distribution calculations. This in essence causes the mass mean diameter equation to reduce to the same form as Eq. (19) except that it is a small factor ( $\sim 3$ ) larger. However, based on subsequent studies it is now known that a large distribution of droplet sizes is produced in the initial (primary) stripping process, and that the larger of these droplets then undergo further (secondary) breakup. The calculation of the wavelengths that determine the final (observed) droplet size distribution should therefore in principle include the secondary breakup process. However the results of this calculation show that the preceding direct functional relationship between the final number and mass mean droplet sizes is essentially retained, and thus the preceding procedure appears to represent an approximate manner of by-passing the secondary breakup calculations. It was also found that the functional dependence of droplet size on viscosity given by Eq. (19) is larger than found by experiment, and that this appears to be a defect in the fundamental equations on which this equation is based.

The solution of the breakup equations including secondary breakup is very complex and cannot be considered here. However based on the preceding results it is possible to modify the previous model so that it retains most of the important physics of the breakup process (including the effect of shear rate on the effective viscosity), and simultaneously is essentially accurate in its predictive behavior. To begin with, as just noted the experimental overall effect of viscosity on the mass or number mean droplet size found in the literature from studies on small

jets and drops is much lower than the 2/3 power value given by Eq. (19). For example Ingebo and Foster<sup>6</sup> correlated a variety of studies and found the approximate value to be 0.25, while in a similar correlation Young<sup>7</sup> found 0.2. Weiss and Worsham<sup>8</sup> obtained a value 1/3 in their measurements, which are generally considered to be some of the most reliable available. It was found that most of the fire retardants given in Figure 50 also correlate quite well at the theoretical shear rate using the value of 0.333. Thus for practical purposes the viscosity dependence in Eq. (19) should tentatively be modified to this value.

In Eq. (81) of ref. 3, an expression for the parameter beta was given which was obtained in the shock tube studies. In the air velocity range of interest to fire fighting this equation can be simplified to

$$\beta = \frac{489.7}{V^{0.94}} \eta^{1/6} \quad (21)$$

where V is in cm/sec. Substituting this equation into Eq. (19) (considering the  $\eta^{1/6}$  term to be included in the modified  $\eta^{1/3}$  term of that equation) then gives the expression for mean droplet size. In order to improve the reliability of the equation for predictive purposes, the equation was fit to the mass mean droplet size (3.5 mm) of the 0.42 Phos-Chek XA solution and will be given subsequently.

The evaluation of the mean droplet size by the modified Eq. (19) requires the value of the effective viscosity, which depends on the shear rate. The shear rate is given by Eq. (28) of ref. 3, i.e.,

$$\dot{S} = 2f/L^{1/2} - 2g/L^2 \quad (22)$$

The number mean wavelength is given by  $(9/2)(g/f)^{2/3}$  and the mass mean wavelength by a factor approximately three times this value. Using a value of 3.6 (to improve the correlation) in Eq. (22) and including Eq. (21) then gives the shear rate.

The final equations for estimating the mass mean droplet size, effective viscosity and shear rate are then given by

$$d_m = \frac{15}{V^{0.7}} (\sigma \eta_e / \rho_1)^{1/3} \quad (23)$$

$$\dot{S} = \frac{16.36 V^{1.414}}{\rho_1^{1/3} \sigma^{2/3} \eta_e^{1/9}} \quad (24)$$

where the units of  $d_m$  is mm, V is knots,  $\dot{S}$  is  $\text{sec}^{-1}$ ,  $\sigma$  is dyne/cm,  $\rho_1$  is gm/cc and  $\eta_e$  is poise. In the calculation of  $d_m$ , the value of  $\eta_e$  is first determined by solving Eq. (24) simultaneously with the experimental relation between  $\eta_e$  and  $\dot{S}$  for the particular fluid.

### 5.1.2 Droplet Size In and Near the Effective Ground Pattern

In using Eq. (23) and (24) to estimate the droplet size, the proper velocity must be used. As previously pointed out, the liquid initially (in the ineffective ground pattern region) undergoes stripping at the full aircraft velocity. In this region then,  $V = V_a$ , where  $V_a$  is the aircraft velocity. However, the stripping occurs at a lower velocity in the effective (heavy) region of the ground pattern, since the liquid has been slowed as the result of the Taylor breakup process. In ref. 4 an analysis was made of the velocity of the liquid particles subsequent to liquid deceleration during the Taylor breakup process. It was concluded that except for very large load size and extreme values of length/diameter ratio of the tank, the effective air velocity for particle stripping is about 0.69 of the aircraft velocity,  $V_a$ . In the present program an additional analysis was made for the test liquids and conditions for the No. 5 compartment of the ETAGS tank. It was concluded that to very good approximation in all cases the velocity,  $V$ , of the liquid after Taylor breakup is given by

$$V = 0.7 V_a \quad (25)$$

This result is thus consistent with the previous conclusion.

Table IX summarizes the droplet sizes, shear rate and effective viscosity for the various retardants in the effective ground pattern region computed using Eq. (23)-(25).

TABLE IX. COMPUTED DROPLET SIZES OF THE RETARDANTS IN AND NEAR THE EFFECTIVE GROUND PATTERN

Retardant	Drop Speed (knots)	$d_m$ (mm)	$\dot{\gamma}$ ( $\text{sec}^{-1}$ )	$\eta_e$ (poise)
1.6 Phos-Chek XA	130	6.5	444	18.9
Phos-Chek XA	130	5.2	553	12.5
Phos-Chek XA	180	4.0	884	11.4
0.42 Phos-Chek XA	130	3.5	757	5.25
Fire-Trol 100	130	2.3	481	0.60
Fire-Trol 931	130	2.1	547	0.48
Water	130	0.6	928	0.01

The computed droplet sizes may be compared with the experimental values given in Table VIII. It is seen that the general agreement is quite good except for water, whose experimental value is significantly larger than the computed value. The deviation for water may be due in part to the fact that evaporation and/or wind drift of the smaller water droplets may have

caused the experimental droplet size to be larger than the actual value, and this may also have been true to a smaller extent for the two Fire-Trol liquids. Another possible explanation is that the actual viscosity dependence may differ to some extent from that given in Eq. (23).

The shear rates given in Table IX are generally slightly smaller than computed earlier.<sup>4</sup> Using a factor of three for the mass mean to number mean wavelength ratio rather than the value 3.6 used in obtaining Eq. (24) (the ratio actually varies slightly with conditions) would increase the constant in this equation by 29% (to 21.11) with an approximately corresponding increase in shear rate. This in some cases would result in slightly smaller droplet sizes. For example for the retardants given in Table IX the values would become 6.3, 5.1, 4.0, 3.5, 2.1, 2.0 and 0.6, respectively. Thus the change in droplet size only amounts to several percent.

The calculations for the 1.6 Phos-Chek XA solution are based on the corrected effective viscosity curve given in Figure 50. As discussed earlier, the experimental shear rate range of the elasticity measurements of the fluids using the Rotoviscometer is very limited and it is necessary to extrapolate the experimental data over a large range for use. However the Phos-Chek XA curve is known to be correct, and the 0.42 Phos-Chek XA curve is consistent with the XA results. On the other hand the 1.6 Phos-Chek XA solution elasticity curve (as well as others) deviated in a manner that didn't appear correct. Moreover the experimental effective viscosity curve of the 1.6 solution is not consistent with the other curves in explaining the droplet sizes.

In view of this, an attempt was made to correct the elasticity curve of the 1.6 solution. From the studies of ref. 9, 10 it was concluded that the recoverable shear,  $s$ , should be roughly relatable to the relative gum thickener concentration,  $C$ , and the shear rate over a restricted shear rate range by the equation

$$s = k(\dot{S}/C)^n \quad (26)$$

where  $k$  and  $n$  are constants. The constants were evaluated by fitting the equation to the recoverable shear vs shear rate curve of Phos-Chek XA at  $\dot{S} = 10^2$  and  $10^3 \text{ sec}^{-1}$ , giving  $k = 0.459$  and  $n = 0.514$ . The equation was tested by calculating  $s$  for the 0.42 Phos-Chek XA solution at the same shear rates. The computed values were 7.65 and 24.97, which are in very good agreement with the experimental values (8.82 and 24.85), thus giving support to the use of Eq. (26) to correct the 1.5 Phos-Chek XA curve. The computed values of  $s$  for 1.6 Phos-Chek XA at the preceding shear rates are 3.84 and 12.56, which when combined with the apparent viscosity gives the corrected curve for effective viscosity given in Figure 50. Similar corrections should be applicable to the other concentration solutions discussed earlier.



### 5.1.3 Effect of Gum Thickener Concentration

Figure 51 shows the computed effect of gum thickener concentration on the mean droplet size, and can be compared with Figure 45. The droplet size increases in a slightly non-linear manner with increase in gum concentration over the studied range, and drops off rapidly at small concentrations. The value for the 1.6 solution is consistent with the lower value given in Figure 45, giving support to that value. If the larger value is correct it would imply that the power of the effective viscosity in Eq. (23) becomes larger for this higher concentration solution.

### 5.1.4 Effect of Aircraft Velocity

Table IX shows that increasing the aircraft speed from 130 to 180 knots reduced the computed droplet size of Phos-Chek XA from 5.2 to 4mm. This reduction is consistent with the smaller experimental value given in Table VIII. The other values suggest a slightly smaller dependence on drop speed. The theoretical dependence on aircraft speed given in Eq. (23), i.e.,  $d_m \propto v^{-0.7}$ , is consistent with ref. 6 where a 0.75 power dependence was found. Reference 7 found a 1.0 power velocity dependence, and this value seems to appear most often in the literature. Reference 8 found a 4/3 power dependence.

The aircraft speed not only enters in the droplet size equation (Eq. (23)) in a direct manner, but it also affects the shear rate - which controls the effective viscosity of a non-Newtonian liquid. Figure 52 shows the computed effect of aircraft speed on droplet size. The relatively rapid rate of increase in droplet size of some of the retardants with reduction in air speed is due to the velocity effect on the shear rate. The use of a larger constant factor in the shear rate equation (Eq. (24)) would cause the curves of the two Fire-Trol solutions to cross at a lower velocity than shown in the figure.

### 5.1.5 Application to Retardant Development

The successful correlation of the experimental droplet sizes (within the experimental accuracy of the data) by Eq. (23), (24) and (25), indicates that these equations can be used as a guide in the development of liquid fire retardants with controlled rheological properties for producing droplets with a desired size. Thus Eq. (23) and (25) show that for a given airspeed, a liquid retardant with a specified density and surface tension would require a certain effective viscosity in order to produce the desired droplet size. However Eq. (24) shows that the stripping would then occur at a certain shear rate whose value depends on the effective viscosity. Thus it would be necessary for the retardant to have an experimental effective viscosity vs shear rate relationship (see Figure 50) such that (Eq. (23-25)) can be satisfied simultaneously. Table IX indicates that for airspeeds of about 130 knots the important shear rate range is about 400-800  $\text{sec}^{-1}$  for the various retardants studied on this program. However in general the shear rate that controls the mean droplet size of a particular retardant depends both on the physical properties of that retardant (especially effective viscosity) and the aircraft speed at which the retardant is dropped.

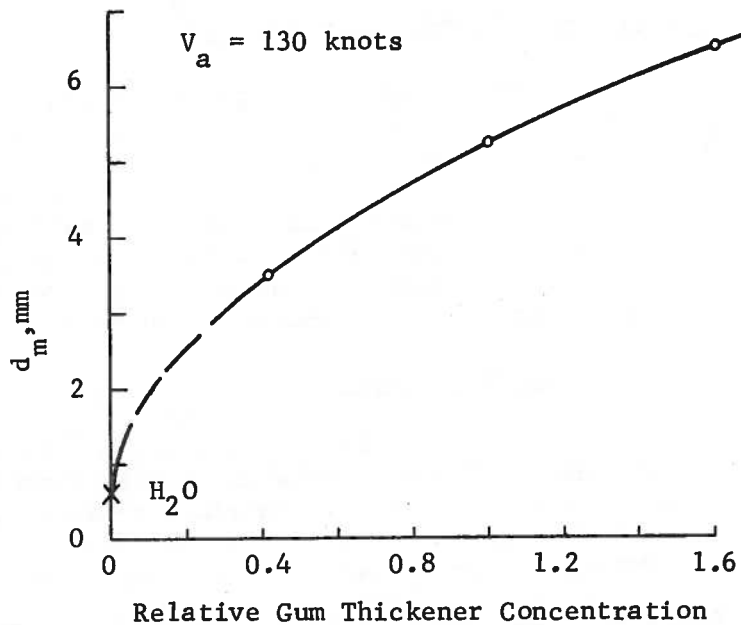


Figure 51. Computed Effect of Gum Thickener Concentration on the Mass Mean Droplet Diameter of the Phos-Chek XA Solutions.

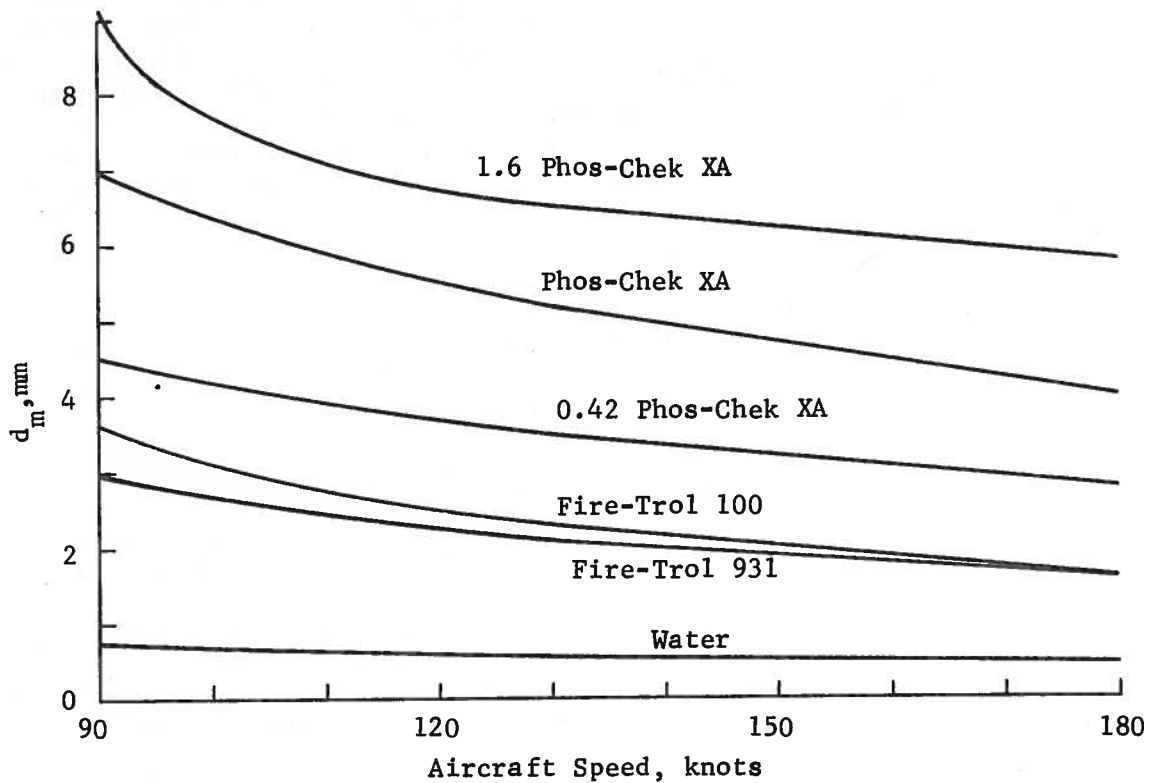


Figure 52. Computed Effect of Aircraft Speed on the Mass Mean Droplet Diameter of the Retardants.

Thus in general the important shear rate range over which the effective viscosity of fire retardants should be investigated experimentally for various practical aerial dissemination applications is about 10 to 1000  $\text{sec}^{-1}$ , and this finding has now been written into retardant development specifications (Section 3.5 of ref. 11).

In summary then, the mean terminal droplet size of an aeri-ally-dispersed liquid fire retardant can be controlled by means of a thickener that will give the retardant an effective viscosity whose magnitude at the shear rate at which the droplet stripping occurs results in the desired droplet size being produced. The approximate relationships between the mean droplet size, shear rate, aircraft speed and the physical properties of the retardant (including the effective viscosity) are given by Eq. (23-25). It may be seen then, that the specification of the effective viscosity that is desired of a retardant should include the applicable shear rate range, and this range will depend on the conditions under which the retardant is to be dispersed (e.g., aircraft speed).

#### 5.1.6 Droplet Size in the Ineffective Ground Pattern

As discussed before, the droplet size in the initial peripheral stripping region should theoretically be smaller than in the effective ground pattern because the stripping takes place at the aircraft velocity rather than at the reduced velocity resulting from Taylor breakup. Since the latter stripping occurs at about 0.7 of the aircraft speed (Eq. (25)), the difference in droplet sizes between the two regions should be a factor of about  $(1/0.7)^{0.7} = 1.28$  due to the velocity difference. In addition there will be a small factor resulting from the change in effective viscosity due to shear rate difference.

An examination of the droplet sizes on the impact cards located upstream of the effective (heavy) ground pattern showed that in all cases the droplet sizes are definitely smaller than in and near the heavy pattern. It was not possible to establish a specific relationship between the two patterns due to the general scatter in the data, the locations of some of the cards and wind effects, but the preceding theoretical difference appeared to be roughly applicable in several cases. In general however the trend seemed to indicate a slightly larger difference. Nevertheless in view of the various uncertainties involved, the preceding treatment offers a reasonable way of estimating the differences in droplet sizes in the roughly two different ground concentration regions (the grouping of the overall pattern into two separate regions is of course idealized).

#### 5.1.7 Droplet Size Distribution

Table IX lists the computed mass mean droplet diameter of the aeri-ally disseminated retardants. In actuality, however, a distribution of droplet sizes is produced, and Figures 30-44 show the experimental distributions obtained by the camera and rotating impact samplers (the distributions on the cards were also reduced). The droplet sizes can be estimated by assuming that they obey a log normal probability distribution,<sup>3,4</sup> and Figure 53 shows the results of the calculations. This figure can be compared

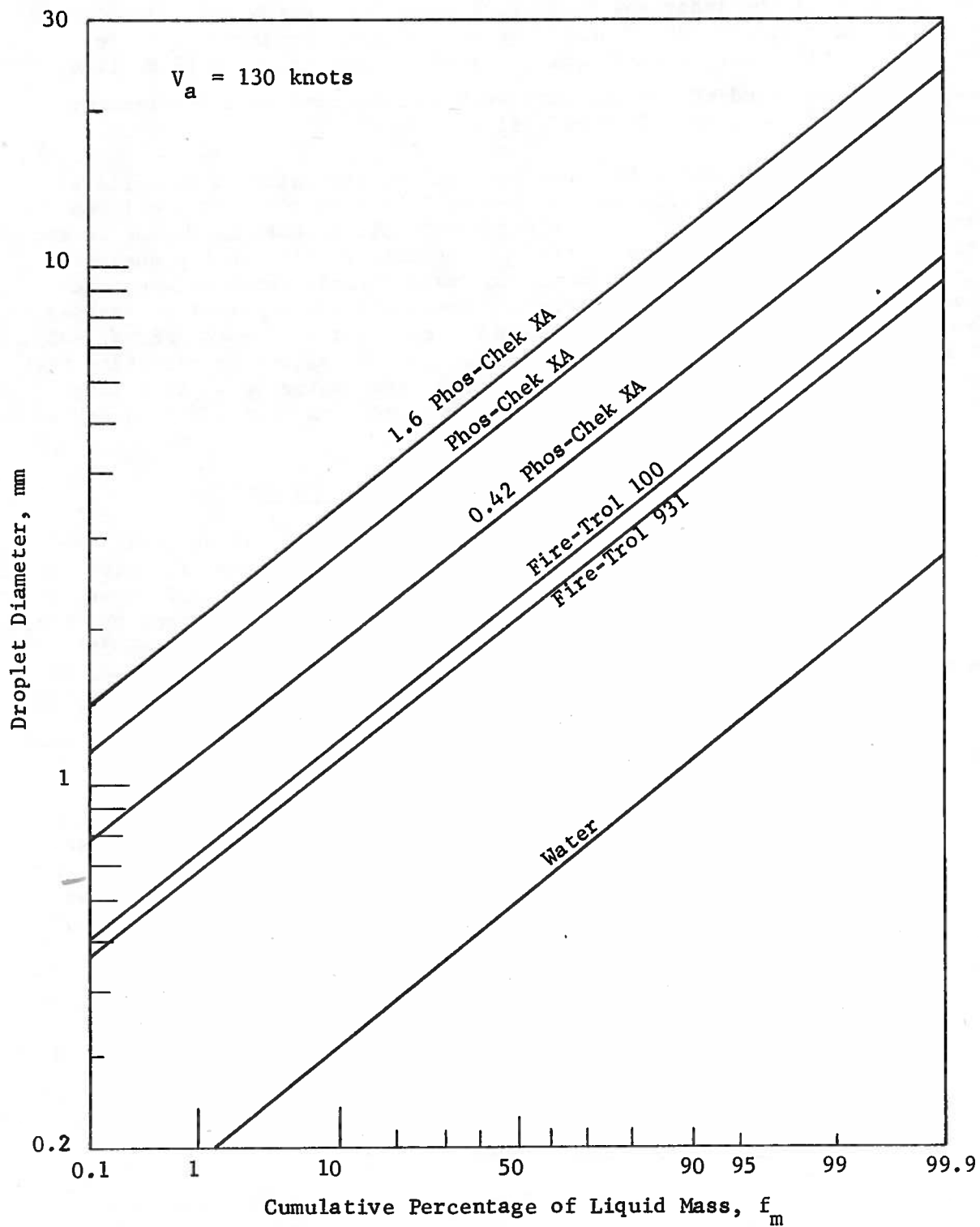


Figure 53. Computed Size Distribution of the Retardant Droplets in and Near the Effective Ground Pattern.

with the experimental distributions. Generally speaking, the computed results appear reasonable. The experimental curves sometimes show some smaller droplets for the Phos-Chek XA solutions than given by theory. This is due to the fact that on a number basis, the minimum droplet size is a factor of 3.36 (as used before) smaller than on a mass basis. Thus all of the curves in Figure 53 should in principle eventually (and smoothly) decrease by this factor at very small values of  $f_m$ . This complication was not included for practical reasons. The smallest droplet sizes for the low viscosity fluids are smaller than for those with higher viscosity. These droplet sizes were not measured, and in most cases were either largely blown away or evaporated so that they did not appear on the impact samplers. The overall effect is that the experimental droplet size distributions (based on mass) are more narrow for the low viscosity fluids than for those with higher viscosity.

## 6. CONCLUSIONS

In this program experimental measurements were made in the field of the droplet sizes produced by the actual aerial dissemination of the contemporary liquid retardants Phos-Chek XA, Fire-Trol 100, Fire-Trol 931 and water, and two Phos-Chek XA solutions whose gum thickener concentration was a factor of 1.6 and 0.42 of that of the standard Phos-Chek XA solution. The rheological properties of these fluids encompass a wide range, and measurements of these properties were made on the Phos-Chek XA solutions as a function of gum thickener concentration to complement those made earlier on the standard retardants. The measured droplet sizes were compared with those estimated earlier on the basis of theory, and the theory was modified and simplified for practical use.

The results of the droplet size measurements showed conclusively what has long been believed from experience in aerial fire fighting technology, viz, that different droplet sizes are produced by different retardants when disseminated under the same conditions. The experimental relative ordering of the retardants with respect to decreasing droplet size was 1.6 Phos-Chek XA, Phos-Chek XA, 0.42 Phos-Chek XA, Fire-Trol 100, Fire-Trol 931 and water. The relative droplet size ordering for the four standard retardants is consistent with experience in the field use of the retardants. Thus from ground recovery experiments (evaporation effects), cloud settling times and wind-drift and other observations it has been determined qualitatively that the droplet size of Phos-Chek XA is significantly larger than those of Fire-Trol 100 and Fire-Trol 931, which are roughly comparable, which in turn are a little larger than that of water.<sup>1,12</sup>

The experimental data provided quantitative values for the droplet sizes, some information regarding the general uncertainty of the values and how the values vary in the ground pattern. There was some evidence that the droplet size may increase in localized areas of very high liquid ground concentration but the trend was not consistent. The droplet size is slightly smaller in the initial low concentration region of the pattern than in the subsequent effective high concentration contour as predicted by theory. It is also - in the absence of ground wind - smaller on the periphery than in the interior of the ground pattern (due to turbulent diffusion), and

smaller on the downstream side of the pattern if there is a ground wind. The droplet size increased with decrease in aircraft speed, and for the Phos-Chek XA solutions the droplet size increased with increase in gum thickener concentration.

The theoretical studies conducted earlier on the program showed that for constant aircraft speed and retardant drop conditions, the mean terminal droplet size of the dispersed retardant should increase with increase in the effective viscosity of the fluid. The effective viscosity incorporates the effects of apparent fluid viscosity and fluid elasticity at the shear rate at which the liquid stripping occurs (effective viscosity is shear-rate dependent). In this program it was found that the experimental droplet sizes of the various retardants could be correlated in a quantitative manner (within the accuracy of the experimental data) by the previously-used liquid breakup model, if the theoretical two-thirds power dependence of effective viscosity on droplet size was empirically reduced to a one-third power dependence. The one-third power dependence is also in essential agreement with droplet size data given in the literature on the stripping breakup of liquid jets. The theory also describes the effect of other fluid properties (surface tension and density), thickener concentration (as manifested by effective viscosity) and aircraft speed on the terminal droplet size (neglecting evaporation effects).

The successful correlation of the experimental droplet sizes by the modified theory has resulted in the development of a simple equation for the prediction of the mass mean droplet size as a function of the rheological properties of the retardant and the aircraft velocity. This equation should be useful in the development of retardants having rheological properties which will produce droplets of a desired size when the retardant is disseminated. However additional field studies should eventually be conducted to provide further information regarding the distribution of droplet size in the ground contour pattern (including concentration effects), and the effect of the release characteristics of the retardant (tank and gating system) on the droplet size. Further theoretical studies of the mechanics of liquid breakup (both Taylor and surface stripping) and its relation to ground concentration pattern,<sup>3,13,14</sup> and droplet size would also be useful in the elucidation of the effects of retardant rheology and tank and gating system design on the dissemination of liquid fire retardants.

## REFERENCES

1. C. W. George and A. D. Blakely, "An Evaluation of the Drop Characteristics and Ground Distribution Patterns of Forest Fire Retardants," USDA Forest Service Res. Paper INT-134, IFR Experiment Station, Ogden, Utah, March 1973.
2. C. W. George, A. D. Blakely and G. M. Johnson, "Forest Fire Retardant Research," Report INT-31, USDA Forest Service, Ogden, Utah, 1976.
3. W. H. Andersen, R. E. Brown, K. G. Kato and N. A. Louie, "Investigation of Rheological Properties of Aerial-Delivered Fire Retardant," Report 8990-04 (Final), to Northern Forest Fire Laboratory, U. S. Forest Service, June 1974.
4. W. H. Andersen, R. E. Brown, N. A. Louie, P. J. Blatz and J. A. Burchfield, Ibid, Extended Study, Report 8990-05 (Final), December 1974.
5. E. B. Anderson, et al, "Aerial Delivery Systems Program," Final Report, ATR-74(7299)-1, to U. S. Forest Service, The Aerospace Corporation, Dec. 1973.
6. R. D. Ingebo and H. H. Foster, "Drop-Size Distribution for Crosscurrent Breakup of Liquid Jets in Airstreams," NACA TN 4087, October 1957.
7. G. A. Young, "The Physics of the Base Surge," NOLTR 64-103, June 1965.
8. M. A. Weiss and C. H. Worsham, ARS Journal 29, 252 (1959).
9. B. H. Zimm, in Rheology, Vol. III, Eirich, Ed., Academic Press, 1960, pp. 1-16.
10. H. C. Hershey and J. L. Zakin, Chem. Eng. Sci. 22, 1847 (1967).
11. "Specification for Retardant, Forest Fire, Dry or Liquid Chemical For Aircraft or Ground Application," Interim Specification 5100-00303, USDA, Forest Service, April 1976.
12. C. W. George, "Fire Retardant Ground Distribution Patterns from the CL-215 Air Tanker," USDA Forest Service Res. Paper INT-165, IFRES, Ogden, Utah, May 1975.
13. D. H. Swanson, "High Altitude Retardant Drop Mechanization Study," Final Report, Vol. 1, to Northern Forest Fire Laboratory, Missoula, Montana, Honeywell, April 1973.
14. D. H. Swanson and T. N. Helvig, "Extended High Altitude Retardant Drop Mechanization Study," January 1974.

5  
2  
7  
1

1  
2  
3  
4  
5